Applications of Generalised Supply-Demand Analysis

by

Carl David Christensen

Thesis presented in partial fulfilment of the requirements for the degree of Master of Science in Biochemistry in the Faculty of Science at Stellenbosch University

Department of Biochemistry,
University of Stellenbosch,
Private Bag X1, Matieland 7602, South Africa.

Supervisor: Prof JM Rohwer
Co-supervisor: Prof J-HS Hofmeyr

March 2013

Declaration

By submitting this thesis electronically, I declare that the entirety of the work contained therein is my own, original work, that I am the sole author thereof (save to the extent explicitly otherwise stated), that reproduction and publication thereof by Stellenbosch University will not infringe any third party rights and that I have not previously in its entirety or in part submitted it for obtaining any qualification.

Date: 2012/12/21 .....

Abstract

Supply-demand analysis (SDA) is a tool that allows for the control, regulation and behaviour of metabolic pathways to be understood. In this framework, reactions are grouped into reaction blocks that represent the supply and demand of a metabolic product. The elasticities of these supply and demand blocks can be used to determine the degree of control either block has over the flux in the pathway and the degree of homoeostasis of the metabolic product that links the blocks. Rate characteristic plots, on which the rates of supply and demand blocks are plotted as functions of the concentration of the linking metabolite, represent a powerful visual tool in this framework.

Generalised supply-demand analysis (GSDA) allows for the analysis of metabolic models of arbitrary size and complexity without prior knowledge of the regulatory structure of the pathway. This is achieved by performing SDA on each variable metabolite in a pathway instead of choosing a single linking metabolite. GSDA also provides other benefits over SDA as it allows for potential sites of regulation and regulatory metabolites to be identified. Additionally it allows for the identification and quantification of the relative contribution of different routes of regulation from an intermediate to a reaction block.

Moiety-conserved cycles present a challenge in performing *in silico* SDA or GSDA, as the total concentration of a moiety must remain constant, thereby limiting the range of possible concentrations of the metabolites between which it cycles. The first goal of this thesis was to develop methods to perform GSDA on two-membered and interlinked moiety-conserved cycles. We showed that by expressing the members of a moiety-conserved cycle as a ratio, rather than individual metabolite concentrations, we can freely vary the ratio without breaking moiety conservation in a GSDA. Furthermore, we showed that by linking the concentrations of the members of two interlinked two-membered moiety-conserved cycles to a "linking metabolite", we could vary the concentration of this metabolite, within constraints, without

breaking moiety conservation.

The Python Simulator for Cellular Systems (PySCeS) is a software package developed within our group that provides a variety of tools for the analysis of cellular systems. The RateChar module for PySCeS was previously developed as a tool to perform GSDA on kinetic models of metabolic pathways by automatically generating rate characteristic plots for each variable metabolite in a pathway. The plots generated by RateChar, however, were at times unclear when the models analysed were too complex. Additionally, invalid results where steady-states could not be reached were not filtered out, and therefore appeared together with valid results on the rate characteristic plots generated by RateChar. We therefore set out to improve upon RateChar by building plotting interface that produces clear and error-free rate characteristics. The resulting RCFigure class allows users to interactively change the composition of a rate characteristic plot and it includes automatic error checking. It also provides clearer rate characteristics with effective use of colour.

Using these tools two case studies were undertaken. In the first, GSDA was used to investigate the regulation of aspartate-derived amino acid synthesis in *Arabidopsis thaliana*. A central result was that the direct interaction of aspartate-semialdehyde (ASA), a metabolite at a branch point in the pathway, with the enzyme that produces it only accounts for 7% of the total response in the flux of supply. Instead, 89% of the observed flux response was due to ASA interacting with of the downstream enzymes for which it is a substrate. This result was unexpected as the ASA producing enzyme had a high elasticity towards ASA.

In a second case study moiety-conserved cycles in a model of the pyruvate branches in lactic acid bacteria were linearised using the above mentioned method. This served to illustrate how multiple reaction blocks are connected by these conserved moieties. By performing GSDA on this model, we demonstrated that the interactions of these conserved moieties with the various reaction blocks in the pathway, led to non-monotonic behaviour of the rate characteristics of the supply and demand for the moiety ratios. An example of this is that flux would increase in response to an increase in product for certain ranges.

This thesis illustrates the power of GSDA as an entry point in studying metabolic pathways, as it can potentially reveal properties of the regulation and behaviour of metabolic pathways that were not previously known, even if these pathways were subjected to previous analysis and a kinetic model is available. In general it also demonstrates how effective analysis tools and metabolic models are vital for the study of metabolism.

Opsomming

Vraag-en-aanbod analise (VAA) is 'n analisemetode wat mens in staat stel om die beheer, regulering en gedrag van metaboliese paaie beter te verstaan. In hierdie raamwerk word reaksies gegroepeer as reaksieblokke wat die aanbod (produksiestappe) en die aanvraag (verbruik-stappe) van 'n metaboliese produk verteenwoordig. Vanaf die elastisiteite van hierdie aanbod- en aanvraag-blokke kan die graad van beheer van elkeen van die blokke oor die fluksie, asook die graad van homeostase van die metaboliese koppelingsintermediaat, bereken word. Snelheidskenmerk-grafieke, waarop die snelhede van die vraag- en aanbod-blokke as funksies van die konsentrasie van die koppelingsmetaboliet uiteengesit word, verteenwoordig 'n kragtige visuele hulpmiddel in hierdie raamwerk.

Veralgemeende vraag-aanbod analise (VVAA), die veralgemeende vorm van VAA, maak dit moontlik om metaboliese modelle van arbitrêre grootte en kompleksiteit te analiseer sonder enige vooraf-kennis van die regulatoriese struktuur van die paaie. Die prosedure is om VAA op elk van die veranderlike metaboliete in die pad uit te voer, eerder as om 'n enkele koppelingsmetaboliet te kies. VVAA het ook ander voordele bo VAA aangesien dit potensiële setels van regulering en regulatoriese metaboliete kan identifiseer. Daarbenewens kan dit die relatiewe bydrae van verskillende regulerings-roetes van vanaf 'n intermediaat na 'n reaksieblok identifiseer en hulle kwantifiseer.

Groep-gekonserveerde siklusse bied 'n uitdaging vir *in silico* VAA of VVAA, aangesien die totale konsentrasie van die gekonserveerde groep konstant moet bly. Dit beperk die waardes van moontlike konsentrasies van die metaboliete wat die siklus uitmaak. Die eerste doelstelling van hierdie tesis was dus om metodes te ontwikkel waarmee VVAA op tweeledige en saamgebonde groep-gekonserveerde siklusse uitgevoer kan word. Deur die lede van groep-gekonserveerde siklusse eerder as verhoudings uit te druk in plaas van as individuele metabolietkonsentrasies, het ons gewys dat ons hierdie verhouding vrylik kan varieer sonder om die groep-

konservering te breek in 'n VVAA. Ons het ook gewys dat die konsentrasies van die lede van 'n saamgebonde groep-gekonserveerde siklus gekoppel kan word aan 'n "koppelingsmetaboliet", waarvan die konsentrasie dan binne perke gevarieer kan word sonder om die groep-konservering te breek.

Die "Python Simulator for Cellular Systems" (PySCeS) is 'n programmatuur-pakket wat binne ons navorsingsgroep ontwikkel is met die doel om sellulêre sisteme numeries te analiseer. Die RateChar module vir PySCeS was reeds voor die aanvang van hierdie projek ontwikkel om VVAA op kinetiese modelle van metaboliese paaie uit te voer deur outomaties snelheidskenmerke vir elke veranderlikke metaboliet te genereer. Die grafieke wat deur RateChar gegenereer is, was egter soms onduidelik wanneer die modelle te groot of kompleks geraak het. Daarbenewens is ongeldige resultate, waar 'n bestendige toestand nie bereik kon word nie, nie uitgefiltreer nie, en het dus saam met geldige resultate op die snelheidskenmerke verskyn. Een van die doelstellings was dus om RateChar te verbeter deur 'n koppelvlak vir grafieke te ontwikkel wat duidelike en foutlose snelheidskenmerke kon produseer. Dit het gelei tot die RCFigure klas wat outomatiese foutopsporing uitvoer en gebruikers in staat stel om op 'n interaktiewe wyse die samestelling van 'n snelheidskenmerk-grafiek te verander. Dit bied ook duideliker snelheidskenmerke deur effektief van kleur gebruik te maak.

Met hierdie ontwikkelde gereedskap is twee gevallestudies onderneem. In die eerste is VVAA gebruik om die regulering van aspartaat-afgeleide aminosuursintese in *Arabidopsis thaliana* te bestudeer. Die belangrikste resultaat was dat die direkte interaksie van aspartaat-semialdehied (ASA), 'n metaboliet by 'n vertakkingspunt in die pad, met die ensiem wat dit produseer, slegs vir 7% van die totale respons in die aanbod-fluksie verantwoordelik was. Daarteen was 89% van die waargenome fluksierespons die gevolg van die interaksie van ASA met drie van die stroomaf-ensieme, waarvoor dit 'n substraat is. Hierdie resultaat was onverwag aangesien die ensiem wat ASA produseer 'n hoë elastisiteit teenoor ASA toon.

In 'n tweede gevallestudie is die groep-gekonserveerde siklusse in 'n model van die pirovaat-takke in melksuurbakterie-metabolisme gelineariseer deur gebruik te maak van die bo beskrewe metode. Dit illustreer hoe verskeie reaksieblokke verbind word deur hierdie gekonserveerde groepe. M.b.v. 'n VVAA van hierdie model het ons gedemonstreer dat die interaksies van die gekonserveerde groepe met die verskeie reaksieblokke in die pad kan lei tot nie-monotoniese gedrag van die snelheidskenmerke van die vraag- en aanbod-reaksies vir die verhouding van die gekonserveerde groep-komponente. 'n Voorbeeld hiervan is die onverwagte

waarneming dat die fluksie toeneem met toenemende produk-konsentrasie oor sekere gebiede.

Hierdie tesis illustreer die krag van VVAA as 'n beginpunt vir die studie van metaboliese paaie, aangesien dit onbekende regulatoriese eienskappe en gedragspatrone kan ontbloot, selfs al is die paaie vantevore m.b.v. kinetiese modelle geanaliseer. Oor die algemeen demonstreer dit die noodsaaklikheid van effektiewe analisegereedskap en metaboliese modelle vir die bestudering van metabolisme.

Acknowledgements

I would like to express my sincere gratitude to the following people and organisations:

My supervisor, Prof Johann Rohwer for his guidance, especially towards the completion of this thesis. He provided me with enough freedom to do follow whichever path I chose to, while making sure that I did not stray too far from the right one.

My co-supervisor, Prof Jannie Hofmeyr.

Theo van Staden for his input towards developing a method of performing generalised supply-demand analysis on moiety conserved cycles. The work he did during his honours project served as a significant inspiration towards my work on moiety-conserved cycles.

My friends and family for all the support they provided.

The NRF for funding during my MSc studies.

Contents

List of Figures

List of Tables

Nomenclature

Abbreviations

SDA Supply-demand analysis

GSDA Generalised supply-demand analysis

MCA Metabolic control analysis

G6P Glucose-6-phosphate

GSH Glutathione

Asp Aspartate

AspP Aspartyl-phosphate

ASA Aspartate-semialdehyde

Hser Homoserine

PHser Phosphohomoserine

Thr Threonine

Ile Isoleucine

Lys Lysine

AK1 Aspartate kinase 1

AK2 Aspartate kinase 2

AKI Aspartate kinase I

AKII Aspartate kinase II

ASADH Aspartate-semialdehyde dehydrogenase

HSDHI Homoserine dehydrogenase I

HSDHII Homoserine dehydrogenase II

DHDPS1 Dihydrodipicolinate sythase 1

DHDPS2 Dihydrodipicolinate sythase 2

HSK Homoserine kinase

TS Threonine synthase

LKR Lysine ketoglutarate reductase

AC Acetate

Acal Acetaldehyde

AcCoA Acetyl coenzyme A

Acet Acetoin

AcLac Acetolactate

Acp Acetyl Phosphate

But 2,3-Butanediol

CoA Coenzyme A

EtOH Ethanol

Glc Glucose

Lac Lactate

Pyr Pyruvate

GLYC Glycolysis

LDH Lactate dehydrogenase

PDH Pyruvate dehydrogenase

PTA Phosphotransacetylase

ACK Acetate kinase

ACALDH Acetaldehyde dehydrogenase

ADH Alchohol dehydrogenase

ALS Acetolactate synthase

ALDC Acetolactate decarboxylase

ACETEFF Acetoin efflux

ACETDH Acetoin dehydrogenase

NOX NADH oxidase

NEALC Non-enzymic acetolactate decarboxylase

Symbols

J_x The flux of reaction x

R_x^y Response coefficient of y towards x

C_i^y Control coefficient of v_i on y

$\varepsilon_x^{v_i}$ Elasticity coefficient of v_i for x

K The total concentration of a moiety (Section 3.3.1)

r_x The ratio of the members of a moiety-conserved cycle x (Section 3.3.1)

L The linking metabolite between interlinked moiety-conserved cycles (Section 3.3.2)

Chapter 1

Introduction

The main goal of systems biology is to build a system-level understanding of how the properties, functions and behaviour of biological systems arise from the properties of, and interactions between, the constituents that make up these systems [1]. Cellular metabolism is an example of one of the most fundamental biological systems, yet the behaviour and regulation of these metabolic systems are far from fully understood.

Supply-demand analysis (SDA) was developed in order to aid in filling this gap in understanding. It is a framework of analysis that allows for the study of the behaviour, control and regulation of metabolic pathways [2] within the metaphor of a supply-demand economy. It combines various theories and approaches relating to metabolic control and regulation into a single framework. The central theme of this framework is that regulation and function in metabolic pathways are inextricably linked. The authors argue that the function of the block of reactions that make up the demand for a metabolite should be responsible for controlling flux in a pathway, while supply blocks determine the degree of homoeostasis of the metabolite [2–4]. With the experimental application of SDA, this previous argument has been both confirmed [5] and contradicted [5; 6].

SDA, in its generalised form, allows for the analysis of metabolic pathways of arbitrary size and complexity by performing SDA for each variable metabolite in a pathway [7]. It has various advantages over SDA. The requirement that supply and demand blocks must be isolated from each other is relaxed in generalised supply-demand analysis (GSDA) and it allows for identification and the quantification of the regulatory importance of these routes of interaction. In spite of this, to date GSDA has not been employed in any published studies of metabolism.

Performing GSDA *in silico* requires a kinetic model of the pathway to be investigated. In addition to the previous requirement, software to perform this analysis is also required. The software package RateChar was developed by Rohwer and Hofmeyr [7] for just this purpose. While adequate in performing GSDA on smaller models, this software has some shortcomings in terms of usability and clarity, especially when dealing with complex metabolic pathways as will be discussed in subsequent chapters.

1.1 Aims and Outline

The aim of the project described in this thesis was to build upon the current computational implementation of GSDA and utilise the framework to investigate the regulation of two metabolic pathways. Specifically we set out to:

- Improve RateChar, especially the component that is responsible for the visual representation of results as rate characteristic plots.
- Investigate and develop a method to deal with moiety-conserved cycles when performing GSDA.
- Use GSDA to analyse a metabolic pathway of aspartate-derived amino-acids in *Arabidopsis thaliana*, focusing on routes of regulation.
- Use GSDA to analyse a metabolic pathway of pyruvate branches in lactic acid bacteria, focusing on moiety-conserved cycles.

Chapter 2 gives a brief review of pertinent literature. It covers metabolic pathways and their regulation, metabolic control analysis, SDA, GSDA and examples of SDA in the literature. Chapter 3 covers the development of the RCFigure class for RateChar and a method to perform GSDA on models with conserved moieties. The next two chapters are the case studies employing GSDA, and cover the analysis of the model of aspartate-derived amino-acids and the model of pyruvate branches respectively. The thesis is concluded by a general discussion in Chapter 6.

Chapter 2

Supply-demand analysis of metabolism

Many different concepts and techniques are employed within the framework of metabolic supply-demand analysis [2; 7; 8]. The following chapter will be dedicated to exploring supply-demand analysis and its associated techniques in detail, and to an overview of some examples of its use in literature.

2.1 The metabolic pathway

If we had the ability to peer into the cell and witness every reaction taking place at any moment, we would see thousands of reactions, involving thousands of different molecules with numbers potentially in the millions[1] taking place simultaneously with interactions between all levels of organisation within the cell. With this vast number of reactions and molecules taking part in metabolism it might be easy to mistake these reactions as random. This is however not the case.

The metabolic system is made up of a complex reaction network. This reaction network consists of chains of enzyme catalysed reactions that are that are interlinked by common intermediates, where the product of the previous reaction acts as the substrate of the next [11–13]. The reaction network consists of various common structures such as linear chains of reactions, branch points at either enzymes or intermediates, or cycles with conserved moieties. These structures are shown in Figure 2.1 as (A), (B) and (C) respectively [13]. The metabolic system is also an open system, meaning that metabolites such as products and substrates are exchanged

[1] Based on a cell volume of 3.7×10^{-16}L[9] and an internal glucose concentration 15mM in *Lactococcus lactis* [10]

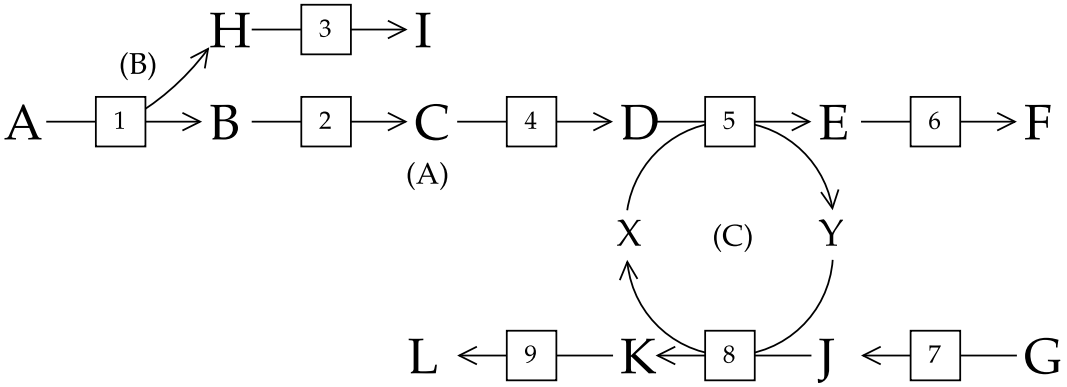

Figure 2.1: A metabolic pathway with (A) a linear portion between metabolites A and F, (B) a branch point at reaction 1 and (C) a moiety-conserved cycle between metabolites X and Y.

between the cell and outside environment [11; 12]. Transport of metabolites forms part of the metabolic system for this reason [11; 12].

The complete reaction network is subdivided into smaller reaction networks, or metabolic pathways. These subdivisions are somewhat arbitrary, but are generally made according to function, where different metabolic pathways have different and specific functions such as the production of amino acids or secondary metabolites. Within metabolic pathways, reactions may also be organised into blocks of successive reactions according to their function. The catabolic block breaks down complex molecules into simple carbon skeletons as well as providing phosphorylation and reducing equivalents. The biosynthetic block builds more complex molecules for use in macromolecular synthesis and the growth block is responsible for maintaining the cellular structure and gene and enzyme machinery [2]. The two latter mentioned blocks typically utilise phosphorylation and reducing equivalents. These reaction blocks are linked to one another via either a common intermediate or a pair of intermediates in a moiety-conserved cycle [2].

Events within the reaction network may also be classified according to the time scale on which they occur [11; 14]. Events with rates measurable during observation lasting seconds to an hour, such as enzyme catalysed reactions, comprise the metabolic time scale. Events may also occur on two other time scales at rates that are either immeasurably fast (eg. enzyme binding to pathway intermediates) or immeasurably slow (eg. changes in the concentrations of conserved moieties) on the metabolic time scale [11].

The open nature of metabolism results in a flow of matter through the metabolic

pathways. This is in contrast to closed systems where equilibrium is eventually reached [11]. The flow of matter also tends to converge to a steady-state, where the flow of matter, or flux, remains constant. This means that the rates of the individual reactions in a pathway are equal. Another property of the steady-state is that intermediate concentrations also remain constant, as the constant flow of matter means that intermediates are produced at the same rate at which they are consumed. Various steady-states are possible for a system and they depend on the parameters of the system. Any change in a system, such as a sudden addition of intermediates, will be met by a change in the reaction rates and metabolite concentrations in the system. In the case of a dynamically stable steady-state, however, the system will eventually return to the same steady-state as long as the parameters of the system remain constant. The steady-state is an important property of metabolic systems and can be seen as the normal working order of metabolism [11].

2.2 Regulation of metabolic pathways

Regulation in metabolism refers to the phenomena whereby the properties of the components that make up the system, as well as the stoichiometry of the system, allow the system to meet the demands of the organism, to maintain homoeostasis of intermediates and to respond to changes in the environment [2; 12]. As stated previously, open metabolic systems have the potential to reach steady-states, but this potential also exists in open reaction networks existing outside of metabolism, due to mass action. The cell, however, requires a system that fulfils specific functions rather than a system whose properties are solely dependent on stoichiometry and mass action. The difference lies in that the reactions in the metabolic system are enzyme catalysed [2; 12]. These enzymes allow the metabolic system to reach different steady-states compared to an uncatalysed network by counteracting or enhancing the mass action effect. The kinetics of enzymes are also affected by various parameters of the system, and therefore they allow the system to react to changes to the environment by allowing for dynamic behaviour. Enzymes can therefore be considered as the primary handles though which evolution creates metabolic function.

Metabolic function can be classified into different levels [2]. Within a specific pathway the most basic function of enzymes is to catalyse a reactions. The pathway itself may similarly have the function of producing some product, such as a amino acid, from a substrate though a series of steps. Higher, systemic level functions can also be attributed to enzymes such as the determination and control of the steady state variables of the pathway. Regulation is measured in terms of the performance

of these functions [11; 12].

In the face of changes to the external environment of the metabolic pathway, the regulation of the system though environmental interaction with system components allows it to adjust its steady state. A system where steady state flux can adapt sensitively to certain changes, while keeping the steady state concentrations relatively constant, can regarded as a well-regulated system. When describing the regulation of the system these factors need to be considered.

Regulation can be described using concepts from control analysis, as will be discussed in the following section. Regulators can be classed into external and internal regulators [11]. The former class represents any chemical species through which environmental changes are communicated to the pathway while the latter are internal species that form part of feedback loops around which regulation is coordinated. Any enzyme that these regulators affect are known as regulatory enzymes. The regulability of these enzymes refers to the extent to which a change in a regulator has an effect on the enzyme rate, while regulatory capacity refers to the effect that a change in the rate of the reaction catalysed by the enzyme has on the steady state variables of the pathway. These two definitions are measured in terms of enzyme elasticity (Section 2.3.1) and control coefficients (Section 2.3.3), respectively. The regulatory importance of an enzyme can be taken as the product of the regulability of an enzyme in regard to a regulator and the regulatory capacity of an enzyme.

2.3 Metabolic Control Analysis

In the previous section, an overview of the organisation and the properties of the metabolic system was given. The steady-state is an important property of metabolic systems and it depends on the structure and parameters of the system. Metabolic control analysis (MCA) has since its inception in the early 1970s enabled scientists to quantify the behaviour of metabolic systems at their steady-states [15; 16]. It allows us to relate the steady-state to the variables in the systems, such as intermediate concentrations and fluxes, to the parameters of the system, such as enzyme concentrations or the kinetic properties of enzymes. Some of the basic concepts of MCA will be discussed in this section.

2.3.1 Elasticity coefficients

If we look at an enzyme in isolation from its metabolic pathway we can describe the sensitivity of its rate to any particular metabolite that interacts with it as its

elasticity towards that species. This species may be an external effector or it may be a variable metabolite which is generated somewhere in the system itself. For instance, if we have an enzyme with a rate v and an effector x we can express the elasticity of the enzyme towards the effector as

$$\varepsilon_x^v = \frac{\partial v/v}{\partial x/x} \tag{2.3.1}$$

This represents the fractional change in reaction rate $\partial v/v$ over the fractional change in effector concentration $\partial x/x$. It is noteworthy that because these fractional changes are scaled, elasticity is dimensionless.

We can also express elasticities as the change in the logarithm of v over the change in the logarithm of x as follows

$$\varepsilon_x^v = \frac{\partial \ln v}{\partial \ln x} \tag{2.3.2}$$

This expression of elasticity is of special importance as it allows one to read off the elasticity from a rate characteristic plot in double logarithmic space, as shall be discussed later. The elasticity of the enzyme catalysed reaction to the concentration of the enzyme itself is 1, as enzyme concentration is a multiplier in the rate equation.

2.3.2 Response Coefficients

When looking at a complete pathway instead of an isolated enzyme we can define the flux, J, as the steady-state reaction rate of whole pathway. The sensitivity of flux towards any particular parameter or effector x in the pathway, i.e. the flux response coefficient, can be defined as follows

$$R_x^J = \frac{\partial \ln J}{\partial \ln x} \tag{2.3.3}$$

It is clear that this definition is similar to elasticity coefficients, as it is also the change in a rate in log form, $\partial \ln J$, over the change of an effector or parameter in log form, $\partial \ln x$, but in this case we are considering at the global rate, flux.

Response coefficients are not limited to flux and may also describe the sensitivity of a steady-state concentration towards a perturbation in another species of the pathway. We may therefore more generally define the response coefficient as

$$R_x^y = \frac{\partial \ln y}{\partial \ln x} \tag{2.3.4}$$

where y represents any steady-state variable.

Figure 2.2: A simple four step linear pathway. The concentrations of metabolites A and E are fixed.

2.3.3 Control Coefficients

Another coefficient that is important towards describing the behaviour of a metabolic pathway is the control coefficient. It quantifies how a perturbation in a certain reaction rate affects a steady-state variable in a metabolic pathway. It is also a property of the pathway itself, meaning that it does not arise from the properties of any single enzyme, but rather from how all the enzymes in the pathway are arranged. It can be defined as

$$C_i^y = \frac{\partial \ln x}{\partial \ln v_i} \tag{2.3.5}$$

where $\partial \ln y$ represents the change in a steady-state variable in logarithmic form and $\partial \ln v_i$ represents the change the rate v of a specific step i in the pathway in logarithmic form.

2.3.4 Relationships between coefficients

MCA finds its strength in that all the previously defined coefficients are related to one another. We shall now explore some of these relationships.

The most obvious relationship is the following

$$R_x^y = C_i^y \varepsilon_x^{v_i} \tag{2.3.6}$$

Here we see that any parameter x affecting the rate v of a step i could ultimately lead to a change in a steady-state variable y as determined by the control that step i has on variable y. We call this the combined response relationship [15]. This relationship is defined specifically for external effectors and other parameters (V_{max}, K_m, K_{eq} etc.) that interact with an enzyme and not for variable metabolites of the system.

A second relationship is the summation property. It relates the control coefficients of each step on a specific steady-state variable. For instance, if we consider a simple four step linear pathway as shown in Figure 2.2 the summation property for the steady-state flux will be

$$C_1^J + C_2^J + C_3^J + C_4^J = 1 \tag{2.3.7}$$

The value of unity for this property demonstrates that the control of flux is shared by all the steps in a pathway. We can express this relationship for a system more generally as

$$\sum_{i=1}^{n} C_i^J = 1 \tag{2.3.8}$$

where n represents the number of steps in the system.

The summation property for steady-state concentrations differs slightly. If we use metabolite C as an example, the summation property is as follows

$$C_1^c + C_2^c + C_3^c + C_4^c = 0 \tag{2.3.9}$$

Here the coefficients add up to zero as some reactions have a positive effect on the concentration of C, such as reactions 1 and 2, while others such as 3 and 4 affect it negatively. We can express this relationship more generally as

$$\sum_{i=1}^{n} C_i^S = 0 \tag{2.3.10}$$

where S is any steady-state concentration and n represents the number of steps in the pathway.

The third relationship is known as the connectivity property. Similarly to the combined response relationship, it combines the elasticity coefficients with the control coefficients, but does so for the elasticities towards variable metabolites rather than external parameters. The connectivity property illustrates that it is possible to change the concentration of a certain variable metabolite in a pathway without altering the flux or the concentrations of the other metabolites in the pathway by altering the rates of the enzymes connected to the changed metabolite to counter its effect. For instance, if we consider the pathway in Figure 2.3 we can express the connectivity between the flux-control coefficient and the elasticities of the enzymes towards C as

$$\varepsilon_c^{v_1} C_1^J + \varepsilon_c^{v_2} C_2^J + \varepsilon_c^{v_3} C_3^J = 0 \tag{2.3.11}$$

or more generally as

$$\sum_{i=1}^{n} \varepsilon_x^{v_i} C_i^J = 0 \tag{2.3.12}$$

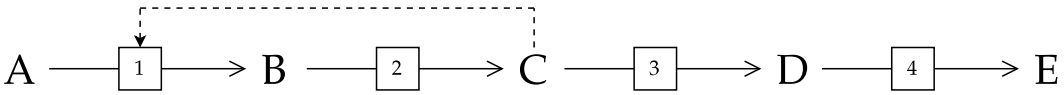

Figure 2.3: A simple four step linear pathway with inhibition of reaction 1 by metabolite C.

where x is a variable metabolite and n is the number of reactions.

As previously mentioned, the concentrations of the other variable metabolites in the pathway also remain constant. We can therefore express the connectivity between the concentration-control coefficients of B and the elasticities of the enzymes towards C as

$$\varepsilon_c^{v_1} C_1^b + \varepsilon_c^{v_2} C_2^b + \varepsilon_c^{v_3} C_3^b = 0 \tag{2.3.13}$$

or more generally as

$$\sum_{i=1}^{n} \varepsilon_x^{v_i} C_i^y = 0 \qquad (x \neq y) \tag{2.3.14}$$

where y is any metabolite in the pathway that is not x.

The connectivity between the concentration-control coefficients of C and the elasticities of the enzymes towards C is slightly different than the two previously defined connectivities as the concentration of C does change. It can be expressed as

$$\varepsilon_c^{v_1} C_1^c + \varepsilon_c^{v_2} C_2^c + \varepsilon_c^{v_3} C_3^c = -1 \tag{2.3.15}$$

The general form of this property is

$$\sum_{i=1}^{n} \varepsilon_x^{v_i} C_i^x = -1 \tag{2.3.16}$$

The following section will integrate the concepts and techniques described up to this point to introduce the framework of SDA.

2.4 Supply-Demand Analysis

Successive reactions in a metabolic pathway can be grouped into reaction blocks [17; 18]. These blocks can be considered as complete units in the metabolic pathway, with their own elasticity coefficients and control properties. The producing and consuming blocks of an internal regulator are referred to as the supply and demand blocks, respectively [2; 11]. With this concept, the regulation of a metabolic system can be approached and analysed within the metaphor of a supply-demand economy [2]. Supply-demand analysis utilises the concepts of regulation and control described in previous sections as well a visual component in the form of combined rate characteristic plots. This allows for the quantification of the behaviour, control and regulation of metabolism in terms of the elasticities of the supply and demand blocks.

2.4.1 Quantitative analysis of supply-demand systems

The combined rate characteristic plot shows the rates of the different reaction blocks as a function of the variable linking metabolite. It allows for the visual analysis of the behaviour of the system at steady-state. It also demonstrates how concentration and flux control depends on the properties of the supply and demand blocks [2; 8].

Figure 2.4 is a rate characteristic plot of the supply-demand system of the linear four step pathway shown in Figure 2.2 around metabolite C. The supply block represents reactions 1 and 2 while the demand block represents reactions 3 and 4. The logarithms of the rates of the supply and demand blocks are plotted against the logarithm of the concentration of C. The point where the supply and demand curves intersect represents the steady-state, where the steady-state flux, or J, can be read off the y-axis and the steady-state concentration of C, or $\bar{c}$, may be read off the x-axis [2; 8]. The block elasticities for supply are also defined in Figure 2.4 and describe the change in the rate of a reaction block towards a change in the metabolite C.

The use of the double-logarithmic scale allows for the direct comparison of the steady-state responses to perturbations of C. As mentioned in Section 2.3.1, it also allows for the elasticity coefficients to be be read off as gradients of the tangents to the curves at steady state [2; 8].

The general equation for control coefficients was given in Section 2.3.3 as Equation (2.3.5). Figure 2.5 is a visual representation of how flux and concentration control is quantified in the supply-demand system. The flux control by supply and

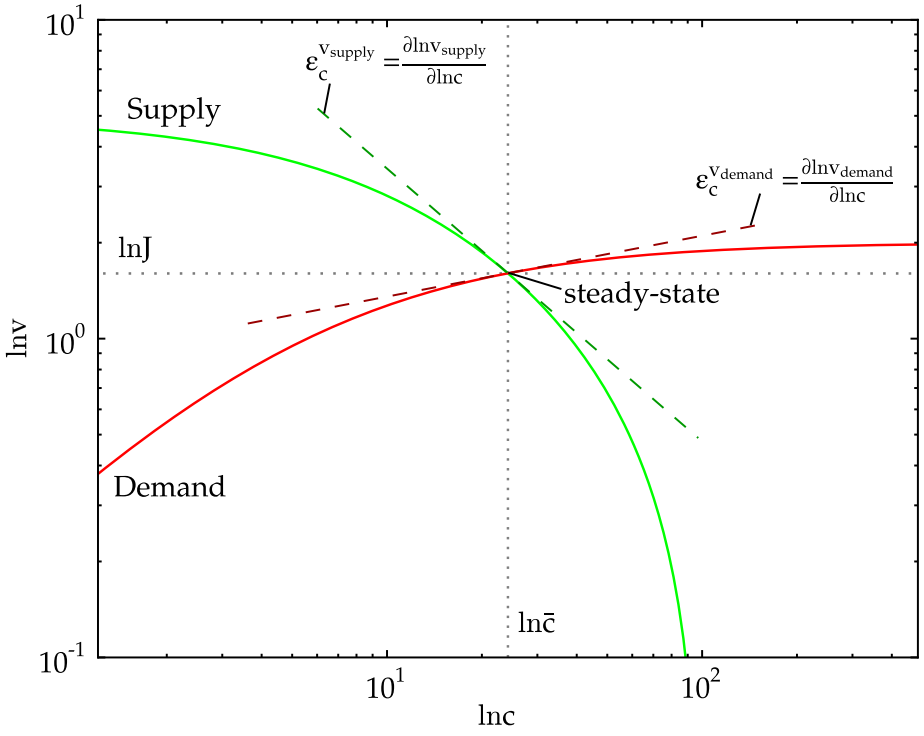

Figure 2.4: The rate characteristic plot of the supply-demand system for the intermediate *C* in Figure 2.2.

demand can therefore be given as:

$$C^J_{supply} = \frac{\partial \ln J_1}{\partial \ln v_{supply}} \tag{2.4.1}$$

and

$$C^J_{demand} = \frac{\partial \ln J_2}{\partial \ln v_{demand}} \tag{2.4.2}$$

and the concentration-control as:

$$C^c_{supply} = \frac{\partial \ln c}{\partial \ln v_{supply}} \tag{2.4.3}$$

and

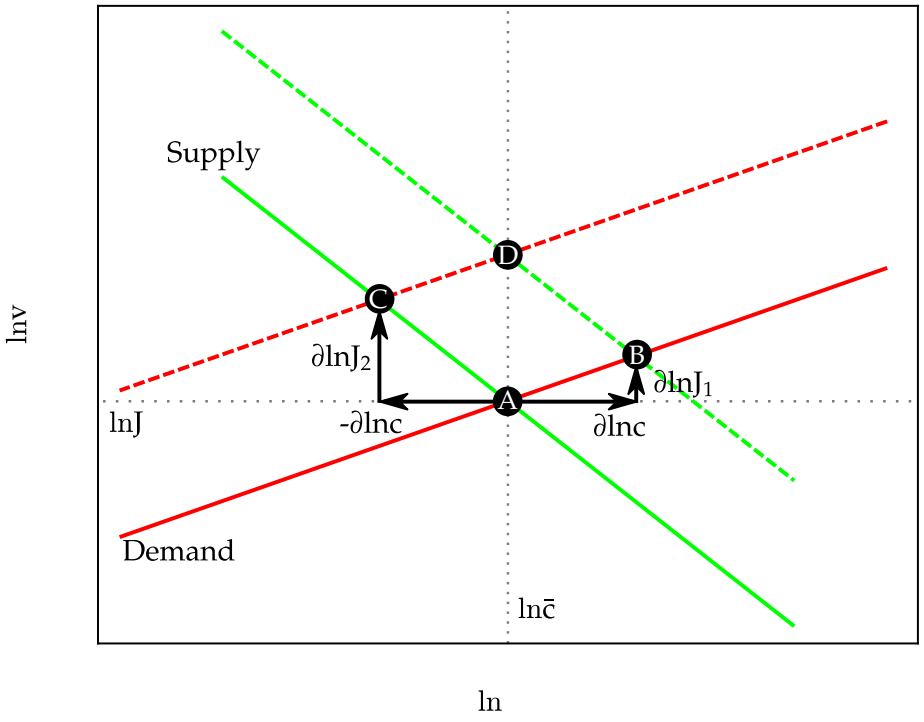

Figure 2.5: The response of the steady-state (A) to a change of $\partial \ln v$ to supply, demand or both activities [2]. This leads to new steady states at (B), (C) and (D) respectively.

$$C^{c}_{demand} = \frac{-\partial \ln c}{\partial \ln v_{demand}} \tag{2.4.4}$$

It follows that according to the definitions of the summation theorems (Equations (2.3.8) and (2.3.10)) and connectivity theorems (Equations (2.3.12),(2.3.14) and (2.3.16)) we can express the control coefficients in terms of the elasticities of supply and demand. The flux-control coefficients are:

$$C^{J}_{supply} = \frac{\varepsilon_c^{v_{demand}}}{\varepsilon_c^{v_{demand}} - \varepsilon_c^{v_{supply}}} \tag{2.4.5}$$

and

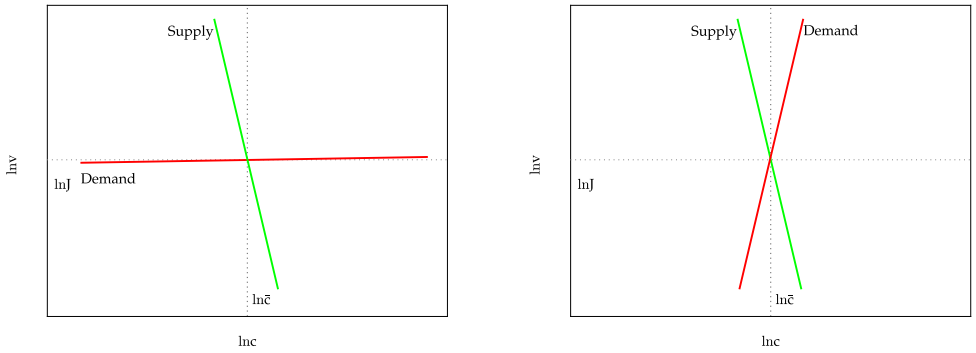

Figure 2.6: The rate characteristics of (A) a system where the supply and demand blocks are almost completely functionally differentiated in terms of flux control and determination of the degree of homoeostasis and, (B) a system where there is no differentiation in the functions of the supply and demand blocks.

$$C^{J}_{demand} = \frac{-\varepsilon_c^{v_{supply}}}{\varepsilon_c^{v_{demand}} - \varepsilon_c^{v_{supply}}} \tag{2.4.6}$$

while the concentration-control coefficients are:

$$C^{c}_{supply} = -C^{c}_{demand} = \frac{1}{\varepsilon_c^{v_{demand}} - \varepsilon_c^{v_{supply}}} \tag{2.4.7}$$

The ratio of the supply elasticity to the demand elasticity determines the distribution of flux control. In the case where

$$\left| \frac{\varepsilon_c^{v_{supply}}}{\varepsilon_c^{v_{demand}}} \right| < 1 \tag{2.4.8}$$

the flux is predominantly demand controlled, while in the opposite case of

$$\left| \frac{\varepsilon_c^{v_{supply}}}{\varepsilon_c^{v_{demand}}} \right| > 1 \tag{2.4.9}$$

the flux is predominantly supply controlled. If the ratio is equal to 1, flux control is shared exactly between the two blocks. The block with the smallest absolute elasticity is therefore the block with the most control over flux. In the case of

concentration control, the control is distributed equally among the two blocks [2; 8]. Here the magnitude in the variation of $\bar{c}$, or the degree of homoeostasis, is of interest. The degree of homoeostasis depends on the value of $\varepsilon_c^{v_{demand}} - \varepsilon_c^{v_{supply}}$, where the larger it is, the smaller the absolute values of the concentration control coefficients are [2; 8].

In Figure 2.6A the value of $\varepsilon_c^{v_{demand}}$ is zero, while the value of $\varepsilon_c^{v_{supply}}$ is very high as can be seen by the gradients of the curves. This means that the condition in Equation (2.4.8) is true and the flux of is controlled by the demand block. As previously stated, the concentration control of $\bar{c}$ is shared equally among the two blocks. In the case of this system $\varepsilon_c^{v_{demand}} - \varepsilon_c^{v_{supply}} = \varepsilon_c^{v_{demand}}$, therefore the supply block plays no role in the determination of the degree homoeostasis of $\bar{c}$.

In Figure 2.6B, the supply block has the same value for $\varepsilon_c^{v_{supply}}$ as in Figure 2.6A, but now $\varepsilon_c^{v_{demand}} = -\varepsilon_c^{v_{supply}}$. Therefore $|\varepsilon_c^{v_{demand}} / \varepsilon_c^{v_{supply}}| = 1$ and flux control is shared equally among the two blocks. Because the absolute values of supply and demand elasticities are equal, they both contribute equally to the degree of homoeostasis of $\bar{c}$.

With the above two examples it becomes clear that when one block has the most control over flux, it does not contribute to the degree of homoeostasis, which is then the function of the other block. The functions of flux and concentration are therefore mutually exclusive [2; 8].

2.5 Generalised Supply-Demand Analysis

A limitation of supply-demand analysis is that it requires a researcher to choose one intermediate that links supply and demand blocks. This linking metabolite must be the only route of interaction between the different blocks. In certain cases, such as linear pathways, the choice of a linking may be trivial, but in more complex pathways there may be branch points or multiple routes of interaction between blocks, which complicates the this choice.

Generalised supply-demand analysis (GSDA) was developed to overcome this limitation by eliminating human bias. Here each variable metabolite concentration is clamped in turn, turning it into a parameter of the system, and varied over a range of concentration values. Flux values generated by these parameter scans are used to draw combined rate characteristic plots for each variable metabolite and the supply and demand blocks that are linked by it.

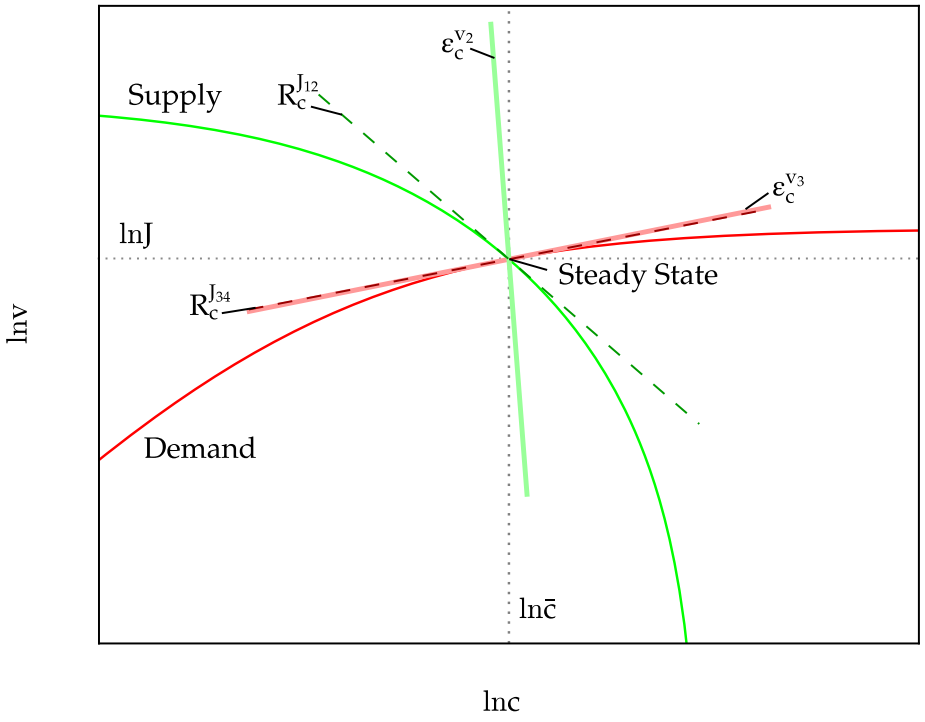

Figure 2.7: The rate characteristic plot of the supply-demand system for the intermediate *C* in Figure 2.3. The response coefficients are equivalent to block elasticities as shown in Figure 2.4. Enzyme elasticities are also indicated.

In addition to being able to identify sites of functional differentiation in a pathways, GSDA allows for (1) the identification of potential sites of regulation and (2) regulatory metabolites as well as for (3) the quantification of the relative contribution of the different routes of interaction from an intermediate to a supply or demand block.

2.5.1 Adaptations from supply-demand analysis

As the limitation on the communication between supply and demand blocks via only the linking metabolite has been lifted in GSDA, some modifications need to be made to the definitions made in the previous section.

Figure 2.7 shows the rate characteristic plot for metabolite *C* in the system shown in Figure 2.3. In this system a feedback loop has been introduced where metabolite *C* inhibits the activity of reaction 1. The control analysis in (2.4.5), (2.4.6) and (2.4.7) holds for metabolite *C* in Figure 2.3, as *C* is the only route of communication between

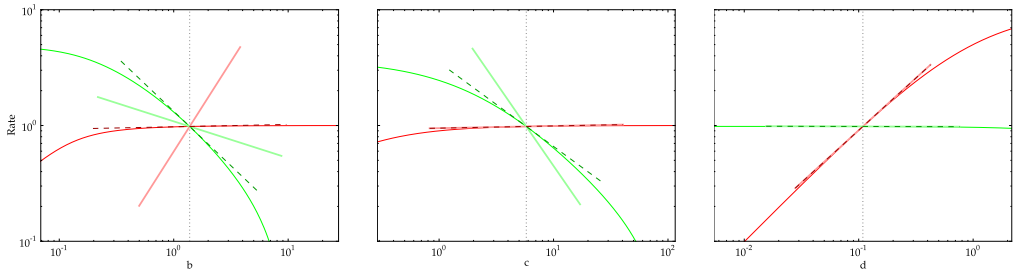

Figure 2.8: The rate characteristics for the clamped metabolites C-D in the system shown in Figure 2.3. Green curves represent the supply flux while red curves represent the demand flux. Dashed lines represent the response coefficients of the supply and demand blocks in the clamped system, while the solid lines represent the elasticities of the enzymes towards the clamped metabolite.

the supply and demand blocks. In the case of metabolite B however, communication occurs with the supply block through the direct interaction with enzyme 1 and via the interaction that C has with enzyme 1. Figure 2.7 also introduces response coefficients that are equivalent to the block elasticities in Section 2.4.1.

2.5.2 The interpretation of rate characteristic plots of GSDA

In addition to indicating functional differentiation in a pathway as explained in Section 2.4.1, the rate characteristic plots generated for use in GSDA can be used to deduce various features of regulation by interpretation on various levels.

2.5.2.1 Rate characteristic shapes

The most simple feature that may be used for assessment is the general shapes of the supply and demand curves. In Figure 2.8 the shape of the supply and demand curves for metabolite D differs from those of metabolite B and C. In this specific examples enzyme 3 is insensitive to changes in concentration of metabolite C and therefore has a very low value for $\varepsilon_c^{v_3}$. Changes in rate characteristic shape such as this point to sites of regulation.

2.5.2.2 Flux response and enzyme elasticities

By comparing the flux response and elasticity coefficients of a reaction block and enzyme towards a certain metabolite, a site of regulation can be identified. According to the response property in Equation (2.3.6), if $R_x^J = \varepsilon_x^{v_i}$, then $C_{v_i}^J$ must equal one, meaning that the enzyme catalysing the reaction has full control over its own flux in the system where the intermediate is clamped. This points to a site of regulation. The metabolite towards which the block and enzyme has a corresponding response

and elasticity may also be classified as a regulatory metabolite as changes in enzyme activity due to variation in the concentration of the metabolite are transmitted fully through the specific block.

A trivial case exists where in the last and first enzymes of a metabolic branch, as in this case the enzyme represents the only member of their demand or supply blocks, respectively. In these cases the responses and elasticities will therefore always be equal.

A further case of matching response and elasticities is where the enzyme is completely insensitive to changes in metabolite concentration. This means that the enzyme elasticity is zero and therefore the left hand term in Equation (2.3.6) must also be zero. In this case the particular block with the zero response has complete flux control for the complete (as opposed to the split) system. We see an example of this in Figure 2.7, where $R_c^{J_{34}} = \varepsilon_c^{v_3} \approx 0$. This system may be classified as functionally differentiated.

2.5.2.3 Multiple Routes of interaction

As previously stated, multiple routes of interaction are possible between a clamped metabolite and a supply or demand block. The response of a particular block may therefore be divided into partial response coefficients. An example of this is metabolite C in Figure 2.3 that may interact with the supply block through either enzyme 3 as a product or with enzyme 1 as an allosteric inhibitor. The complete response of the supply block can be written as

$$R_c^{J_{12}} = \varepsilon_c^{v_1} C_{v_1}^{J_{12}} + \varepsilon_c^{v_2} C_{v_2}^{J_{12}} = {}^1R_c^{J_{12}} + {}^2R_c^{J_{12}} \tag{2.5.1}$$

Figure 2.9B is a visual representation of these partial responses. Here it is possible to see the contribution of the two routes of interaction of C with the supply block. In this specific case $|{}^1R_c^{J_{12}}| > |{}^2R_c^{J_{12}}|$, which means that the allosteric inhibition of enzyme 1 by metabolite C contributes more to the response of the supply block than the product inhibition effect by C on enzyme 2.

Figure 2.9A shows the contribution of the two routes of interaction of metabolite B with the supply block, in this case consisting of only enzyme 1. These routes are the product inhibition of enzyme 1 by B and the interaction of B with enzyme 2 that is transmitted back towards enzyme 1 via allosteric inhibition by metabolite C. Here

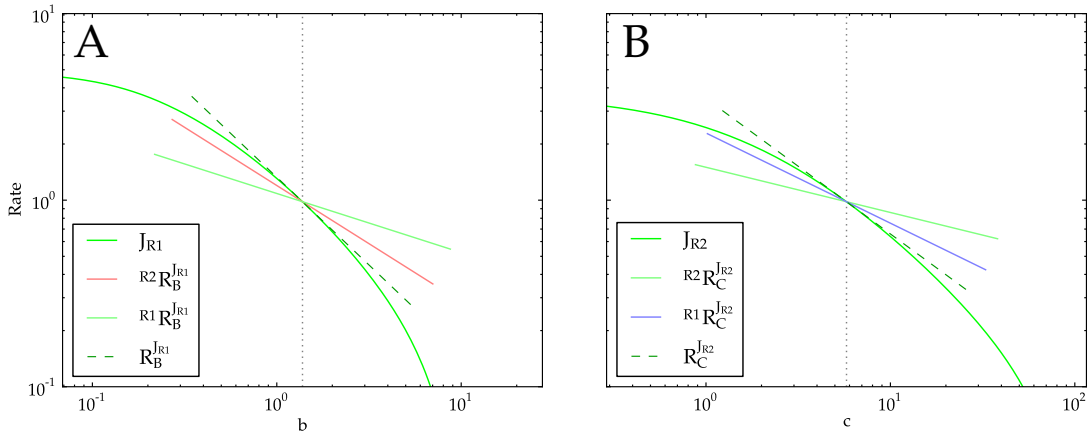

Figure 2.9: The rate characteristics of the supply blocks for clamped metabolites (A) B and (B) C in the system shown in Figure 2.3.

$|^2R_b^{J_1}| > |^1R_b^{J_1}|$ which means that more inhibition of supply flux is transmitted via the demand block than via direct product inhibition by B.

2.6 Examples of Supply-Demand Analysis

Various groups have utilised the supply-demand paradigm in their investigations into metabolism. Studies thus far have predominantly followed the experimental approach, as opposed to a modelling approach where the kinetics of enzymes in each block were determined before analysis. There have also been no studies following the generalised approach thus far. In the following paragraphs, a selection of studies employing SDA together with their findings will be highlighted.

Glycolysis has been a favourite topic of study for biochemists, because of its industrial importance and because it is an important pathway in energy metabolism. Koebmann *et al.* [5] utilised SDA to determine where the control of glycolytic flux lies in *E. coli* and *L. lactis*. They divided their system into supply and demand blocks around ATP and made the assumption that ATP was the only linking metabolite. Using *in vivo* flux data for ATP/ADP supply and demand in *E. coli* and *L. lactis* during the growth phase, Koebmann *et al.* [5] demonstrated contrasting results between these two organisms.

In *E. coli* it was found that $\varepsilon_{ATP}^{supply}$ was -0.89 and $\varepsilon_{ATP}^{demand}$ was 0.04 while in *L.lactis* $\varepsilon_{ATP}^{supply}$ was -0.02 and $\varepsilon_{ATP}^{demand}$ was 0.22. The control coefficients for the supply and demand blocks were calculated using Equations (2.4.1) and (2.4.2). While the high

control coefficient of 0.96 for the control of demand reactions over flux in *E. coli* correlated well with the prediction made by Hofmeyr and Cornish-Bowden [2], the opposite was true for *L. lactis*. Here the flux control coefficient of demand over flux was only 0.1, indicating that control was vested in the supply. When the flux measurements were repeated in non-growing *L. lactis* it was found that an increase in ATP demand did in fact increase the flux. These results showed that, while the flux control did lie in demand, as previously predicted [2], for the case of glycolysis it depended on the degree of excess capacity of the pathway.

A study with a similar premise was performed by Kroukamp *et al.* [6], substituting *S. cerevisiae* for the two bacterial species. In this study the authors also set out to determine the flux control coefficients of supply and demand for ATP in glycolysis. It was shown that flux control lied in the supply reactions rather than demand reactions. It should be noted that, in contrast to the research by Koebman *et al.* [5; 19], this result was determined under low-glucose conditions.

A pathway that shares some reactions with glycolysis, is glycogenesis. This pathway is important as is produces the energy storage molecule, glycogen. Schafer *et al.* [20] studied the control of flux in glycogen synthesis in mammalian muscle using a supply-demand system around glucose-6-phosphate (G6P). Interestingly they found that flux control resided in the supply of G6P while the degree of homoeostasis was determined by the demand for G6P, especially under low blood-glucose levels. Under high blood-glucose levels, however, they found that the immediate and sustained increase in flux led to homoeostasis being disturbed and a drastic build up of intermediates. This situation was countered by the allosteric and covalent regulation of both enzymes upstream and downstream from G6P due to an increase in blood insulin levels via an as-of-yet unknown mechanism. The stimulation of downstream enzymes, specifically glycogen synthase allowed homoeostasis to be maintained in the face of increased flux.

Jørgensen *et al.* [21] studied the role that CTP synthase plays in the synthesis of CTP in *Lactococcus lactis*. They found that the supply of CTP, in this case CTP synthase, had no control over the flux towards CTP as increasing the levels of CTP synthase had no effect on the growth rate of the organism except at very low expression levels of the gene encoding for this enzyme. CTP synthase did however had a strong control over CTP concentration. The authors did not investigate the effect that CTP demand has on CTP flux and concentration, but their findings correlated well with the predictions made by SDA regarding the role of the supply block [2].

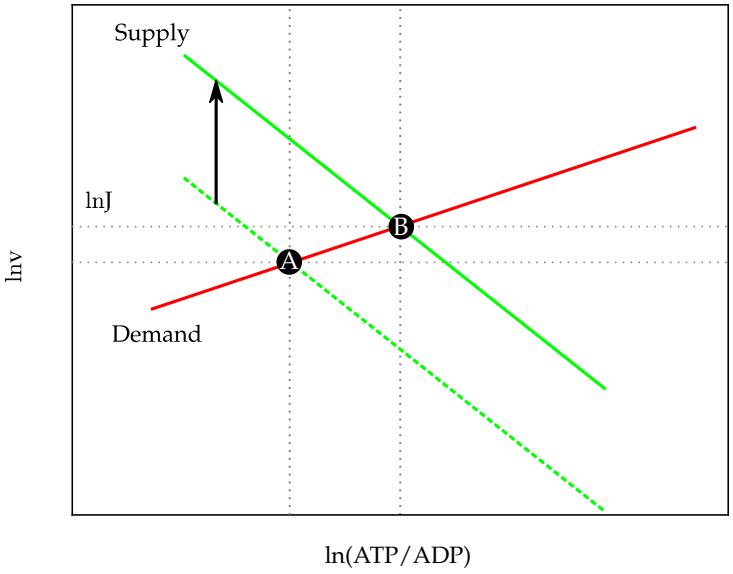

Figure 2.10: The rate characteristic plot of a the system described by Aledo *et al.* [23]. This rate characteristic plot demonstrates that as supply flux increases, the ATP/ADP ratio is expected to increase as depicted by the points (A) and (B). In the system exhibiting the ATP paradox, an increase in supply flux led to a decrease in the ATP/ADP ratio.

Glutathione (GSH) is an important metabolite which plays many roles in cell metabolism. One of these roles is the protection against heavy metals as GSH is a precursor to phytochelatins which accumulate heavy metals in the vacuole. Mendoza-Cozatl and Moreno-Sanchez [22] investigated the control of GSH flux and concentration by investigating a kinetic model of GSH metabolism under both stressed and unstressed conditions using SDA. Under unstressed, low demand conditions it was found that demand for GSH had the majority of flux control with supply providing a reasonably high degree of GSH homoeostasis. In the model for stressed conditions, demand increased and flux control shifted towards the supply block, ultimately leading to flux control being shared between supply and demand blocks and where GSH concentration was more sensitive to changes in flux due to the low elasticities of both supply and demand.

The ATP paradox refers to the curious phenomenon that occurs in yeast when there is a transition from glucose limitation to glucose excess. Aledo *et al.* [23] utilised the principles of SDA in an attempt to explain the ATP paradox. During this transition flux through glycolysis increases while the ATP concentration decreases.

Using the illustrative power of a rate characteristic plot of a supply-demand system around the ATP/ADP ratio (reproduced in Figure 2.10) the authors demonstrated that according to conventional knowledge of such systems, one would expect the ATP/ADP ratio to increase along with the increase in supply flux. Even in a system where there is a positive cooperative effect on demand reactions by ATP, it seems that ATP itself may not the effector of this observed paradox. The authors, however, present a theoretical basis whereby ATP could in fact be responsible for the paradox. Simply put, it involves a system where the rate of two enzymes responsible for the interconversion of a protein between active (W*) and inactive (W) forms, partly depends upon the ATP concentration. The protein in its active form is responsible for the modulation of ATP demand reactions. In the proposed system, there are certain cases where multiple possible steady-state concentrations of W* exist for the same ATP concentration and where the specific steady-state depends on ATP concentration crossing certain threshold values. This enables the demand activity to be stimulated when ATP concentration increases and crosses a threshold value, in turn decreasing ATP concentration to lower level than before the initial increase, but critically not low enough so that a lower threshold is reached that would reverse demand activation. While the authors do not specifically explore the control or elasticity coefficients in this study, the use of the supply-demand paradigm was vital in illustrating and understanding their proposed system.

The current chapter described the concepts and techniques associated with SDA and GSDA. We briefly introduced metabolic pathways and their regulation. The core concepts of metabolic control analysis were discussed in detail before covering SDA and GSDA and some examples of these techniques in the literature. In the next chapter we will discuss the concepts of kinetic modelling of metabolic pathways using computer software and the computational implementation of GSDA.

Chapter 3

Computational implementation of generalised supply-demand analysis

3.1 Introduction

With the power of computers it has become easier than ever to study metabolic pathways. However, the use of computers in studies of metabolism is not entirely new, as researchers in the field of enzyme kinetics have used analogue computers as early as the 1960s [24–27]. More recently various software applications have become available that were specifically designed to model and analyse metabolic systems such as COPASI [28], ScrumPy [29] and Jarnac [30]. The number of metabolic models available for study has also increased in recent years [7; 31] with model databases such as JWS Online [32] and the Biomodels Database providing easy access to these models [33].

Olivier *et al.* [34] presented a proof of concept where they used Python, a powerful scripting language that follows various programming paradigms, to model metabolic pathways and to perform certain analyses. While this was not the first time Python was used to model cellular metabolism [29], the authors wanted to build an open source modelling tool that fulfilled their requirements in terms of functionality. The same researchers later presented PySCeS, or the Python Simulator for Cellular Systems [35]. PySCeS, as its name implies, is a Python based application with various features such as time-course simulations of kinetic models of metabolic pathways and tools to perform metabolic control analysis. It can also visualise results with the use of a plotting interface. One of the main advan-

tages over the proof of concept is that PySCeS allows researchers to perform these analyses without needing to use lower-level programming techniques.

In the following sections, we will describe kinetic modelling of metabolic pathways in general and within the PySCeS modelling software. We will then discuss our contribution towards modelling conserved moieties. The final section of this chapter will be dedicated to describing our contributions towards the RateChar module for PySCeS and demonstrating its use in performing GSDA on kinetic metabolic models.

3.2 Kinetic Models

Models of metabolic pathways are essential for the study of metabolism with computational methods, as will be demonstrated in our case studies in Chapters 4 and 5. These models are a translation of the metabolic network into mathematical terms and may be relatively simple, containing only stoichiometric information [36–38]. In order to study the dynamic behaviour of a metabolic system using methods such as GSDA, however, more detailed kinetic models that include information about the rates of reactions in a pathway are necessary [7; 36–38].

The stoichiometry of a system defines the number of intermediates consumed or produced in the system. The stoichiometric coefficient indicates this number and may be positive, indicating production, or negative, indicating consumption of a specific intermediate in a reaction. Therefore the stoichiometry shows how reactions are connected in a metabolic network. We can summarise the stoichiometry of a system in a stoichiometric matrix $\boldsymbol{N}$. Below the stoichiometric matrix for the system in Figure 2.1 is shown with metabolites A, F, L and G as external (or fixed) metabolites, and Y and X as a moiety-conserved cycle.

$$N = \begin{array}{c} \\ B \\ C \\ D \\ E \\ J \\ K \\ X \\ Y \end{array} \begin{array}{c} \begin{array}{ccccccccc} 1 & 2 & 3 & 4 & 5 & 6 & 7 & 8 & 9 \end{array} \\ \begin{pmatrix} 1 & -1 & 0 & 0 & 0 & 0 & 0 & 0 & 0 \\ 0 & 1 & 0 & -1 & 0 & 0 & 0 & 0 & 0 \\ 0 & 0 & 0 & 1 & -1 & 0 & 0 & 0 & 0 \\ 0 & 0 & 0 & 0 & 1 & -1 & 0 & 0 & 0 \\ 0 & 0 & 0 & 0 & 0 & 0 & 1 & -1 & 0 \\ 0 & 0 & 0 & 0 & 0 & 0 & 0 & 1 & -1 \\ 1 & 0 & 0 & 0 & -1 & 0 & 0 & 1 & 0 \\ 1 & 0 & 0 & 0 & 1 & 0 & 0 & -1 & 0 \end{pmatrix} \end{array} \tag{3.2.1}$$

While the stoichiometry of a system provides useful information regarding the manner in which reactions are put together, it cannot describe the behaviour of the system in regards to a change in any variable or parameter of the system, or how the system behaves over any time period. In order to study this behaviour, the rate of each enzyme must be defined as a enzyme kinetic rate law [36–38]. These rate laws are functions of the concentrations of various parameters and variables of the system such as enzyme or reactant concentrations, respectively. The structure of a rate law depends on the enzyme mechanism and the stoichiometry of the reaction and the the parameters such as the maximal velocity (V_{max}) and binding constants (K_m) may be measured in vivo or in crude cell extracts [36; 38]. Rate laws do not need be completely mechanistic, as generic rate laws describe reactions adequately without needing as many parameters [36]. Below is an example of a reversible Michaelis-Menten rate law which defines the rate of enzyme 2 in Figure 2.1.

$$v_2 = \frac{\frac{V_f}{K_b}\left(B - \frac{C}{K_{eq}}\right)}{1 + \frac{B}{K_b} + \frac{C}{K_c}} \tag{3.2.2}$$

The reaction rates for a specific system may be collected in a vector $\boldsymbol{v}$ and the reactant concentrations in a vector $\boldsymbol{S}$ [36]. Using these vectors and the matrix $\boldsymbol{N}$, a kinetic model of a metabolic system can be defined using a set of ordinary differential equations (ODEs) [36] as follows

$$\frac{dS}{dt} = Nv \tag{3.2.3}$$

With this set of ODEs various different types of analyses such as time-course simulations, steady-state analysis and metabolic control analysis may be performed.

3.2.1 Kinetic models in PySCeS

The mathematical representation of a kinetic model shown in Equation (3.2.3) must be coded in terms the PySCeS Model Description Language (MDL) for use with PySCeS. In this file format variables such as intermediate concentrations and parameters of the system such as the V_{max} values or enzyme concentrations, as well as the stoichiometry and rate equations for each reaction, are coded in human readable format as opposed to a purely mathematical representation [39; 40]. Figure 3.1 shows an excerpt of a simple PySCeS model file for the pathway in Figure 2.1.

In addition to defining a kinetic model based on Equation (3.2.3), the PySCeS MDL format allows for various additional features such as time dependent events, directly encoded ODEs, conditional assignments and forcing functions [39; 40]. Forcing functions are of particular importance for the next section, as they allow for model attributes to be set to a value with a function instead of directly hard-coding them.

3.3 Modelling moiety-conserved Cycles

Moiety-conserved cycles are features in metabolic pathways where chemical groups are transferred between molecules in a cyclical manner [2; 7; 14]. This means that the concentration of specific moiety remains constant and therefore the sum of the concentrations of the molecules that the specific moiety is associated with also remains constant. This provides a stoichiometric constraint in otherwise open reaction networks.

We therefore set out to develop a method to perform GSDA on moiety-conserved cycles. In the following subsections two different cases of moiety conservation will be reviewed in terms how they are modelled and we will describe how they can be approached within the context of supply-demand analysis.

3.3.1 Common Case: Two membered moieties

The most common and simple case of moiety conservation found in metabolism, is the two membered moiety (shown in Figure 3.2A). Common examples two membered moieties are the NAD/NADH$^+$ and ADP/ATP couples. Here a single moiety is transferred between two different molecules, as represented by X and Y in Figure 3.2A. The sum of the concentrations of Y and X remains constant and can be represented as K [14], so that

$$K = [X] + [Y] \tag{3.3.1}$$

If we assume for Figure 3.2A, that the external reactions producing A and C and consuming B and D are named R_a, R_c, R_b, and R_d respectively and that external metabolites are not shown, the stoichiometric matrix, $\boldsymbol{N}$, is as follows

```
#External Metabolites
FIX: A I X Y Z

#Reactions
Reaction_2:
    B = C
    ((Vf2/KB2)*(B-C/Keq2))/(1 + B/KB2 + C/KC2)

#External Metabolite Concentrations:

A       = 10.0
I       = 25.5
X       = 2.35
Y       = 0.15
Z       = 500.0

#Variable Metabolite Concentrations:
#Reaction 2:

B       = 12.0
C       = 5.0


#Model Parameters:
#Reaction 2:

Vf2     = 50.0
Keq2    = 2.0
KB2     = 20
KC2     = 15
```

Figure 3.1: An excerpt of a PySCeS MDL file. This particular example encodes a part of the example pathway shown in Figure 2.1.Lines starting with # are comments and ignored during the parsing of the file. The fixed and variable metabolites are defined along with their concentration values as shown under the headings "External Metabolites" and "External Metabolite Concentrations". The stoichiometry and rate equation for reaction 2 are shown under the heading "Reactions". Variables and Model parameters each have their own section as shown by their respective headings.

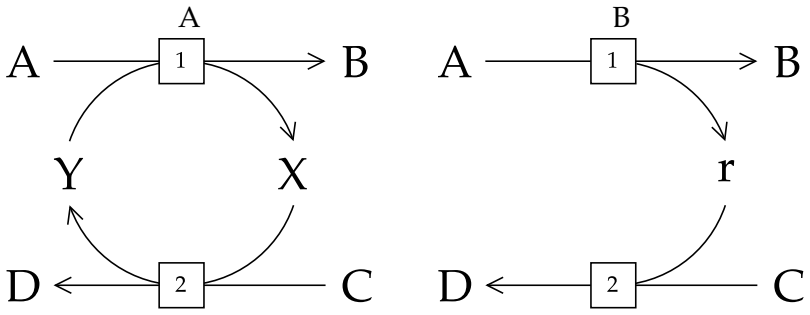

Figure 3.2: A two-membered moiety-conserved cycle. (A) Metabolites X and Y form a moiety-conserved cycle, with reactions 1 and 2 catalysing their interconversion. (B) In the modified system $r = [X]/[Y]$.

$$N = \begin{array}{c} \\ A \\ B \\ C \\ D \\ X \\ Y \end{array} \begin{array}{c} \begin{array}{cccccc} R_a & R_b & 1 & 2 & R_c & R_d \end{array} \\ \begin{pmatrix} 1 & 0 & -1 & 0 & 0 & 0 \\ 0 & -1 & 1 & 0 & 0 & 0 \\ 0 & 0 & 0 & -1 & 1 & 0 \\ 0 & 0 & 0 & 1 & 0 & -1 \\ 0 & 0 & 1 & -1 & 0 & 1 \\ 0 & 0 & -1 & 1 & 0 & 0 \end{pmatrix} \end{array}$$

It is clear that while A, B, C and D are free to take on any concentration, this is not true for X and Y in light of the constant K, and the stoichiometry of the system. However, X and Y may be represented as a ratio, as shown in Figure 3.2B, where the ratio may be perturbed freely without constraint. Here r represents the ratio of X to Y so that

$$r = \frac{[X]}{[Y]} \tag{3.3.2}$$

This modification to the system alters the stoichiometry of the system by removing the two metabolites, X and Y, that form part of the moiety-conserved cycle and replacing them with a single metabolite, r, as defined above. For the modified system in Figure 3.2B the stoichiometry simplifies to

$$
N = C \begin{array}{c} \\ A \\ B \\ C \\ D \\ r \end{array}
\begin{array}{c}
\begin{array}{cccccc} R_a & R_b & 1 & 2 & R_c & R_d \end{array} \\
\begin{pmatrix}
1 & 0 & -1 & 0 & 0 & 0 \\
0 & -1 & 1 & 0 & 0 & 0 \\
0 & 0 & 0 & -1 & 1 & 0 \\
0 & 0 & 0 & 1 & 0 & -1 \\
0 & 0 & 1 & -1 & 0 & 1
\end{pmatrix}
\end{array}
$$

As rate equations are included in a kinetic model, one of two changes must be made to the model to accommodate the modified stoichiometry. Either the rate equations of reactions 1 and 2 must either be adapted to be functions of r instead of X and Y or, more simply, the concentrations of X and Y need to be determined from the ratio r without modifying the rate equations. The concentrations of X and Y may be determined by combining Equations (3.3.1) and (3.3.2) so that

$$[X] = \frac{K.r}{r+1} \tag{3.3.3}$$

and

$$[Y] = \frac{K}{r+1} \tag{3.3.4}$$

In PySCeS the alteration to the model may be encoded by modifying the stoichiometries of the individual reactions, in this case reactions 1 and 2, and by utilising forcing functions to set the values of $[X]$ and $[Y]$ using Equations (3.3.3) and (3.3.4) without altering the rate equations.

Using the modified system, parameter scans (Section 3.4) of r may now be performed. This is demonstrated in Figure 3.3A which shows a rate characteristic plot for the modified system in Figure 3.2B while Figure 3.3B shows the concentrations of X and Y in relation to the change in r. A rate characteristic plot similar to Figure 3.3A was previously contructed by du Preez *et al.* [41] for the GSH/GSSG moiety conserved cycle using the ratio of GSH to GSSG.

The application of this method will be demonstrated in Chapter 5, where we will perform GSDA on a model with three two-membered moiety-conserved cycles.

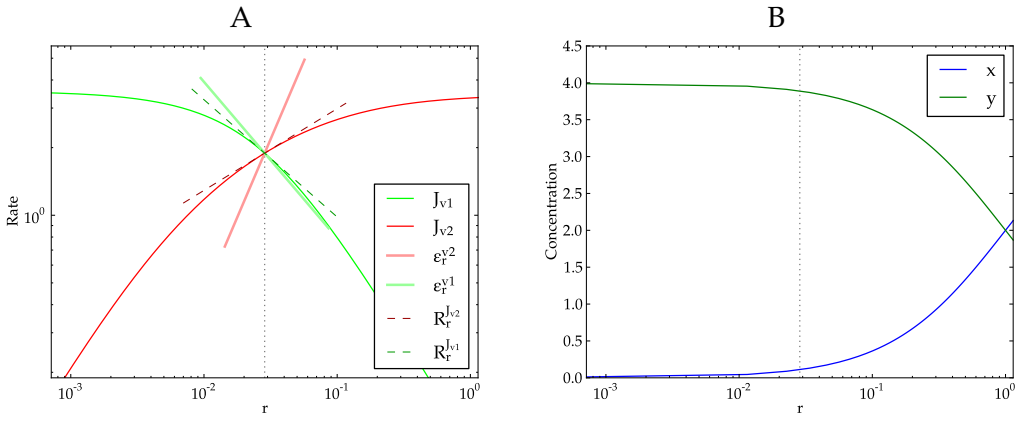

Figure 3.3: Both figures are drawn with results from a parameter scan of r over the same range. A) A rate characteristic plot where reactions 1 and 2 represent the supply and demand blocks, respectively, for the metabolite ratio r. B) The concentrations of X and Y are shown in relation to the value of r.

3.3.2 A special case: Interlinked moiety-conserved Cycles

A special case occurs when a moiety-conserved cycle exists within a linear pathway in such a way that it is coupled with two reactions that share a common intermediate so that two moiety-conserved cycles are interlinked. This is demonstrated in Figure 3.4 A, where both Y and X *and* Y and B form moiety-conserved cycles. As in the previous case the concentrations of these intermediates are not free to vary because the sum of the concentrations of the two different pairs must remain constant. Making the assumption that R_a produces A while R_c consumes C, the stoichiometry of this system is as follows

$$N = \begin{array}{c} \\ A \\ B \\ C \\ X \\ Y \end{array} \begin{array}{c} \begin{array}{cccc} R_a & 1 & 2 & R_c \end{array} \\ \begin{pmatrix} 1 & -1 & 0 & 0 \\ 0 & 1 & -1 & 0 \\ 0 & 0 & 1 & -1 \\ 0 & 1 & -1 & 0 \\ 0 & -1 & 1 & 0 \end{pmatrix} \end{array}$$

To overcome this limitation the model can be altered so that the three metabolite concentrations can be modified in concert while keeping the sum of their concentrations constant when performing a parameter scan. Assume that $B > X$, $[X]+[Y] = K_1$ and $[B] - [X] = K_2$. We can define a new variable L, as shown in Figure 3.4 B. The value of L is equal to $[X]$ so that the values of $[X]$, $[Y]$ and $[B]$ may be determined

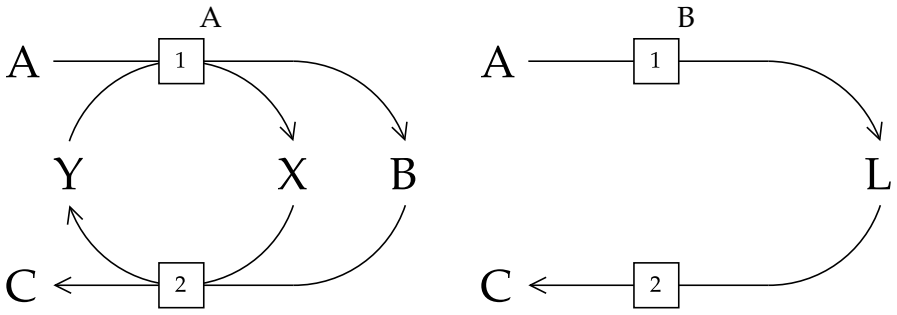

Figure 3.4: Two interlinked two-membered moiety-conserved cycles. (A) Metabolites X and Y, as well as Y and B form moiety-conserved cycles, with reactions 1 and 2 catalysing their interconversion. (B) In the modified system $L = [X]$.

as follows

$$[X] = L \tag{3.3.5}$$

$$[Y] = K_1 - L \tag{3.3.6}$$

$$[B] = L + K_2 \tag{3.3.7}$$

This modification changes the stoichiometry of the system to

$$N = \begin{array}{c} \\ A \\ L \\ C \end{array} \begin{array}{c} \begin{array}{cccc} R_a & 1 & 2 & R_c \end{array} \\ \begin{pmatrix} 1 & -1 & 0 & 0 \\ 0 & 1 & -1 & 0 \\ 0 & 0 & 1 & -1 \end{pmatrix} \end{array},$$

while, as with two-membered moiety-conserved cycles, leaving the rate equations unmodified and introducing forcing functions for Equations (3.3.5), (3.3.6) and (3.3.7) into the model to determine the values of X, Y and B from the value of L.

With these modifications the value of L may be perturbed in the range $0 < L < K_1$ during a parameter scan to produce results as shown in the example, Figure 3.5.

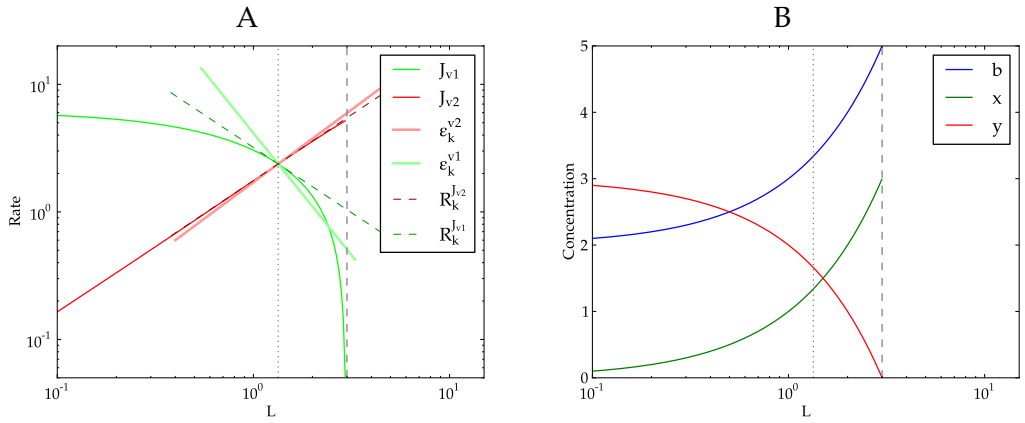

Figure 3.5: Both figures are drawn with results from a parameter scan of L over the range $0 < L < K_1$. A) A rate characteristic plot where reactions 1 and 2 represent the supply and demand blocks, respectively, for the linking metabolite L. B) The concentrations of $[X]$, $[Y]$ and $[B]$ are shown in relation to the value of L.

3.4 RateChar

It was previously mentioned that PySCeS is an open source tool. This means that anyone is free to view the source code of PySCeS and to change it to their needs. It also means that anyone is free to contribute to the project by adding new features and modules. The functionality to perform GSDA on metabolic models was implemented by Rohwer and Hofmeyr [7] as the RateChar module for PySCeS.

The procedure followed by RateChar when performing GSDA is as follows: The model of the metabolic pathway to be analysed is loaded by RateChar and the concentrations of the variable metabolites are fixed (or clamped), in turn. If ratios of concentrations are present, as with conserved moieties, the ratios are treated in exactly the same way as variable metabolite concentrations as previously discussed. The concentrations of the clamped metabolites are then varied over a predetermined concentration range in a parameter scan. These parameter scans produce flux data for the supply and demand blocks of the clamped metabolites. Additionally, MCA is performed, producing elasticity coefficients, response coefficients and partial response coefficients. These data are then combined to produce rate characteristic plots as described in Figures 2.7 and 2.9. This whole process is carried out automatically by RateChar.

While the version of RateChar originally developed by Rohwer and Hofmeyr [7] produced adequate results when performing GSDA on small models, larger models produced very cluttered rate characteristic plots. These rate characteristic plots

used only one colour each for supply and demand block rates, which led to unclear results when pathway models had more than one supply or demand block for any variable metabolite. There was also no way to customise rate characteristic plots to overcome this limitation, to display only relevant results or to produce higher quality plots. Additionally, in cases where the steady-state solver could not converge to a solution, invalid steady-states were produced. When these invalid steady-states were encountered during parameter scans, they were included in the data used to draw the rate characteristic plots and there was no way to discard or differentiate these erroneous results.

These limitations in RateChar prompted us to improve and extend it by adding error handling and developing an interactive plotting interface, in the form of the RCFigure class, as discussed below.

3.4.1 RateChar module overview

The RateChar module was integrated into PySCeS via the PyscesLink module. The module has three classes, RateChar, RateCharData and RCFigure.

The RateChar class instantiates an object that loads a PySCeS compatible kinetic model. This class can be regarded as the main class of the RateChar module. It contains functions for performing the parameter scans for the variable metabolites in the pathway model and it calls the RateCharData class as a container for results. A separate RateCharData instance is called to store the results for each parameter scan. This class can then instantiate a RCFigure object which is used to plot the rate characteristics for the results stored in the RateCharData object.

3.4.2 The RCFigure class

This RCFigure class contains various functions to draw rate characteristics. It makes use of the functionality provided by the matplotlib library [42], which is a very powerful figure drawing library for Python. This class was developed to address the problem of dissecting combined rate characteristic plots of metabolites that link multiple supply or demand blocks as well as to enable researchers to interactively customise these plots. The features of the newly developed RCFigure class are summarised below. These features were not present in the previous version of RateChar.

Coloured rate characteristic plots The rate of each supply and demand block is assigned a colour from a selection of 11 hues (Figure A.1). Lines representing

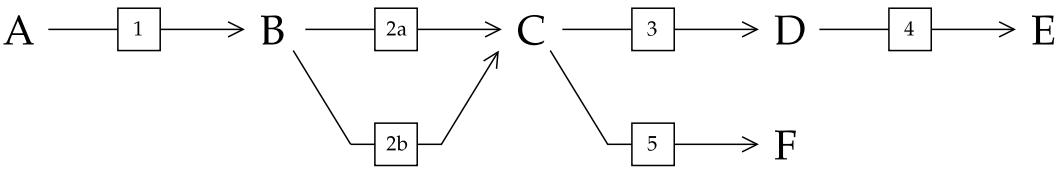

Figure 3.6: A pathway with two isoenzymes with differing kinetics, 2*a* and 2*b*, converting metabolite *B* to metabolite *C* and two separate reactions, 3 and 5, consuming metabolite *C* to produce metabolites *D* and *F*, respectively.

elasticity coefficients and response coefficients have the same hues, but lower saturation and value parameters respectively, according to the HSV computer graphics colour model [43].

Interactive rate characteristic plots This new feature allows the user to alter the composition of a rate characteristic plot while it is displayed on screen. Specifically, the rate curves of reactions block and their associated elasticity, response and partial response coefficients may be enabled or disabled interactively as the user sees fit.

Convenience functions In addition to having full control over the appearance of rate characteristic plots, a set of predefined functions allows the user to display basic rate characteristics, such as those shown in Figures 2.7 and Figures 2.9, without having to use any of the interactive features. If specified, rate characteristics can be generated and saved without any further user input.

Additional options The user has the option to define the dimensions of a rate characteristic plot, the output format of a rate characteristic plot and to define the location of the legend before generating a rate characteristic.

Integration with standard matplotlib While the previous version of RateChar used the matplotlib library to generate rate characteristic plot, this version gives the user the ability to use standard matplotlib functions on the generated rate characteristic plots, as they provide instantiated matplotlib figure objects to which the user has access.

In addition to these features, error handling was also implemented. Invalid steady-states produced by during parameter scans are now determined after the scan discarded automatically.

A detailed description of all the functions of the RCFigure class is given in Appendix A and the source code can be found as part of the RateChar module at

http://pysces.sourceforge.net/download.html. Examples of the rate characteristic plots generated by RCFigure and those generated by the older version of RateChar are given in Figures A.2 and A.3 respectively.

3.4.3 RateChar usage example

In the following text, we shall demonstrate the interactive plotting feature of RateChar. This demonstration was performed on a computer with a Linux based operating system in an IPython session, but will also work under Windows or with the standard interactive Python session.

Figure 3.6 shows the pathway on which we will perform our analysis. To show the capability of the RCFigure class, a rate characteristic plot will be drawn for the supply and demand blocks linked by *C*.

We start by importing PySCeS into our IPython session:

```
In [1]: import pysces

**********************************************************************
* Welcome to PySCeS (0.8.0rc1) - Python Simulator for Cellular Systems*
*                http://pysces.sourceforge.net                       *
* Copyright(C) B.G. Olivier, J.M. Rohwer, J.-H.S. Hofmeyr, 2004-2011  *
* Triple-J Group for Molecular Cell Physiology                       *
* Stellenbosch University, South Africa                              *
* PySCeS is distributed under the PySCeS (BSD style) licence, see     *
* LICENCE.txt (supplied with this release) for details               *
**********************************************************************
```

The model file "rateCharExample.psc" can now be loaded via the PyscesLink module. We create an object "rc" of the RateChar class:

```
In [2]: rc = pysces.PyscesLink.RateChar('rateCharExample')

**********************************************************************
*           Welcome to the RateChar add-on module for PySCeS         *
* Does generic supply-demand parameter scans around internal         *
* metabolites species of a model and optionally plots the results.   *
*                                                                    *
* Copyright(C) J.M Rohwer, C.D. Christensen, J.-H.S. Hofmeyr, 2007-2011*
* Triple-J Group for Molecular Cell Physiology                       *
* Stellenbosch University, South Africa                              *
* RateChar is distributed under the PySCeS (BSD style) licence, see  *
* LICENCE.txt (supplied with this release) for details               *
**********************************************************************
```

A parameter scan of intermediate metabolite C may now be performed using the doRateChar() function.

```
In [3]: rc.doRateChar('C')

Fixed species is Substrate for:  ['J_R3', 'J_R5']
Fixed species is Product for:    ['J_R2a', 'J_R2b']
Scanner user output:  ['C', 'J_R2a', 'J_R2b', 'J_R3', 'J_R5']
MaxMode 0
0 min 0 sec
SCANNER: Tsteps 256

SCANNER: 256 states analysed
```

The results generated by the parameter scan is saved in a RateCharData object with a name corresponding that of the scanned metabolite. A RCFigure object can be created with these results. In this case we shall name the object "fig".

```
In [4]: fig = rc.C.figure()
```

Using the plotElasRC() function of the RCFigure class, a rate characteristic plot may be drawn. The result is shown in Figure 3.7. It should be noted that this plot, and all those shown in this example, is representative of output by the RCFigure class under default settings, meaning that it is not of publication quality, but rather for use as an analysis tool. These figures may be manipulated further using standard matplotlib functions to the end of creating figures more suitable for publication.

```
In [5]: fig.plotElasRC()
```

The rate characteristic plot in Figure 3.7 indicates the fluxes of the various supply and demand reactions linked by metabolite C as well as the total supply and demand fluxes. Response and elasticity coefficients are also indicated. This specific plot demonstrates that when multiple supply or demand reactions are linked by a single metabolite, the resulting rate characteristics may become cluttered and difficult to pick apart. We may overcome this by using the plotElasRCIndiv() function to plot each reaction block linked to C individually as shown in below, with the resulting rate characteristics in Figure 3.8.

```
In [6]: fig.plotElasRCIndiv()
```

The functions set_visible() and set_type_visible() can be used on the rate characteristics to display whatever curves or coefficients a researcher desires. The code

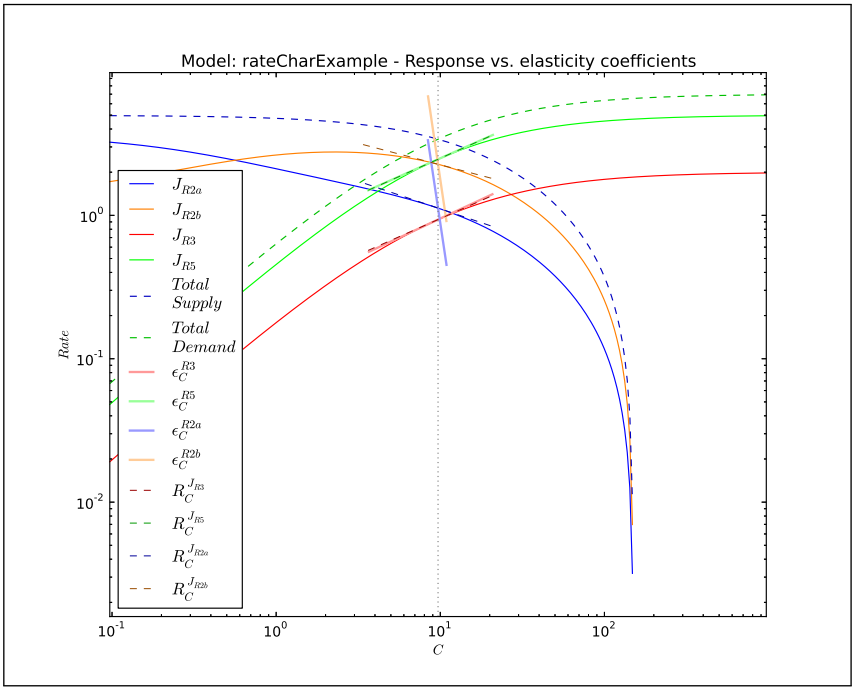

Figure 3.7: A combined rate characteristic plot of the reaction blocks linked by metabolite C as generated by RCFigure with the default settings.

below demonstrates clearing figure using the clear() function, plotting the flux of reaction 2a along with its elasticity towards C using set_visible() and plotting all demand reactions using set_type_visible() and finally updating the figure using show(). The result is shown in Figure 3.9.

```
In [7]: fig.clear()

In [8]: fig.set_visible('J_R2a',f=True)

In [9]: fig.set_visible('J_R2a',f=True,e=True)

In [10]: fig.set_type_visible('demand_flux', visibility =  True)

In [11]: fig.show()
```

In the current chapter we discussed a method to perform GSDA on models with conserved moieties and the use and development of RCFigure. We shall demonstrate their practical application in the following chapters. In Chapter 4, the ability to customise rate characteristic plots was vital, as the model analysed had multiple supply and demand blocks for certain metabolites as a result of numerous isoenzymes and branch points.

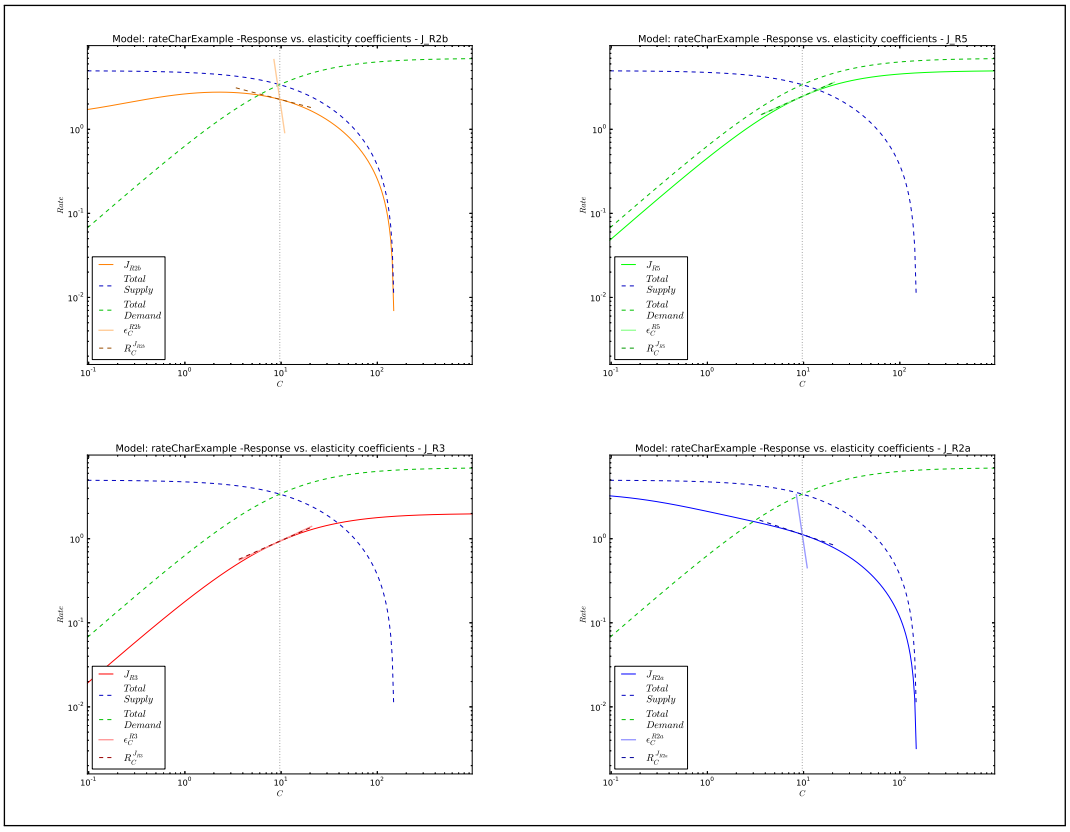

Figure 3.8: Individual rate characteristic plots for each reaction block linked by metabolite *C* as generated by the RCFigure class with the default settings

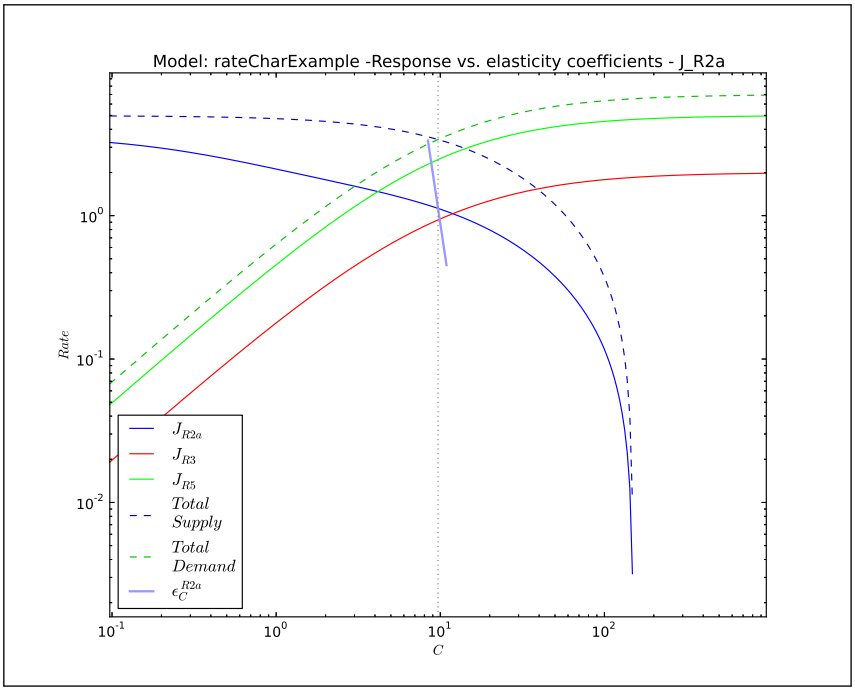

Figure 3.9: A combined rate characteristic plot of the supply flux through reaction 2*a* together with its elasticity towards *C*, as well as the demand fluxes for metabolite *C* as generated by RCFigure with the default settings.

Chapter 4

Case study 1: Unexpected routes of regulation

4.1 Introduction

In systems biology, kinetic models of metabolic pathways represent an invaluable resource for understanding the control, regulation and behaviour of these pathways [31; 36]. They also provide the potential to greatly reduce the amount of experimental work needed to study these aspects *in vivo* by shifting their study to *in silico* analysis. This is very useful when studying pathways with biotechnological applications (e.g. lactic acid fermentation or ethanol fermentation) as it allows for the components important for control of flux or concentration to be identified relatively easily. This information may then be used as a guide when genetically manipulating organisms to increase the yield of the pathways or quality of the product [44; 45].

The building of metabolic models itself entails a considerable amount of experimental work [46], as each individual enzyme of a pathway must be characterised in terms of its kinetics. This can provide quite challenging when characterising large or complex metabolic pathways. Models are therefore often limited in their scope, simplified or not completely accurate. Models may be simplified by practices such as the omission of feedback loops, the lumping of various reactions into a single reaction [10] step or by clamping the concentrations of certain variable metabolites [31].

A model that has both biotechnological significance and that is relatively complete in terms of characterised and modelled features was published by Curien *et al.* [31]

in 2009. This model of the aspartate-derived amino-acid pathway in *Arabidopsis thaliana* has various important biotechnological applications such as improving nutritional quality in plants [47; 48]. It is also important for plants in resistance against fungal disease [49]. The aspartate-derived amino-acid pathway includes various detailed features such as various branch points, isoenzymes and allosteric control mechanisms which potentially allow for novel routes of regulation. These features, together with its biotechnological applications make the model a prime candidate for studying metabolic regulation. This model has previously been used to show that allosteric interactions in such a branched system do not have the function of coupling supply and demand, but rather to maintain high independence between fluxes in competing pathways. Furthermore, isoforms were shown not to be functionally redundant as they contribute unequally to flux and its regulation [31].

While this model has already provided valuable information regarding the regulation of aspartate metabolism, the system is still not fully understood. In the present study we therefore set out to further characterise the regulation of the aspartate-derived amino-acid pathway, with specific focus on the routes of regulation, with the use of GSDA.

4.2 Methods

4.2.1 Model Reconstruction

The model of the aspartate-derived amino-acid synthesis pathway (Figure 4.1) was provided by Curien *et al.* [31] in two file formats; SBML and Berkeley Madonna. As there were slight inconsistencies between these files, a definitive model description was assembled in PySCeS MDL format (Section 3.2.1) from the two model files and the rate equations provided (Table 4.2). To test the validity and equivalence of this model to the original, all results provided by Curien *et al.* [31] were reproduced. The model file is provided in Appendix C.

4.2.2 Generalised supply-demand Analysis

Using the RateChar module for PySCeS, each variable metabolite in the pathway was parameterised and its concentration varied over a range with the doAllRateChar method. Suitable concentration ranges (Table 4.1) were chosen (1) to show characteristic features of each supply and demand block for the variable metabolite and (2) according to the validity of the steady-states produced. In addition to parameter scans, metabolic control analysis was performed for each clamped

Metabolite	Scan Range (μM)	Steady State Concentration (μM)
AspP	0.01–1.40	0.34
ASA	0.03–3.92	0.96
Lys	4.63–1040.71	69.38
Hser	0.21–1.22	0.94
PHser	9.95–58.86	45.27
Thr	20.16–4535.86	302.39
Ile	3.95–888.71	59.25

Table 4.1: The concentration ranges over which the parameterised variable metabolites were varied.

metabolite. The results were used to draw rate characteristic plots for each variable metabolite in the pathway using the functionality of the RCFigure class of RateChar. To investigate the effect of an increased lysine demand, lysine ketoglutarate reductase (LKR) was introduced at a concentration of 30 μM before performing GSDA. This concentration corresponds the upper level of LKR concentrations found *in vivo* and therefore represents a large increase in Lys demand [31].

4.3 Results

4.3.1 Differences in rate characteristic shapes

The rate characteristic shapes of J_{v_3} and J_{v_4} were very similar (Figure 4.3A) due to the similar kinetics of AK1 and AK2 (Table 4.2). A 1000-fold change in AspP concentration resulted in 10-fold decrease in the rate of J_{v_3} and J_{v_4}. The rate characteristic shapes of J_{v_1} and J_{v_2} were also similar (Figure 4.3A) due to the similar kinetics of aspartate kinase I and II (AKI and AKII) (Table 4.2). These rates were almost unaffected by aspartyl-phosphate (AspP) concentrations below $0.2\mu M$, but above this concentration their rates decreased over 1000-fold for a less than 10-fold change in AspP concentration. There was therefore a marked difference in the response to changes in AspP concentration between threonine (Thr) inhibited and lysine (Lys) inhibited AKs. In contrast to the fluxes through the AK-isoenzymes, the homoserine dehydrogenase (HSDH) isoenzymes and dihydrodipicolinate dehydrogenase (DHDPS) isoenzymes showed very little similarity in their rate characteristic shapes in response to changes in aspartate-semialdehyde (ASA) concentration (Figure 4.3B).

The majority of flux in the pathway goes through the branch towards Thr and isoleucine (Ile) (Figure 4.3 A,B,D,E,F) [31]. In this branch, the rate characteristic

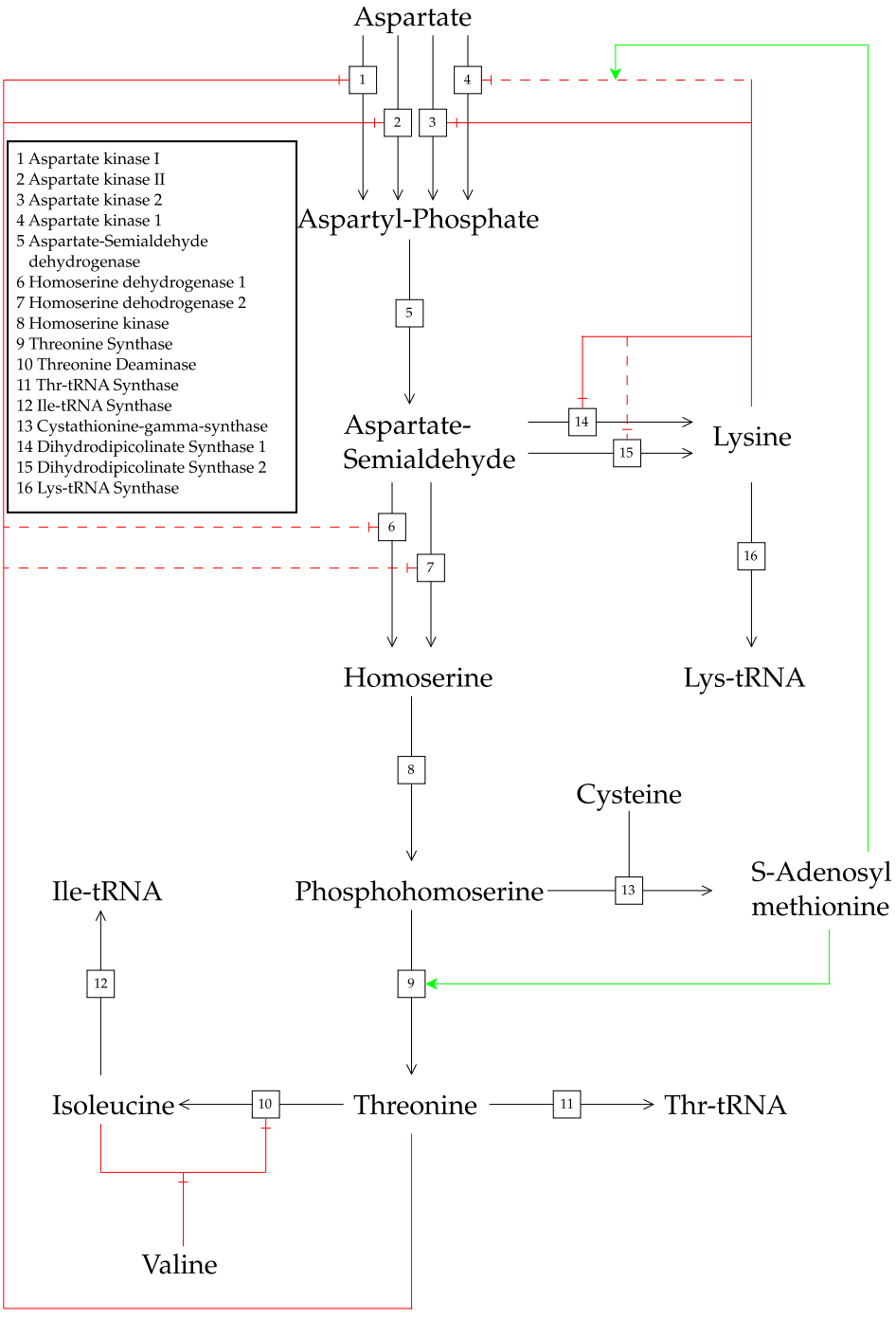

Figure 4.1: The aspartate-derived amino-acid pathway as defined by Curien *et al.* [31]. Reactions are numbered according to the key. Green lines ending in solid arrows indicate activation of a reaction or potentiation of an allosteric effect, while red lines ending with daggers indicate inhibition of reactions or damping of an allosteric effect. Strong allosteric effects are indicated with solid coloured lines, while weak effects are shown in dashed coloured lines. The stoichiometry of each reaction is 1 to 1. This figure was redrawn from the original figure in [31].

Reaction No.	Rate Equation
1	$v_{AKI} = [\text{AKI}] \cdot \frac{0.36 - 0.10[\text{AspP}]}{(1 + [\text{Thr}]/124)^2}$
2	$v_{AKII} = [\text{AKII}] \cdot \frac{1.35 - 0.38[\text{AspP}]}{(1 + [\text{Thr}]/109)^2}$
3	$v_{AK2} = [\text{AK2}] \cdot \frac{3.15 - 0.88[\text{AspP}]}{1 + ([\text{Lys}]\ /22.0)^{1.1}}$
4	$v_{AK1} = [\text{AK1}] \cdot \frac{5.65 - 1.57[\text{AspP}]}{1 + \left[[\text{Lys}]\ / \left(\frac{550}{1+[\text{AdoMet}]/3.5}\right)\right]^2}$
5	$v_{ASADH} = [\text{ASADH}] \cdot (0.9 \cdot [\text{AspP}] - 0.23 \cdot [\text{ASA}])$
6	$v_{HSDHI} = [\text{HSDHI}] \cdot [\text{ASA}] \cdot 0.84 \cdot \left(0.15 + \frac{0.85}{(1 + [\text{Thr}]/400}\right)$
7	$v_{HSDHII} = [\text{HSDHII}] \cdot [\text{ASA}] \cdot 0.64 \cdot \left(0.25 + \frac{0.75}{(1 + [\text{Thr}]/8500}\right)$
8	$v_{HSK} = \frac{[\text{HSK}] \cdot [\text{Hser}] \cdot 2.8}{14 + [\text{Hser}]}$
9	$v_{TS} = [\text{TS}] \cdot \frac{\frac{0.42+3.5\cdot[\text{AdoMet}]^2/73}{1+[\text{AdoMet}]^2/73}[\text{PHser}]}{\left[\frac{250\frac{1+[\text{AdoMet}]/0.5}{1+[\text{AdoMet}]/1.1}}{1+\frac{[\text{AdoMet}]^2}{140}}\right]\left(1 + \frac{[\text{P}_\text{i}]}{1000}\right) + [\text{PHser}]}$
10	$v_{TD} = \frac{[\text{TD}] \cdot [\text{Thr}] \cdot 0.0124}{1 + \left[[\text{Ile}] / \frac{30+73\cdot[\text{Val}]}{615+[\text{Val}]}\right]^3}$
11	$v_{Thr-tRNAS} = \frac{[\text{Thr}] \cdot 0.43}{100 + [\text{Thr}]}$
12	$v_{Ile-tRNAS} = \frac{[\text{Ile}] \cdot 0.43}{20 + [\text{Ile}]}$
13	$v_{CGS} = \frac{[\text{CGS}] \cdot [\text{PHser}] \cdot \frac{30}{1+460/[\text{ Cys}]}}{\left(\frac{2500}{1+460/[\text{ Cys}]}\right) \cdot \left(1 + \frac{[\text{P}_\text{i}]}{2000}\right) + [\text{PHser}]}$
14	$v_{DHDPS1} = \frac{[\text{DHDPS1}] \cdot [\text{ASA}]}{1 + \left(\frac{[\text{ Lys}]}{10}\right)^2}$
15	$v_{DHDPS2} = \frac{[\text{DHDPS2}] \cdot [\text{ASA}]}{1 + \left(\frac{[\text{ Lys}]}{33}\right)^2}$
16	$v_{Lys-tRNAS} = \frac{[\text{Lys}] \cdot 0.43}{25 + [\text{Lys}]}$

Table 4.2: The rate equations for each reaction in the pathway as shown in Figure 4.1. Rate equations were provided in supplementary data S1.1–S1.13 [31].

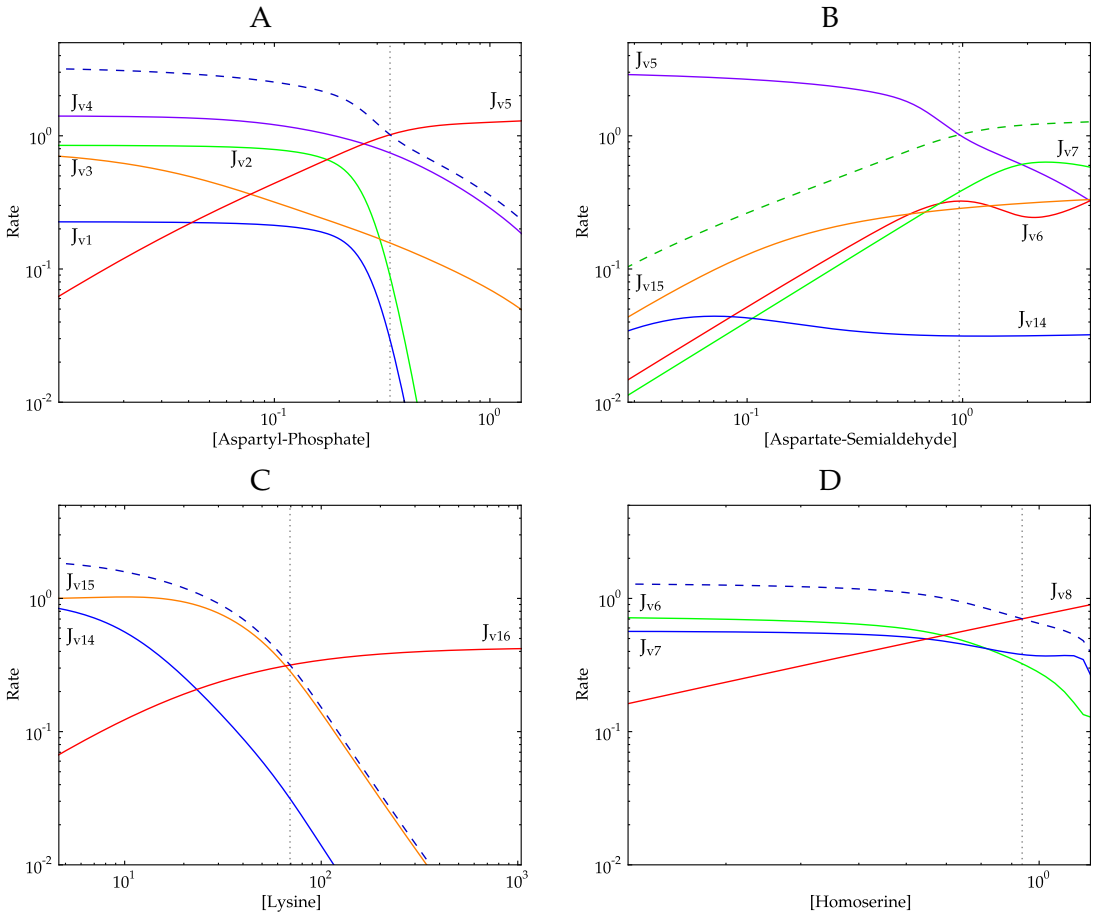

Figure 4.2: The combined rate characteristic plots for each variable metabolite in the pathway. The rate of each reaction linked to a specific metabolite is shown on a single rate characteristic plot. Unlabelled dashed curves represent either total supply (blue) or total demand (green). The steady-state is indicated by the grey dotted line. *continued on next page*.

shapes of the combined supply or demand blocks were similar for almost all variable metabolites. The shape of the curve of the demand block J_{v_8} in response to increasing homoserine (Hser) (Figure 4.3D) and the combined rate of the demand blocks J_{v_9} and $J_{v_{13}}$ in response to phosphohomoserine (PHser) (Figure 4.3E) were exceptions, as these demand blocks increased linearly in response to increased substrate concentrations. This was due to tested substrate concentration ranges being far from saturating for the product insensitive enzymes homoserine kinase (HSK), threonine synthase (TS) and cystathionine γ-synthase (CGS).

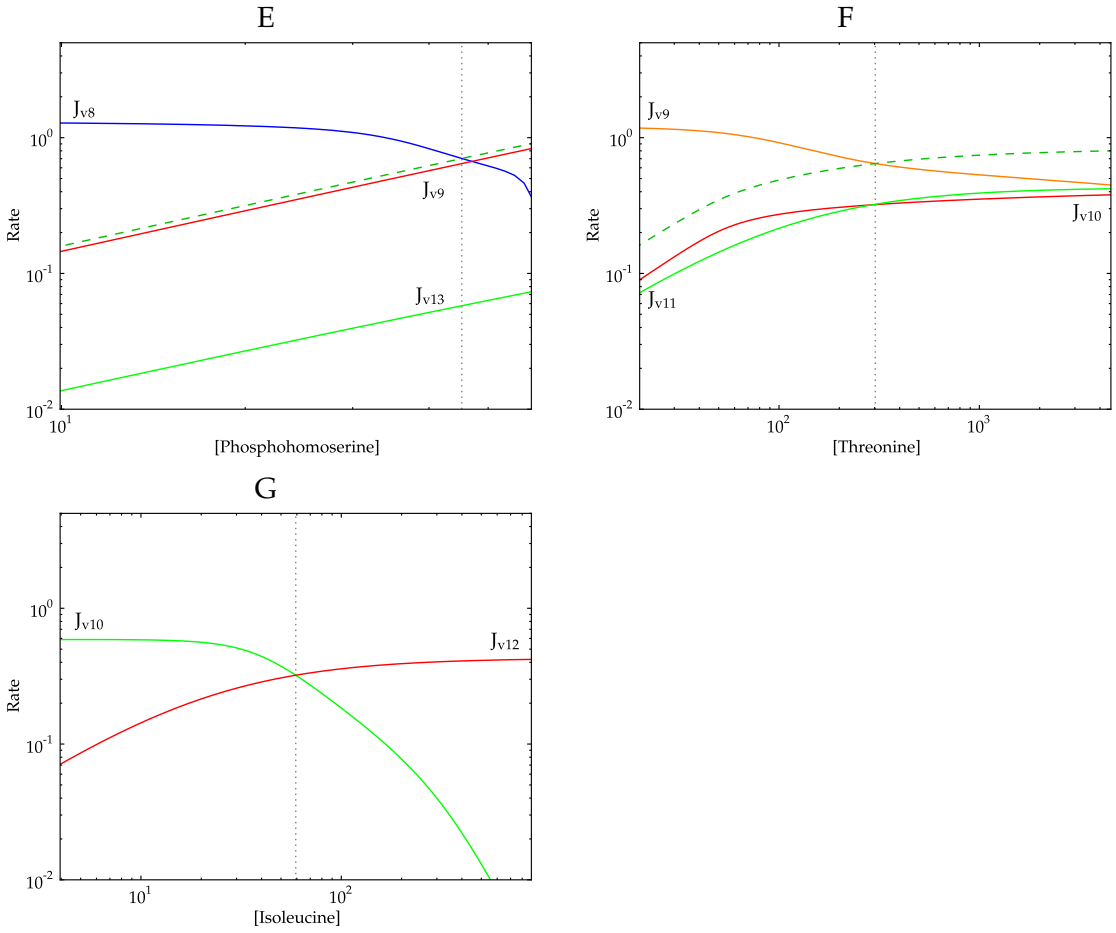

Figure 4.3: *continued from previous page.*

4.3.2 Comparison of elasticities and response coefficients

Each demand-block at the end points of the pathway consists of a single enzyme catalysed reaction with no communication between the supply and demand blocks. The elasticities of CGS, Thr-tRNA synthase, Lys-tRNA synthase and Ile-tRNA synthase towards their substrates were therefore equal to their respective demand flux-response coefficients. This is the trivial case as defined by Rohwer and Hofmeyr [7].

Similarly, the insensitivity of HSK and TS towards all variable metabolites, save for their substrates, means that the responses of their respective demand blocks must be equal to the activity responses of the enzymes. These enzymes therefore have full control over the fluxes of the demand blocks in which they occur.

The flux-response coefficients of the demand-block J_{v_7} towards ASA (Figure 4.4A),

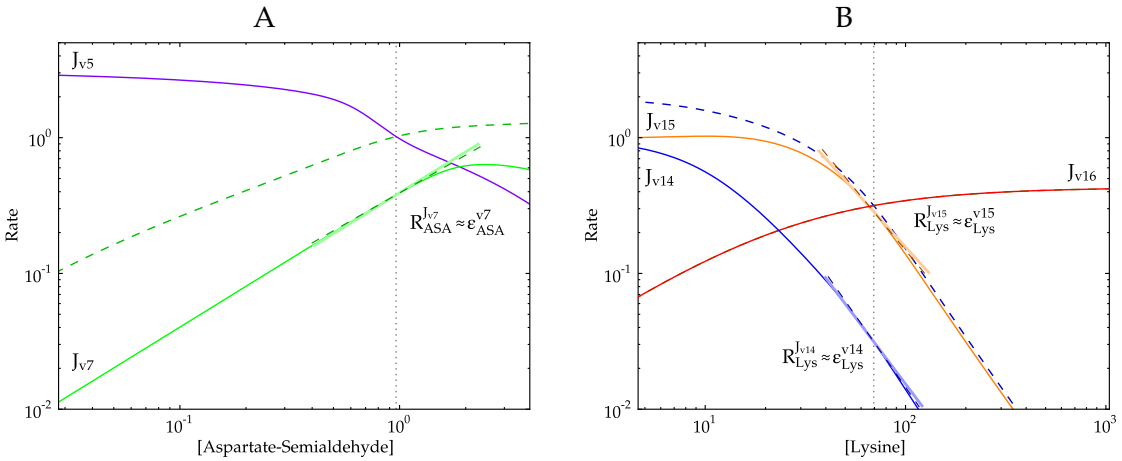

Figure 4.4: The rate characteristic plots for metabolites for which the elasticity equals the flux response. Response coefficients are shown as dashed dark coloured lines, while elasticity coefficients are indicated by solid light coloured lines. Unlabelled dashed curves represent either total supply (blue) or total demand (green). The steady-state is indicated by the grey dotted line.

and the supply-blocks $J_{v_{14}}$ and $J_{v_{15}}$ towards Lys (Figure 4.4B), were approximately equal to the elasticity coefficients of the enzymes HSDHII, DHDPS1 and DHDPS2 the towards the tested metabolites. The existence of various routes of interaction of the metabolites ASA and Lys with these demand and supply blocks results in response coefficients that consist of a number of terms, one for each distinct route. This means that despite the flux and activity responses being equal, the enzymes do not necessarily have full control over their own fluxes. In the case of J_{v_7}, HSDHII does have full control over its own flux, but this was not the case for $J_{v_{14}}$ and $J_{v_{15}}$. These routes of interaction will be addressed in Section 4.3.4.

4.3.3 Functional differentiation and homoeostasis

The branch point at ASA is an important feature of the aspartate pathway. The two branches have to remain independent in the face of changes in flux of the other. In addition, each branch consists of two enzymes making unequal contributions towards the total flux.

The combined demand block of $J_{v_{6+7}}$ had more control over flux than the supply J_{v_5}, which determined the degree of homoeostasis (Figure 4.5A), but the system was not completely functionally differentiated. The same was also true for the demand block of $J_{v_{14+15}}$ (Figure 4.5A), which had slightly more control over its flux than $J_{v_{6+7}}$ had over its own flux, due to the lower response of $J_{v_{14+15}}$ to ASA. For both branches, there was a low degree of homoeostasis of ASA.

When the fluxes J_{v_6}, J_{v_7}, $J_{v_{14}}$ and $J_{v_{15}}$ were taken individually, there was more functional differentiation between supply (J_{v_5}) and the demands of the lowest contributing flux in each branch (J_{v_6} and $J_{v_{14}}$) than for the fluxes that contributed the most to the total flux in each branch (J_{v_7} and $J_{v_{15}}$). This was because both J_{v_6} and $J_{v_{14}}$ had near zero responses to ASA (Figures 4.5C and E).

In spite of the apparent low degree of homoeostasis of ASA, it was found that increasing the demand for Lys had minimal effects on the concentration of ASA and the flux towards Thr [31]. When demand for Lys was increased the combined flux $J_{v_{14+15}}$ increased, while $J_{v_{6+7}}$ remained constant (Figure 4.5B). The individual fluxes toward Lys, $J_{v_{14}}$ and $J_{v_{15}}$ increased by 126% and 87% respectively (Figure 4.5F). We see that in spite of the increased demand for ASA, its concentration remained the same as under low Lys demand. This was due to an increase in J_{v_5} that matched that of the increased demand. This effect was due to the lower concentration of Lys at high Lys demand (Figure 4.6B), which acts as an inhibitor for AK1 and AK2 in the supply block, thereby relieving inhibition.

Together with changes in the fluxes $J_{v_{14+15}}$ and J_{v_5} due to increased Lys demand, their response coefficients towards ASA also changed. The response $R_{ASA}^{J_{v_{14+15}}}$ increased while $R_{ASA}^{J_{v_5}}$ decreased in magnitude (Figure 4.5B), leading to a decrease in the functional differentiated between these demand and supply blocks. While $J_{v_{6+7}}$ and its response towards ASA remained unchanged, the decrease in magnitude of $R_{ASA}^{J_{v_5}}$ lead to a lower degree of functional differentiated between these blocks, with $J_{v_{6+7}}$ and J_{v_5} having almost equal control over flux (Figure 4.5B). In the case of the differentiation between J_{v7} and J_{v_5}, supply had more control over flux than demand (Figure 4.5D). Apparent ASA homoeostasis also decreased for each demand block (Figure 4.5B, D and F).

The individual Lys supply fluxes, $J_{v_{14}}$ and $J_{v_{15}}$, and demand $J_{v_{16}}$ were significantly functionally differentiated, with demand having the most control over flux and supply determining the degree of homoeostasis in both cases (Figure 4.6A). The degree of differentiation between $J_{v_{14}}$ and $J_{v_{16}}$ was larger than between $J_{v_{15}}$ and $J_{v_{16}}$ due to the larger value of $R_{Lys}^{J_{v_{14}}}$ (Figure 4.6A). When the fluxes $J_{v_{14}}$ and $J_{v_{15}}$ are taken as a combined flux $J_{v_{14+15}}$, the degree of functional differentiation between supply and demand was similar to that of the differentiation between $J_{v_{15}}$ and $J_{v_{16}}$, as $J_{v_{15}}$ contributes the most towards the total supply flux (Figure 4.6A).

Lys demand was increased by introducing a second demand reaction catalysed by LKR, rather than increasing the rate of $J_{v_{16}}$. At the steady state $J_{v_{LKR}}$ was higher than

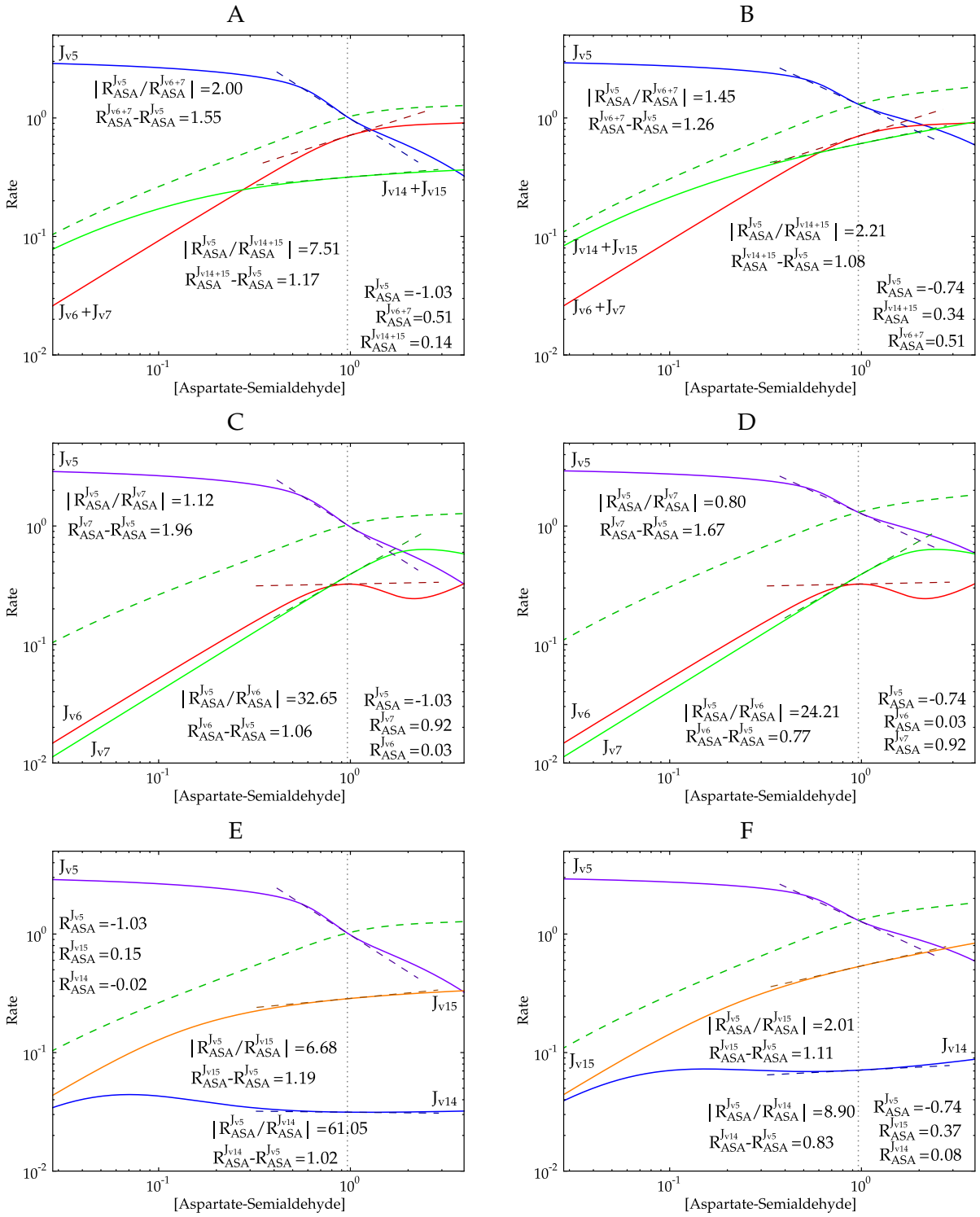

Figure 4.5: The rate characteristic plots for ASA indicating functional differentiation of the supply and demand blocks. The fluxes towards Lys ($J_{v_{14}}$ and $J_{v_{15}}$) and the fluxes towards Thr (J_{v_6} and J_{v_7}) are combined into two individual demand fluxes in A and B, indicating their different responses to ASA. Rate characteristics in the left column are under normal conditions, while those on the right are under increased demand for Lys (see text). Response coefficients are shown as dark coloured dashed lines. The steady-state is indicated by the grey dotted line.

$J_{v_{16}}$ and unsaturated. The degree of functional differentiation between the combined supply $J_{v_{14+15}}$ and demand $J_{v_{16+LKR}}$ was lower than under low Lys demand due to an decrease in magnitude of both $R_{Lys}^{J_{v_{14}}}$ and $R_{Lys}^{J_{v_{15}}}$ and a larger value of $R_{Lys}^{J_{v_{16+LKR}}}$ under high Lys demand than $R_{Lys}^{J_{v_{16}}}$ under low Lys demand (Figure 4.6B). The degree of Lys homoeostasis did, however, increase due to the increase in difference between supply and demand responses (Figure 4.6B).

Ile is at the end point of the Thr branch. Supply and demand of Ile were functionally differentiated, with $J_{v_{12}}$ having the most control over flux and $J_{v_{10}}$ determining the degree of homoeostasis of Ile (Figure 4.7B). Supply (J_{v_9}) and total demand $J_{v_{10+11}}$) around Thr was only slightly functionally differentiated with demand controlling flux (Figure 4.7A). When demand fluxes were taken individually, J_{v_9} and $J_{v_{10}}$ were more functionally differentiated than the total demand and J_{v_9}, and the supply J_{v_9} had slightly more control over flux than $J_{v_{11}}$ (Figure 4.7A). As demonstrated by Curien *et al.* [31], Thr concentration was the least homoeostatically maintained metabolite in the pathway with a value of only 0.41 for $R_{Thr}^{J_{v_{10+11}}} - R_{Thr}^{J_{v_9}}$ (Figure 4.7A). This was due to the low responses of supply and both demand branches towards Thr.

Supply and demand blocks for other metabolites in the pathway were only slightly functionally differentiated with $|R_x^{J_{Supply}}/R_x^{J_{Demand}}|$ having values close to 1.36 for both Hser an PHser and 2.71 for AspP.

4.3.4 Routes of interaction

Besides directly interacting with a specific reaction block as a product or substrate of that block, allosteric effects allow metabolites to interact via various routes with a specific block. In this pathway, the various allosteric effects, such as inhibition by Lys and Thr of the aspartate kinases, and the various enzyme isoforms lead to a variety of routes whereby metabolites may interact with their supply and demand blocks.

4.3.4.1 Interaction with Lysine

Lys is one of two variable metabolites in the pathway that allosterically inhibit enzymes in the pathway (AK1, AK2, DHDPS1 and DHDPS2). Figure 4.8 shows the partial response coefficients of (A) $J_{v_{14}}$ and (B) $J_{v_{15}}$ towards Lys. DHDPS1 and DHDPS2 are allosterically inhibited by Lys and represent the first enzymes in a seven step pathway which converts ASA to Lys. The latter six enzymes were omitted in this model because of their irreversibility and product insensitivity[31].

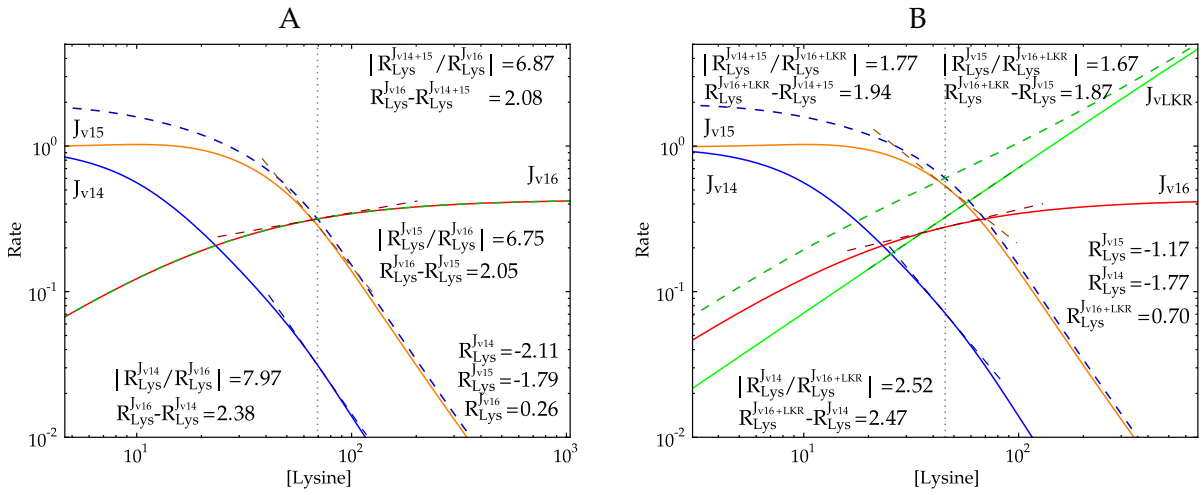

Figure 4.6: The rate characteristic plots for Lys indicating functional differentiation of the supply and demand blocks. In A the rate characteristics were generated under normal conditions, while B represents an increased demand for Lys by the introduction of a second demand reaction catalysed by LKR (see text). Response coefficients are shown as dark coloured dashed lines. The steady-state is indicated by the grey dotted line.

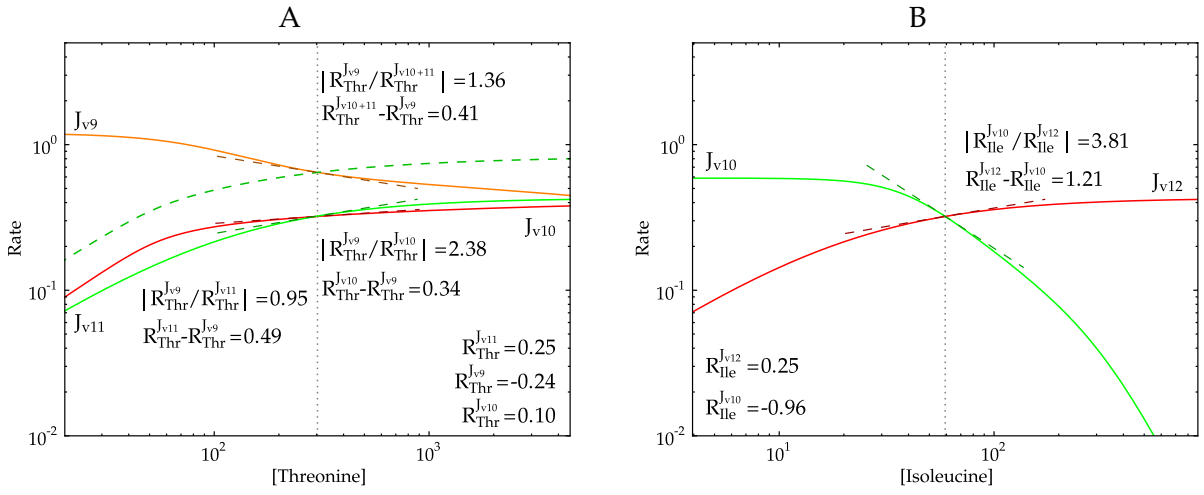

Figure 4.7: The rate characteristic plots for (A) Thr and (B) Ile indicating functional differentiation of the supply and demand blocks. Response coefficients are shown as light coloured lines. The steady-state is indicated by the grey dotted line.

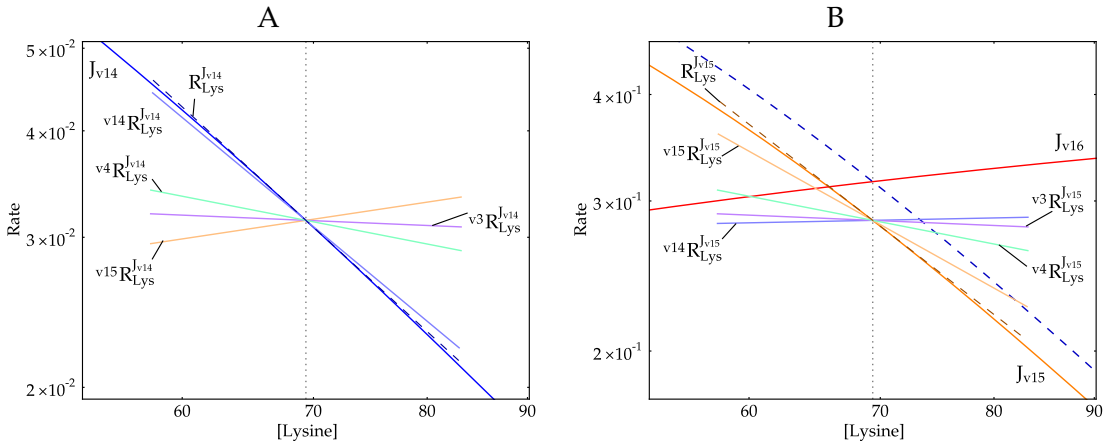

Figure 4.8: The rate characteristic plots for (A) $J_{v_{14}}$ and (B) $J_{v_{15}}$ with their partial responses towards Lys indicating the relative contribution of each route of interaction with each respective supply block. The importance of each route is indicated with a partial response coefficient as a light coloured solid line; these add up to the total response coefficient that is shown as dark dashed line. The steady-state is indicated by the grey dotted line.

x	${}^{x}R_{Lys}^{J_{v_{14}}}$	ε_{Lys}^{x}	$C_{x}^{J_{v_{14}}}$
v_{14}	-1.91	-1.96	0.98
v_{15}	0.35	-1.63	-0.21
v_3	-0.10	-0.86	0.11
v_4	-0.45	-0.84	0.53
$R_{Lys}^{J_{v_{14}}}$	-2.11		

Table 4.3: The individual control and elasticity coefficients that make up the partial response coefficients of $R_{Lys}^{J_{v_{14}}}$.

x	${}^{x}R_{Lys}^{J_{v_{14}}}$	ε_{Lys}^{x}	$C_{x}^{J_{v_{14}}}$
v_{14}	-1.82	-1.91	0.96
v_{15}	0.42	-1.31	-0.32
v_3	-0.10	-0.76	0.13
v_4	-0.27	-0.47	0.57
$R_{Lys}^{J_{v_{14}}}$	-1.76		

Table 4.4: The individual control and elasticity coefficients that make up the partial response coefficients of $R_{Lys}^{J_{v_{14}}}$ under increased Lys demand.

The routes through which Lys makes the most significant contribution towards the complete flux-response of $J_{v_{14}}$ and $J_{v_{15}}$, is the interaction of Lys with DHDPS1 and DHDPS2 respectively (Figure 4.8A and B). The existence of an isoenzyme and the branch point at ASA allows some reactions to have negative control over $J_{v_{14}}$ and $J_{v_{15}}$. This means that even though $C_{v_{14}}^{J_{v_{14}}} = 0.98$ and $\sum_{i=1}^{n} C_{i}^{J_{v_{14}}} = 1$, DHDPS1 does not have nearly full control over $J_{v_{14}}$.

The inhibition of AK1 by Lys made a significant negative contribution towards $R_{Lys}^{J_{v_{14}}}$ and $R_{Lys}^{J_{v_{15}}}$ (Figure 4.8A and B). While the activity response of AK1 and AK2 towards

x	${}^{x}R^{J_{v_{15}}}_{Lys}$	ε^{x}_{Lys}	$C^{J_{v_{15}}}_{x}$
v_{14}	0.05	-1.96	-0.02
v_{15}	-1.29	-1.63	0.79
v_3	-0.10	-0.86	0.11
v_4	-0.45	-0.84	0.53
$R^{J_{v_{15}}}_{Lys}$	-1.79		

Table 4.5: The individual control and elasticity coefficients that make up the partial response coefficients of $R^{J_{v_{15}}}_{Lys}$.

x	${}^{x}R^{J_{v_{15}}}_{Lys}$	ε^{x}_{Lys}	$C^{J_{v_{15}}}_{x}$
v_{14}	0.08	-1.91	-0.04
v_{15}	-0.89	-1.31	0.68
v_3	-0.10	-0.76	0.13
v_4	-0.26	-0.47	0.57
$R^{J_{v_{15}}}_{Lys}$	-1.17		

Table 4.6: The individual control and elasticity coefficients that make up the partial response coefficients of $R^{J_{v_{15}}}_{Lys}$ under increased Lys demand.

Lys were similar, AK2 had much less control over $J_{v_{14}}$ and $J_{v_{15}}$ (Tables 4.3 and 4.5). The difference in control over $J_{v_{14}}$ and $J_{v_{15}}$ between AK1 and AK2 was determined by their different contributions towards the total flux though the supply block with

$$\frac{J_{v_3}}{J_{v_4}} = \frac{C^{J_x}_{v_3}}{C^{J_x}_{v_4}} = 0.21, \quad x = v_{14} \text{ or } v_{15}$$

The interaction of Lys with the supply block of $J_{v_{14}}$ via DHDPS2 contributed positively towards $R^{J_{v_{14}}}_{Lys}$ (Figure 4.8A). This is due to the inhibition of DHDPS2 by Lys and because both compete for the same substrate. Inhibition of one, eases the competition for the other. The same, however was not true for the interaction of Lys with the supply block of $J_{v_{15}}$ via DHDPS1 which had a negligible contribution towards $R^{J_{v_{15}}}_{Lys}$ due to its low control over $J_{v_{15}}$ (Figure 4.8B and Table 4.5). The degree of control that these steps have over the other was determined by their own contribution to the total flux towards Lys and by the elasticity of their counterpart towards ASA and with

$$\frac{J_{v_{14}} \cdot \varepsilon^{v_{15}}_{ASA}}{J_{v_{15}} \cdot \varepsilon^{v_{14}}_{ASA}} = \frac{C^{J_{v_{15}}}_{v_{14}}}{C^{J_{v_{14}}}_{v_{15}}} = 0.11$$

Both enzymes had the same elasticity towards ASA, therefore the observed difference in control was due solely to the difference in flux towards Lys.

Under increased demand for Lys, both $R^{J_{v_{14}}}_{Lys}$ and $R^{J_{v_{15}}}_{Lys}$ decreased in magnitude (Tables 4.4 and 4.6). The elasticities of each enzyme towards Lys decreased. DHDPS1 and DHDPS2 had less control over their own fluxes. This decrease in control and

activity responses of DHDPS1 and DHDPS2 led to partial responses ${}^{v_{14}}R^{J_{v_{14}}}_{Lys}$ and ${}^{v_{15}}R^{J_{v_{15}}}_{Lys}$ that were quantitatively smaller in magnitude. These routes of interaction, however, made larger *relative* contributions towards the complete responses than under low Lys demand. Similarly ${}^{v_{15}}R^{J_{v_{14}}}_{Lys}$ and ${}^{v_{14}}R^{J_{v_{15}}}_{Lys}$ also contributed more towards the complete responses.

The control coefficients of both v_3 and v_4 over $J_{v_{14}}$ and $J_{v_{15}}$ increased. The significant decrease in elasticity of AK2 however lead to ${}^{v_4}R^{J_{v_{14}}}_{Lys}$ and ${}^{v_4}R^{J_{v_{15}}}_{Lys}$ contributing relatively less to the complete responses than under low demand conditions. The quantitative values of ${}^{v_3}R^{J_{v_{14}}}_{Lys}$ and ${}^{v_3}R^{J_{v_{15}}}_{Lys}$ remained the same under high Lys demand, but made relatively larger contributions towards the complete responses.

4.3.4.2 Interaction with Threonine

Thr, like Lys, is an allosteric inhibitor of various enzymes in the pathway (AKI, AKII, HSDHI and HSDHII). This property introduces various routes of interaction of Thr with its supply block through TS.

x	${}^{x}R^{J_{v_9}}_{Thr}$	ε^{x}_{Thr}	$C^{J_{v_9}}_{x}$
v_9	0	0	0.08
v_1	-0.13	-1.77	0.07
v_2	-0.04	-0.71	0.02
v_6	-0.06	-0.33	0.19
v_7	-0.01	-0.03	0.23
$R^{J_{v_9}}_{Thr}$	-0.24		

Table 4.7: The individual control and elasticity coefficients that make up the partial response coefficients of $R^{J_{v_9}}_{Thr}$.

.

Insensitivity of TS towards Thr means that the observed response towards Thr was only due to the interaction of Thr with other enzymes (Figure 4.9). Differences in control over J_{v_9} between AKI and AKII, and HSDHI and HSDHII were due to their contributions towards the flux towards Thr with

$$\frac{J_{v_6}}{J_{v_7}} = \frac{C^{J_{v_9}}_{v_6}}{C^{J_{v_9}}_{v_7}} = 0.85, \qquad \frac{J_{v_1}}{J_{v_2}} = \frac{C^{J_{v_9}}_{v_1}}{C^{J_{v_9}}_{v_2}} = 0.33$$

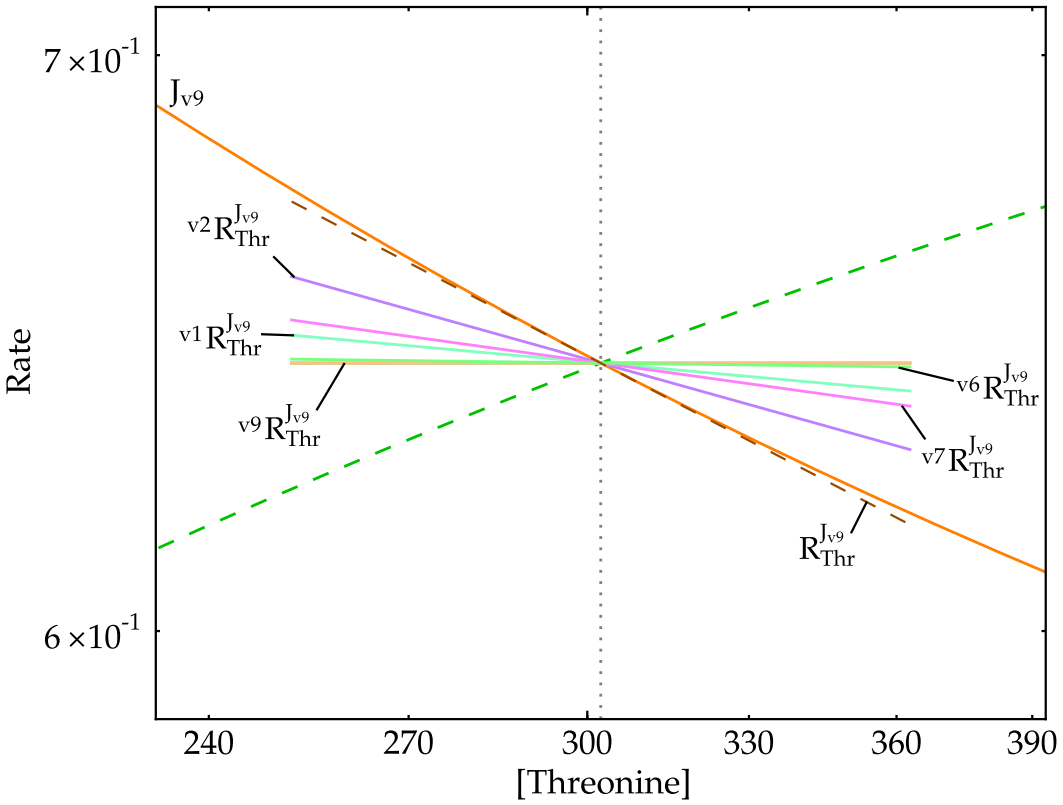

Figure 4.9: The rate characteristic plot for J_{v_9} with its partial responses towards Thr indicating the relative contribution of each route of interaction with the supply block. The importance of each route is indicated with a partial response coefficient as a light coloured solid line; these add up to the total response coefficient that is shown as dark dashed line. The steady-state is indicated by the grey dotted line.

The interaction of Thr with AKI makes the most significant contribution towards $R^{J_{v_9}}_{Thr}$ due to the large elasticity of AKI towards Thr and in spite of the little control it has over J_{v_9} (Table 4.7).

4.3.4.3 Interaction with Aspartate-Semialdehyde

ASA is at the branch point towards Lys and Thr. HSDHI and HSDHII catalyse the conversion of ASA towards Thr and are both inhibited by Thr, while DHDPS1 and DHDPS2 catalyse the conversion of ASA towards Lys which also inhibits them. In addition to these allosteric effects, Thr and Lys also inhibit AKI and AKII, and AK1 and AK2, respectively. These various allosteric effects introduce various routes of interaction of ASA with both its supply and demand blocks.

While aspartate-semialdehyde dehydrogenase (ASADH) is product sensitive and reversible, the direct interaction of ASA with its supply block via this enzyme made

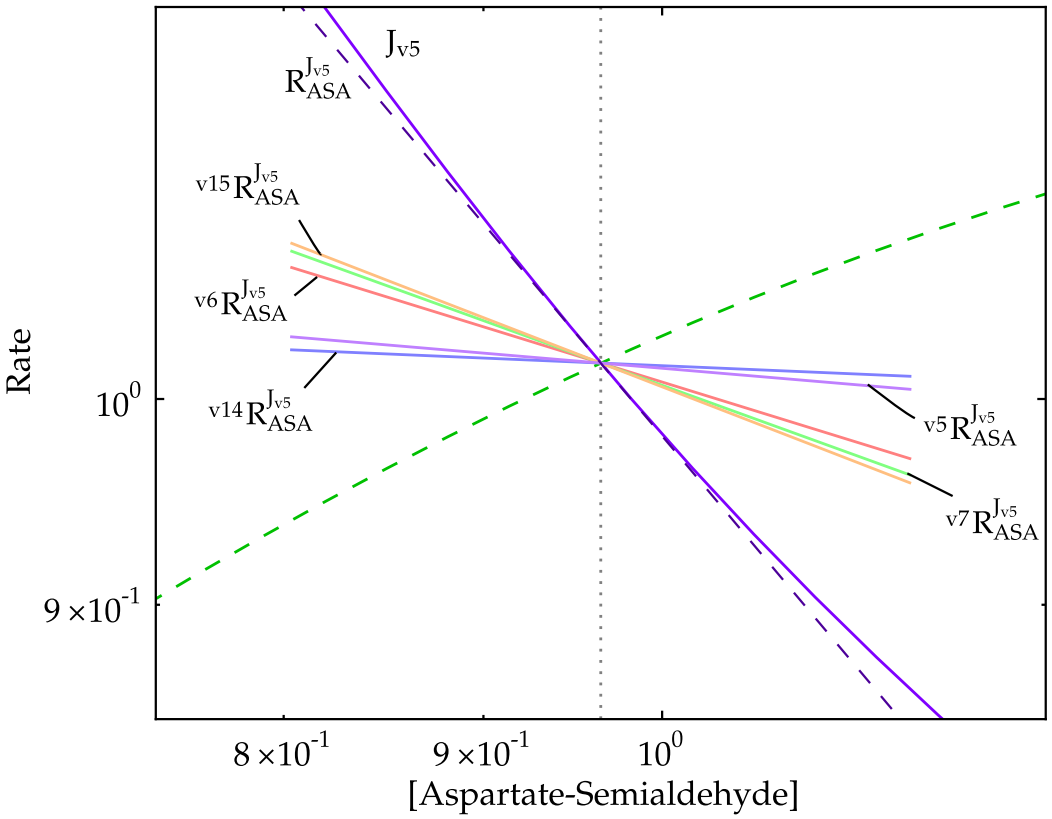

Figure 4.10: The rate characteristic plot for J_{v_5} with its partial responses towards ASA indicating the relative contribution of each route of interaction with the supply block. The importance of each route is indicated with a partial response coefficient as a light coloured solid line; these add up to the total response coefficient that is shown as dark dashed line. The steady-state is indicated by the grey dotted line.

the *second smallest* contribution towards $R^{J_{v_5}}_{ASA}$ (Figure 4.10) in spite of ASADH having a high elasticity coefficient towards ASA (Table 4.8). It was rather the interaction of ASA with HSDHI, HSDHII and DHDPS2 that caused most of the observed response (Figure 4.10). Changes in the flux through these enzymes due to a change in ASA affected both Lys and Thr concentrations, which in turn affected the rate of the AKs in the supply block as a result of their allosteric effects. The difference in control over J_{v_5} between HSDHI and HSDHII was only due to their different contributions towards the total flux towards Thr, as evident by

$$\frac{J_{v_6}}{J_{v_7}} = \frac{C^{J_{v_5}}_{v_6}}{C^{J_{v_5}}_{v_7}} = 0.85$$

The same is also true for DHDPS1 and DHDPS2 in regard to their control over J_{v_5}

x	${}^{x}R^{J_{v_5}}_{ASA}$	ε^{x}_{ASA}	$C^{J_{v_5}}_{x}$
v_5	-0.07	-2.53	0.03
v_6	-0.27	1.00	-0.27
v_7	-0.31	1.00	-0.31
v_{14}	-0.04	1.00	-0.04
v_{15}	-0.34	1.00	-0.34
$R^{J_{v_5}}_{ASA}$	-1.03		

Table 4.8: The individual control and elasticity coefficients that make up the partial response coefficients of $R^{J_{v_5}}_{ASA}$.

x	${}^{x}R^{J_{v_5}}_{ASA}$	ε^{x}_{ASA}	$C^{J_{v_5}}_{x}$
v_5	-0.07	-1.97	0.04
v_6	-0.21	1.00	-0.21
v_7	-0.24	1.00	-0.24
v_{14}	-0.03	1.00	-0.03
v_{15}	-0.19	1.00	-0.19
$R^{J_{v_5}}_{ASA}$	-0.75		

Table 4.9: The individual control and elasticity coefficients that make up the partial response coefficients of $R^{J_{v_5}}_{ASA}$ under increased Lys demand.

with

$$\frac{J_{v_{14}}}{J_{v_{15}}} = \frac{C^{J_{v_5}}_{v_{14}}}{C^{J_{v_5}}_{v_{15}}} = 0.11$$

Under high Lys demand conditions, there was a decrease in $R^{J_{v_5}}_{ASA}$ (Table 4.9). The elasticity of each demand enzyme towards ASA remained the same, while the control their reactions have over J_{v_5} decreased leading to a decreased quantitative contribution of each of these routes towards $R^{J_{v_5}}_{ASA}$. There was an increase in $\varepsilon^{v_5}_{ASA}$, while $C^{J_{v_5}}_{v_5}$ decreased, but the quantitative value of ${}^{v_5}R^{J_{v_5}}_{ASA}$ remained the same. The relative contribution of each route of interaction increased slightly save for the route represented by ${}^{v_{15}}R^{J_{v_5}}_{ASA}$, which decreased. The importance of each route of interaction is therefore different under high Lys demand than under low Lys demand.

Figure 4.11 shows the rate characteristics for each demand block from ASA. The isoenzymes HSDHI and HSDHII were the first enzymes in the demand blocks J_{v_6} and J_{v_7}, while DHDPS1 and DHDPS2 were the first in $J_{v_{14}}$ and $J_{v_{15}}$. There were therefore two routes of interaction of ASA with each demand block; one directly with the first enzyme in a block, and one via the isoenzyme of the first enzyme, as both enzymes catalysed the same reaction. The interaction of ASA with these demand blocks via the indirect routes, made negative contributions towards their total flux responses. These negative partial responses towards ASA resulted in a nearly zero total response towards ASA for both J_{v_6} ($R^{J_{v_6}}_{ASA} = 0.03$), and $J_{v_{14}}$

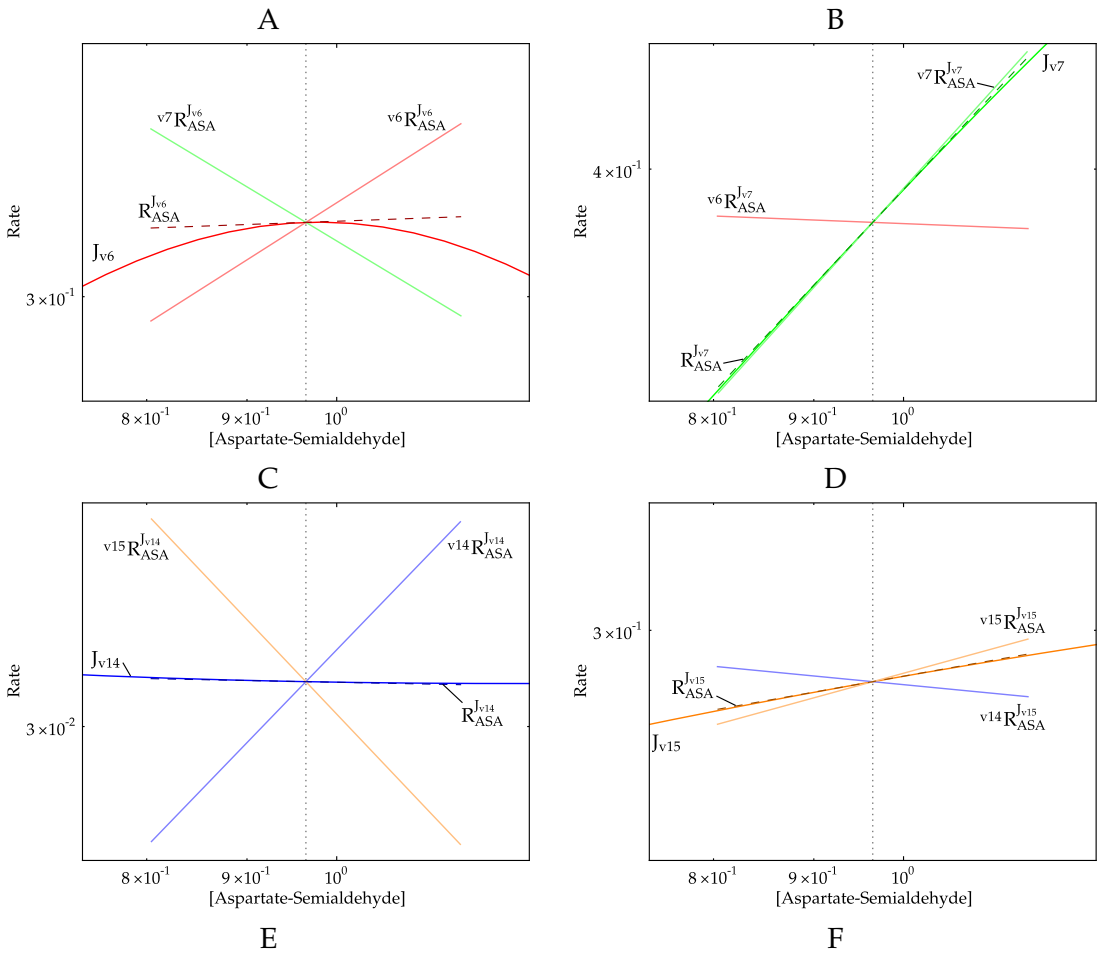

Figure 4.11: The rate characteristic plots for (A) J_{v_6}, (B) J_{v_7}, (C) $J_{v_{14}}$ and (C) $J_{v_{15}}$ with their partial responses towards ASA indicating the relative contribution of each route of interaction with each respective demand block. The importance of each route is indicated with a partial response coefficient as a light coloured solid line; these add up to the total response coefficient that is shown as dark dashed line. The steady-state is indicated by the grey dotted line.

($R_{ASA}^{J_{v_{14}}} = -0.02$) as they counteracted the positive partial responses towards ASA via the direct route of interaction. The shape of the rate characteristic plot in Figure 4.11A also indicates that for concentrations of ASA only slightly larger than the steady state concentration, there is also a negative flux-response towards ASA.

Each demand enzyme from ASA had the same elasticity towards ASA, meaning that the observed responses were due to differences in control of one enzyme over its counterpart. The degree of control of one insoenzyme over the other was determined by the flux through the enzyme and the elasticity of the counterpart towards its inhibitor as indicated by

$$\frac{J_{v_6} \cdot \varepsilon_{Thr}^{v_7}}{J_{v_7} \cdot \varepsilon_{Thr}^{v_6}} = \frac{C_{v_6}^{J_{v_7}}}{C_{v_7}^{J_{v_6}}} = 0.07, \qquad \frac{J_{v_{14}} \cdot \varepsilon_{Lys}^{v_{15}}}{J_{v_{15}} \cdot \varepsilon_{Lys}^{v_{14}}} = \frac{C_{v_{14}}^{J_{v_{15}}}}{C_{v_{15}}^{J_{v_{14}}}} = 0.09$$

In the case of HSDHI and HSDHII, the fluxes J_{v_6} and J_{v_7} were very similar, while the elasticity coefficient, $\varepsilon_{Thr}^{v_7}$ was much lower than $\varepsilon_{Thr}^{v_6}$. This means that the control $C_{v_6}^{J_{v_7}}$ was much smaller than $C_{v_7}^{J_{v_6}}$, predominantly because of the low sensitivity of HSDHII towards Thr. DHDPS1 and DHDPS2 on the other hand, had similar elasticities towards Lys, but $J_{v_{15}}$ was nearly 10-fold larger than $J_{v_{14}}$.

4.4 Discussion

In the above text we demonstrated the importance of the various routes of interaction between supply and demand blocks. We also demonstrated how the communication between supply and demand ensures the independence between the two branches at ASA when the demand for ASA changes in one of the branches.

The regulation of the supply block towards ASA was shown to take place not by the interaction of ASA with the supply enzyme ASADH as product inhibition, but rather by the interaction of ASA with the demand enzymes HSDHI, HSDHII and DHDPS2. This was unexpected, as ASADH had a high elasticity towards ASA, and one would therefore expect the direct interaction of ASA with ASADH to make the largest contribution towards the observed response. In this case however the near zero value of the control coefficient $C_{v_5}^{J_{v_5}}$ lead to the direct route contributing very little to the observed response. We also demonstrated that while the interaction of Lysine with DHDPS1 and DHDPS2 were mainly responsible for the observed responses of $J_{v_{14}}$ and $J_{v_{15}}$, the interaction of Lys with the enzymes AK1 and AK2 also significantly contributed towards the responses of the Lys supply blocks. Similarly

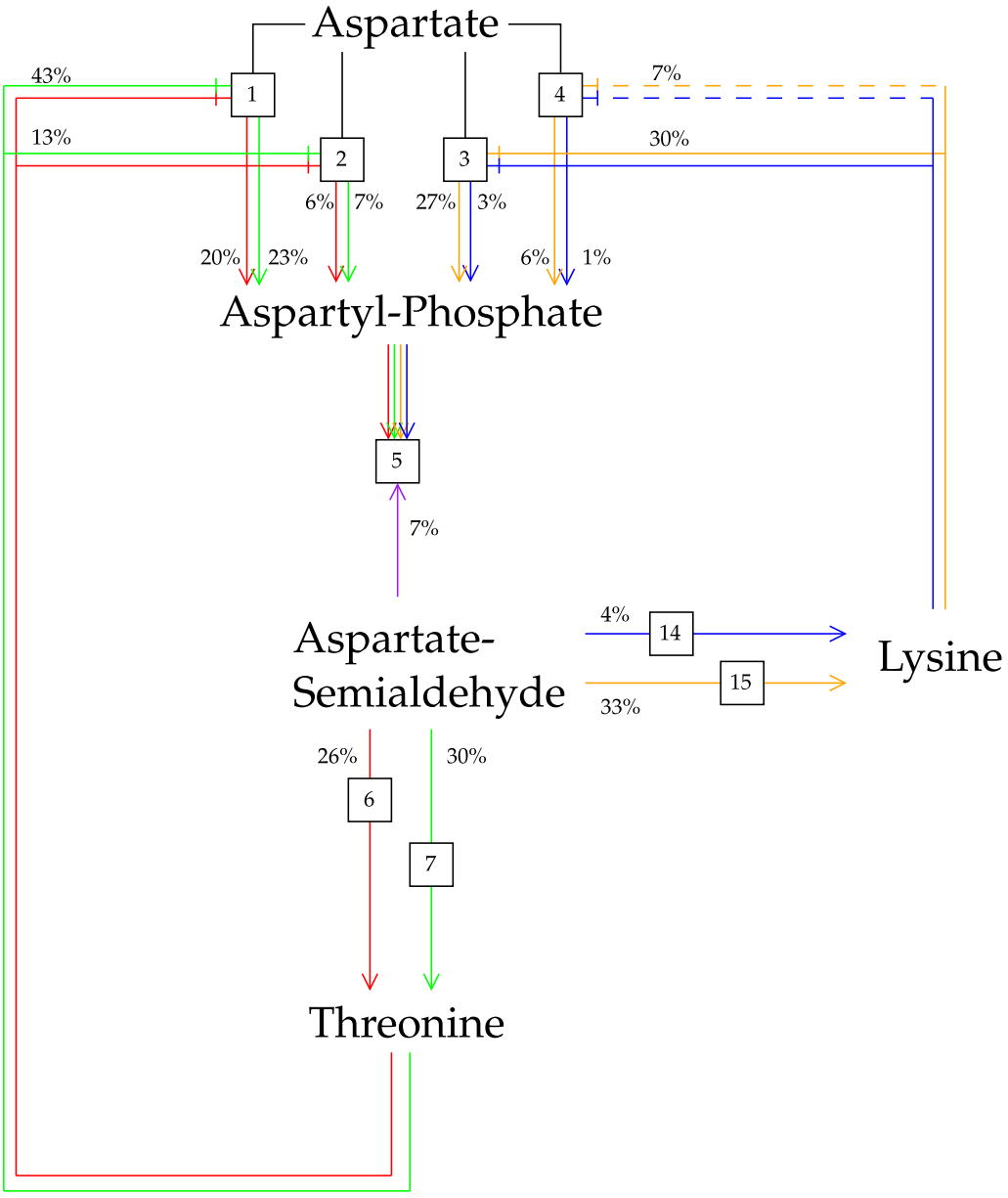

Figure 4.12: A simplified scheme of the aspartate-derived amino acid pathway indicating the percentage contribution towards the complete response of J_{v_5} of each route of interaction of ASA with ASADH. Coloured lines correspond to those used to indicate partial response coefficients in Figure 4.10.

interaction of Thr with AKI and AKII was shown the contribute significantly to the observed response in J_{v_9}. Each of these interactions takes place via ASADH and therefore represents not only their importance towards controlling the flux of $J_{v_{14}}$, $J_{v_{15}}$ and J_{v_9}, but also the importance of each of AK1, AK2, AKI and AKII in controlling ASADH. We also demonstrated that the importance of the different routes

of interaction changed under high Lys demand. This illustrates that regulation of metabolism is dynamic and changes as the needs of the organism changes.

Using these results, we can trace the complete routes of interaction from a metabolite towards an enzyme and quantify the importance of these complete routes in regulating flux. This is demonstrated in Figure 4.12.

It was also found that ASA, like most variable metabolites in this pathway, was not very well homoeostatically maintained. This is due to a relatively low degree of functional differentiation of supply and demand of ASA as well as a supply block that does not decrease very sensitively towards increased ASA concentration. Any increase in ASA demand would therefore lead to significant decreases in ASA concentration at the steady-state.

In spite of the low degree of ASA homoeostasis, when demand for Lys increased, both the flux of ASA supply and ASA demand towards Lysine increased while the flux of the demand towards Thr and ASA concentration remained constant at the steady-state. This was due to the attenuation of inhibition of AK1 and AK2 in the supply block by Lys, as its concentration decreased as a result of the increase in demand. The decrease in the quantitative regulatory importance of the route of interaction of ASA with J_{v_5} via $J_{v_{15}}$ illustrates this attenuation. By making AK1 and AK2 insensitive towards Lysine concentration, the same increase in ASADH flux was not observed in response to an increased Lys demand and steady-state ASA concentration decreased, leading to a decreased flux towards Thr (data not shown). A similar phenomenon was observed when demand for Thr was increased, with a slight increase in ASA concentration and flux towards Lys at the steady-state, but an overall independence between the two branches and a decrease in the quantitative regulatory importance of the route of interaction of ASA with J_{v_5} via J_{v_6} and J_{v_7} (data not shown). It is therefore apparent that by maintaining the homoeostasis of ASA when demand is increased in one branch, the independence of the two branches is maintained.

Curien *et al.* [31] demonstrated that the role of the control of the AKs and DHDPs by Lys was needed for the independence of the branches towards Lys and Thr. Here we confirmed these results. Additionally, by using rate characteristic plots, we could show how the supply and demand of ASA, while not being functionally differentiated or allowing for a high degree of homoeostasis of ASA [50], could, in the context of the complete system, still maintain ASA homoeostasis. We also showed that the change in importance of the different routes of regulation was

important in maintaining this independence through ASA homoeostasis.

The enzymes TS and HSK are product insensitive, this means when Thr demand increases, the decrease in Thr concentration will have no direct effect on the supply flux of Thr through TS, which would lead to no homoeostasis of Thr. However, a decreased Thr concentration does lead to a higher flux of J_{v_9}. This is due to the attenuation of inhibition of HSDHI, HSDHII, AKI and AKII. We also found that the control of flux is shared between supply and demand blocks of Hser and PHser. This allows for an increase in the flux of supply to be transmitted along the Thr branch. A high degree of functional differentiation between these blocks, where demand has full control over flux, would have led to a situation where increased flux from HSDHI and HSDHII would not have been transmitted along the branch towards Thr. In this system it is therefore important that both HSK and TS remain at levels where they are unsaturated by their substrates so that they have the capacity to respond to increased substrate concentrations brought on by increased supply flux. While the 6 reactions from DHDPS1 and DHDPS2 to Lys were not included in this model due to their irreversibility [31], their levels should also allow them to be unsaturated in order to transmit increased flux towards Lys.

While previous research has already shown that manipulation of the genes that encode for certain enzymes, such as DHDPS and AK, in the aspartate-derived amino-acid pathway may lead to increased amino-acid yields [51], further improvement of yields may still be possible, as the system is not yet fully understood. The quantification of the routes of regulation in this study represents a small step towards such an understanding. We demonstrated that the relative importance of the different routes of regulation changed under different conditions and postulated that these changes exist to maintain the independence of different branches though the homoeostatic maintenance of a metabolite at this branch point. Further research regarding the role of these routes of regulation under a wider range of conditions may lead to a better understanding of the roles of the various isoenzymes in the pathway. Further analysis with complementary methods such symbolic metabolic control analysis [52; 53], which can be used to identify and quantify control patterns [54], may also provide answers regarding the importance of different routes of regulation. By expanding the scope of study towards different metabolic pathways with similar features, the same techniques may also be applied in order to investigate possible similarities in regulation between these pathways.

While previous analysis of the model used in this study already produced various results [31], further analysis using different tools such as GSDA can yield novel

findings. Metabolic models, and the tools employed in their study, therefore represent powerful resources in the study of metabolic pathways that can be utilised in different ways to provide a better understanding of metabolism. Additionally, by allowing for the identification of regulatory features, GSDA can also act as an entry point towards more detailed or directed study of metabolic pathways.

In the next chapter we will investigate the regulation of the pyruvate branches in *Lactococcus lactis*. Unlike the pathway in the present case study, there are no allosteric effects in the pathway of the pyruvate branches from glycolysis. The presence of three moiety-conserved cycles, however, also allows for multiple routes of interaction between supply and demand blocks. Using GSDA we will quantify the regulatory effects of these conserved moieties on they reaction blocks they interact with.

Chapter 5

Case study 2: The widespread effect of moiety-conserved cycles

5.1 Introduction

Moiety-conserved cycles are common structures in metabolic pathways. Their presence, however, places constraints on flux in the pathway as the sum of the concentrations of the individual molecules that form part of the moiety-conserved cycle does not change rapidly. The concentration of any individual member of a moiety-conserved cycle is therefore limited by the concentration of all the other members.

The most common moiety-conserved cycles found in metabolism are those of ATP/ADP/AMP and NADH/NAD^+. In addition to the constraints these structures place on a system, the common moiety-conserved cycles also take part in a variety of different reactions in the cell. ATP is often referred to as the "molecular energy currency" of living organisms, with various metabolic pathways dedicated towards producing ATP. It is involved in any reactions that require chemical energy and provides energy for muscle contraction, is involved in active transport of molecules over membranes and it acts as a neurotransmitter [55; 56]. NAD^+ also takes part in numerous reactions as an electron carrier [57; 58]. The NAD^+ and AMP moieties often take part in the same reactions. The ubiquity of these common conserved moieties in metabolism means that they are extremely important for the functioning of biological systems and that changes in the concentration of the members of the moiety-conserved cycles will have effects widespread effect on metabolism [59; 60]. Indeed the ratio of NADH/NAD^+ or the redox state of a cell can be used as a measure of the health of a cell.

Glycolysis and subsequent pyruvate metabolism are two examples of pathways where the ATP/ADP and NADH/NAD^+ moieties are common. Hoefnagel *et al.* [10] constructed and analysed a model of the pyruvate branches in lactic acid bacteria as the products of the various branches have important industrial applications. While the concentrations of the members of moiety-conserved cycles are often modelled as parameters or even omitted, this pyruvate branch model includes three different moiety-conserved cycles, each with members with variable concentrations. They are NADH/NAD^+, ATP/ADP and Acetyl-CoA/CoA. While the work by the original authors includes a full metabolic control analysis of the system, the specific interactions of each of the moiety-conserved cycles with the various reactions they take part in were not investigated.

In the present study we therefore set out to elucidate and quantify the effects of the interactions of these moiety-conserved cycles with the various reactions in the pathway within the framework of generalised supply-demand analysis.

5.2 Methods

5.2.1 Model Modifications

The model constructed by Hoefnagel *et al.* [10] was retrieved from JWS online [35] in Pysces MDL format. The structure of the model is outlined in Figure 5.1 and the rate equations in Table 5.1. In order to perform parameter scans of the moiety-conserved cycles, NADH/NAD^+, ATP/ADP and Acetyl-CoA/CoA (AcCoA/CoA), the ratios r_N, r_A and r_C were defined as outlined in Section 3.3. The concentrations of the members of the moiety-conserved cycle are defined in terms of the their ratios and the total concentration of the moiety as in the equations below. The total moiety concentrations are 1 mM for AcCoA/CoA, 5 mM for ATP/ADP and 10 mM for NADH/NAD^+. In order to test the validity of the modified model, all the results produced by Hoefnagel *et al.* [10] were reproduced. The model file used is provided in Appendix D.

$$r_N = \frac{[NADH]}{[NAD^+]} \qquad r_A = \frac{[ATP]}{[ADP]} \qquad r_C = \frac{[AcCoA]}{[CoA]}$$

$$K_N = [NADH] + [NAD^+] \qquad K_A = [ATP] + [ADP] \qquad K_C = [AcCoA] + [CoA]$$

$$\therefore \qquad \therefore \qquad \therefore$$

$$[NADH] = \frac{r_N \cdot K_N}{1 + r_N} \qquad [ATP] = \frac{r_A \cdot K_A}{1 + r_A} \qquad [AcCoA] = \frac{r_C \cdot K_C}{1 + r_C}$$

$$[NAD] = \frac{K_N}{1 + r_N} \qquad [ADP] = \frac{K_A}{1 + r_A} \qquad [CoA] = \frac{K_C}{1 + r_C}$$

5.2.2 Generalised supply-demand Analysis

Using the RateChar module for PySCeS, pyruvate (Pyr), r_A, r_N and r_C were parameterised varied over a range with the doAllRateChar method as discussed in Sections 3.3.1 and 3.4. Suitable concentration ranges (Table 5.2) were chosen to show characteristic features of each supply and demand block for the variable metabolite. In addition to parameter scans, metabolic control analysis was performed for each clamped metabolite or ratio[1]. The results were used to draw rate characteristic plots for each variable metabolite in the pathway using the functionality of the RCFigure class of RateChar.

5.3 Results

5.3.1 Pyruvate

Pyruvate (Pyr) is the product of glycolysis (GLYC) and is at a branch point with demand blocks towards AcCoA via pyruvate dehydrogenase (PDH), lactate (Lac) via lactate dehydrogenase (LDH) and acetolactate (AcLac) via acetolactate synthase (ALS). At steady state 96.86% of the glucose consumption flux went towards Lac (J_{v_2}), 3.13% towards AcCoA (J_{v_3}) and the remaining 0.001% towards AcLac (J_{v_8}) (Figure 5.2). The rates of J_{v_1} and J_{v_2} saw an initial increase in response to increased [Pyr] after which their rates remained unaffected by further increases above 0.1 mM. The shape of the curve of J_{v_3} was sigmoidal with no further increase in rate at Pyr concentrations above 1 mM while the rate of J_{v_3} increased linearly in response to increasing Pyr.

The supply block J_{v_1} had a response coefficient of close to zero towards Pyr, causing functional differentiation between the supply and demand blocks, where supply had the most control over flux. There was almost no homoeostasis of Pyr due to the small difference between response coefficients of the supply and demand blocks. The demand block J_{v_8} was the only exception as it did determine some degree of homoeostasis as indicated by the value of 2.37 for $R_{Pyr}^{J_{v_8}} - R_{Pyr}^{J_{v_1}}$.

ALS had full control of the flux of J_{v_8} as its activity response towards Pyr was equal to the flux response of J_{v_8}.

[1]The MCA results are given in tables in Appendix B

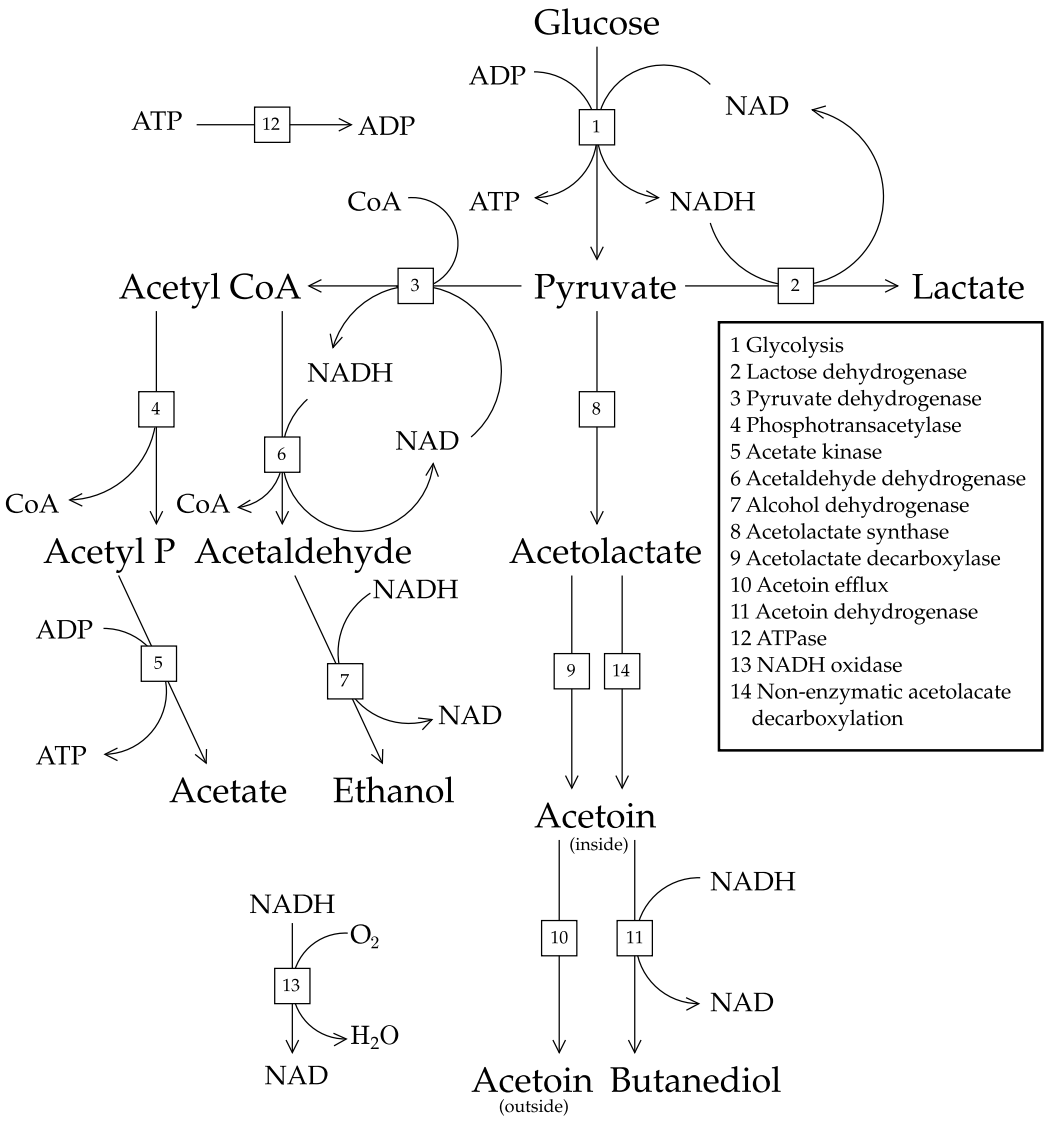

Figure 5.1: The pyruvate branch pathway as defined by Hoefnagel *et al.* [10]. Reactions are numbered according to the key. The stoichiometry of each reaction is 1 to 1, except for reaction 1 where Glc + 2ADP + 2NAD$^+$ → 2Pyr + 2ATP + 2NADH and reaction 8 where 2Pyr ⇌ AcLac. This figure was redrawn from the original as it appears in [10].

Reaction No.	Rate Equation
1	$v_{GLYC} = \frac{2397 \cdot \frac{Glc}{0.1} \cdot \frac{NAD}{0.14} \cdot \frac{ADP}{0.047}}{\left(1 + \frac{Glc}{0.1} + \frac{Pyr}{2.5}\right) \cdot \left(1 + \frac{NAD}{0.14} + \frac{NADH}{0.09}\right) \cdot \left(1 + \frac{ADP}{0.047} + \frac{ATP}{0.019}\right)}$
2	$v_{LDH} = \frac{5118 \cdot \frac{Pyr}{1.5} \cdot \frac{NADH}{0.08} \cdot \left(1 - \frac{Lac \cdot NAD}{Pyr \cdot NADH \cdot 21120.7}\right)}{\left(1 + \frac{Pyr}{1.5} + \frac{Lac}{100}\right) \cdot \left(1 + \frac{NADH}{0.08} + \frac{NAD}{2.4}\right)}$
3	$v_{PDH} = 259 \cdot \frac{\frac{Pyr}{1} \cdot \frac{NAD}{0.4} \cdot \frac{CoA}{0.014}}{\left(1 + \frac{Pyr}{1}\right) \cdot \left(1 + \frac{NAD}{0.4} + \frac{NADH}{0.1}\right) \cdot \left(1 + \frac{CoA}{0.014} + \frac{AcCoA}{0.008}\right)} \cdot \frac{1}{1 + \frac{46.4 \cdot NADH}{NAD}}$
4	$v_{PTA} = \frac{\frac{42}{0.2 \cdot 2.6} \cdot \left(AcCoA \cdot P - \frac{Acp \cdot CoA}{0.0065}\right)}{1 + \frac{AcCoA}{0.2} + \frac{P}{2.6} + \frac{Acp}{0.2} + \frac{CoA}{0.029} + \frac{AcCoA \cdot P}{0.2 \cdot 2.6} + \frac{Acp \cdot CoA}{0.7 \cdot 0.029}}$
5	$v_{ACK} = \frac{2700 \cdot \frac{Acp}{0.16} \cdot \frac{ADP}{0.5} \cdot \left(1 - \frac{AC \cdot ATP}{Acp \cdot ADP \cdot 174.2}\right)}{\left(1 + \frac{Acp}{0.16} + \frac{AC}{7}\right) \cdot \left(1 + \frac{ADP}{0.5} + \frac{ATP}{0.07}\right)}$
6	$v_{ACALDH} = \frac{\frac{97 \cdot NADH \cdot AcCoA}{0.025 \cdot 0.007} - \frac{97 \cdot NAD \cdot CoA \cdot Acal}{0.025 \cdot 0.007 \cdot 1}}{\left(1 + \frac{NADH}{0.025} + \frac{NAD}{0.08}\right) \cdot \left(1 + \frac{AcCoA}{0.007} + \frac{CoA}{0.008}\right) \cdot \left(1 + \frac{Acal}{10}\right)}$
7	$v_{ADH} = \frac{162 \cdot \frac{Acal}{162} \cdot \frac{NADH}{0.05} \cdot \left(1 - \frac{EtOH \cdot NAD}{Acal \cdot NADH \cdot 12354.9}\right)}{\left(1 + \frac{Acal}{162} + \frac{EtOH}{1}\right) \cdot \left(1 + \frac{NADH}{0.05} + \frac{NAD}{0.08}\right)}$
8	$v_{ALS} = \frac{600 \cdot \frac{Pyr}{50} \cdot \left(1 - \frac{AcLac}{Pyr \cdot 9 \times 10^{12}}\right) \cdot \left(\frac{Pyr}{50} + \frac{AcLac}{100}\right)^{2.4-1}}{1 + \left(\frac{Pyr}{50} + \frac{AcLac}{100}\right)^{2.4}}$
9	$v_{ALDC} = \frac{\frac{106 \cdot AcLac}{10}}{1 + \frac{AcLac}{10} + \frac{Acet}{100}}$
10	$v_{ACETEFF} = \frac{200 \cdot Acet}{5 + Acet}$
11	$v_{ACETDH} = \frac{105 \cdot \frac{Acet}{0.06} \cdot \frac{NADH}{0.02} \cdot \left(1 - \frac{But \cdot NAD}{Acet \cdot NADH \cdot 1400}\right)}{\left(1 + \frac{Acet}{0.06} + \frac{But}{2.6}\right) \cdot \left(1 + \frac{NADH}{0.02} + \frac{NAD}{0.16}\right)}$
12	$v_{ATPase} = \frac{900 \cdot \left(\frac{ATP}{ADP}\right)^{2.6}}{6.2^{2.6} + \left(\frac{ATP}{ADP}\right)^{2.6}}$
13	$v_{NOX} = \frac{\frac{\frac{118 \cdot NADH}{0.041} \cdot O}{0.2}}{\left(1 + \frac{NADH}{0.041} + \frac{NAD}{1}\right) \cdot \left(1 + \frac{O}{0.2}\right)}$
14	$v_{NEALC} = 0.0003 \cdot AcLac$

Table 5.1: The rate equations for each reaction in the pathway as shown in Figure 5.1. Rate equations were obtained from the model file and [10].

Metabolite	Scan Range	Steady State Concentration or Ratio
Pyr	0.005–28.87 mM	0.36 mM
r_A	0.06–457.51	5.08
r_N	0.0002–1.77	0.02
r_C	0.01–107.24	1.19

Table 5.2: The ranges over which the parameterised variable metabolites concentrations or ratios were varied.

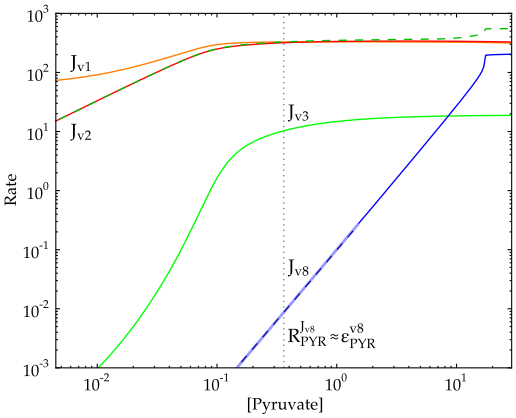

Figure 5.2: The rate characteristic plot for Pyr. The unlabelled green dashed curve represent total demand. The steady-state is indicated by the grey dotted line.

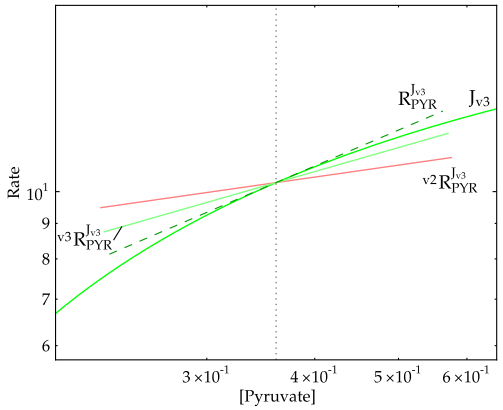

Figure 5.3: The rate characteristic plot for J_{v_3} with its partial responses towards Pyr indicating the relative contribution of each route of interaction with the reaction block. Partial response coefficients are shown as light coloured solid lines, while the total response is shown as a dark dashed line. The steady-state is indicated by the grey dotted line.

5.3.1.1 Routes of interaction of Pyruvate with J_{v_3}

At steady state, $R^{J_{v_3}}_{Pyr}$ was positive with a value of 0.53 (Figure 5.2). Two routes of interaction of Pyr with the J_{v_3} demand block made positive contributions towards the total response. The first was the interaction of Pyr with PDH as a substrate.

The second positive partial response coefficient was ${}^{v_2}R^{J_{v_3}}_{Pyr}$. In the unclamped system (see Section 3.4), v_2 has negative control over J_{v_3}, due to these two reactions competing for the same substrate, Pyr [10]. In the clamped system, where interaction via Pyr was removed, both reactions interact with r_N and may therefore still communicate. r_N is a substrate/product ratio for LDH and a product/substrate ratio for PDH. When Pyr was clamped and increased, the rate of J_{v_2} increased causing a decrease in the NADH/NAD$^+$ ratio with ${}^{v_2}R^{r_N}_{Pyr} = -1.08$. This decrease in product/-substrate ratio for PDH was therefore the source of the observed positive response in J_{v_3} (Figure 5.2).

5.3.2 ATP/ADP

The ATP/ADP moiety-conserved cycle represents one of three moiety-conserved cycles in the pathway. r_A is increased by the lumped GLYC reaction (J_{v_1}) and acetate kinase (AK) (J_{v_5}), while ATPase ($J_{v_{12}}$) decreases the ratio (Figure 5.4). The rate of $J_{v_{12}}$ increases in response to increased r_A, reaching saturation at ratios above 10. Save for a slight initial increase in J_{v_5} when r_A was increased from 0.06 and 0.4 (as shall be discussed in Section 5.3.2.1), both J_{v_1} and J_{v_5} decreased over the tested r_A range (Figure 5.4).

Supply and demand were functionally differentiated, with both supply blocks having more control over supply than demand with $|R^{J_{v_1}}_{r_A}/R^{J_{v_{12}}}_{r_A}| = 0.57$ and $|R^{J_{v_5}}_{r_A}/R^{J_{v_{12}}}_{r_A}| = 0.19$, indicating a higher degree of functional differentiation between $J_{v_{12}}$ and J_{v_5} than between $J_{v_{12}}$ and J_{v_1}. The demand block $J_{v_{12}}$ therefore determined the degree of homoeostasis of r_A with $R^{J_{v_{12}}}_{r_A} - R^{J_{v_{1+5}}}_{r_A} = 2.49$.

5.3.2.1 Routes of interaction of ATP/ADP with J_{v_5}

The demand block J_{v_5} had two negative partial response coefficients towards r_A at the steady state (Figure 5.5). The first negative response originated from the increase of ATP/ADP ratio, where ATP is a product and ADP is a substrate of of the enzyme ACK, thereby negatively affecting the rate of J_{v_5}. The second was through the interaction of r_A with GLYC (J_{v_1}). An increase in r_A decreased the rate of the supply of Pyr, thereby decreasing flux through the whole pathway and negatively affecting J_{v_5}.

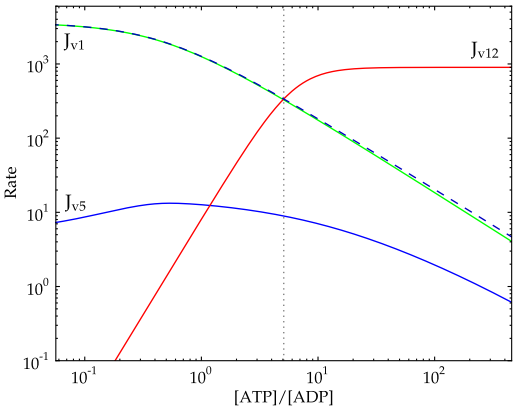

Figure 5.4: The rate characteristic plot for r_A. The unlabelled blue dashed curve represent total supply. The steady-state is indicated by the grey dotted line.

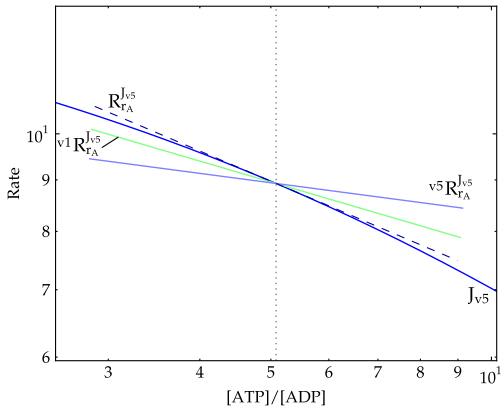

Figure 5.5: The rate characteristic plot for J_{v_5} with its partial responses towards r_A indicating the relative contribution of each route of interaction with the reaction block. Partial response coefficients are shown as light coloured solid lines, while the total response is shown as a dark dashed line. The steady-state is indicated by the grey dotted line.

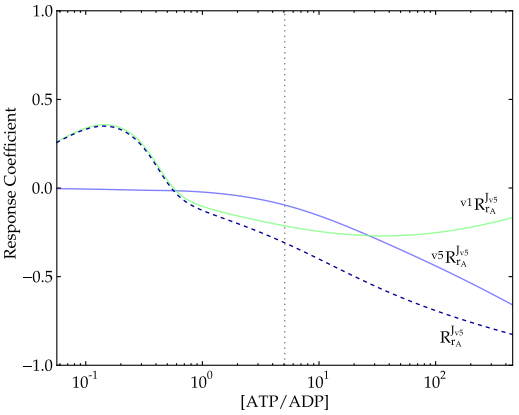

Figure 5.6: Partial response coefficients of J_{v_5} as a function of r_A. Partial response coefficients are shown as light coloured solid lines, while the total response is shown as a dark dashed line.

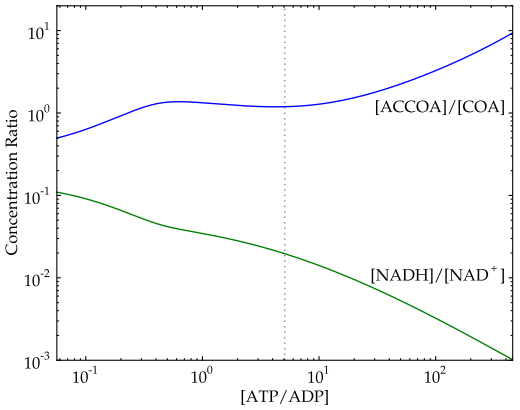

Figure 5.7: The values of the ratios r_C and r_N as a function of r_A.

At r_A values between 0.06 and 0.4, while a negative response in J_{v_1} was still observed, there was a positive response in J_{v_5} (Figure 5.4 and 5.6). In this concentration ratio range, the partial response ${}^{v_5}R_{r_A}^{J_{v_5}}$ was close to zero indicating that an increase in r_A did not affect the rate of ACK (Figure 5.6). In the same range ${}^{v_1}R_{r_A}^{J_{v_5}}$ was positive (Figure 5.6). This indicates that for this range the interaction of r_A with GLYC, which decreased the flux of J_{v_1}, increased flux of J_{v_5}. The ratio r_N also decreased over this range as a result of the decrease in the rate of J_{v_1} for which NAD^+ is a substrate and NADH a product (Figure 5.7).

Over this same r_A range, the rate of J_{v_6} decreased and the rate of J_{v_3} increased slightly (data not shown). The flux relationship

$$J_{v_3} = J_{v_5} + J_{v_6}$$

indicates these changes in flux must be met by an increase in the rate of J_{v_5}.

The change in rates of J_{v_3} and J_{v_6} can be ascribed to the interaction of r_N with PDH in J_{v_3}, acetaldehyde dehydrogenase (ACALDH) in J_{v_6} and alcohol dehydrogenase (ADH) in J_{v_7}. In this way J_{v_1} was linked to J_{v_5} via the interaction of r_N with J_{v_3} and J_{v_6}.

5.3.3 Acetyl-CoA/CoA

The Acetyl-CoA/CoA couple is the second moiety-conserved cycle in the pathway. The r_C supply is represented by J_{v_3} while it has two demand blocks, $J_{v_{14}}$ and J_{v_6}. The rate of J_{v_3} decreased while the rate of J_{v_4} increased for an increase in r_C over the tested range (Figure 5.8). The rate of J_{v_6} increased in response to an increased r_C value up to near steady state, whereafter a decrease in rate was observed (Figure 5.8).

The supply and demand blocks J_{v_3} and J_{v_4} were functionally differentiated with J_{v_3} having the most control over flux with $|R_{r_C}^{J_{v_3}}/R_{r_C}^{J_{v_4}}| = 0.35$. For these two blocks, the demand J_{v_4}, therefore determined the degree of r_C homoeostasis. For the supply and demand blocks J_{v_3} and J_{v_6} the opposite was true, as the demand block J_{v_6} had the most control over flux and J_{v_3} determined the degree of homoeostasis. This was due to the low response of J_{v_6} towards r_A at the steady state ($R_{r_C}^{J_{v_6}} = 0.07$). For these blocks $|R_{r_C}^{J_{v_3}}/R_{r_C}^{J_{v_6}}| = 3.14$.

5.3.3.1 Routes of interaction of Acetyl-CoA/CoA with J_{v_3}

At the steady state, the response of J_{v_3} toward r_C was negative (Figure 5.10A). The direct interaction of r_C with PDH in J_{v_3} made the most significant contribution

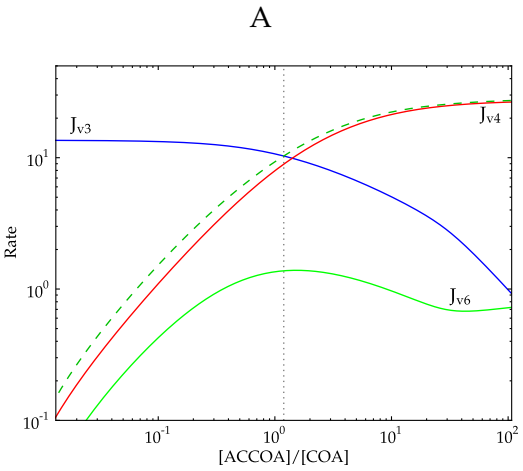

Figure 5.8: The rate characteristic plot for r_C. The unlabelled green dashed curve represents total demand. The steady-state is indicated by the grey dotted line.

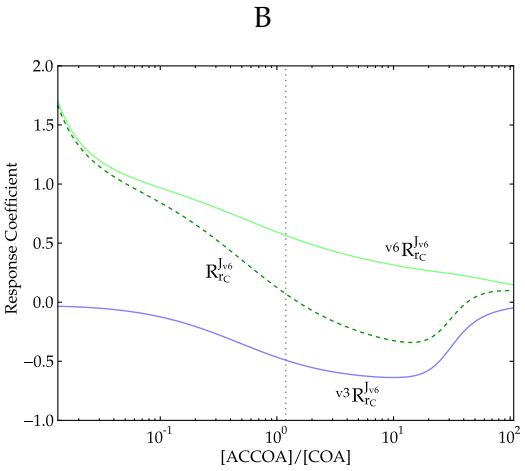

Figure 5.9: Partial response coefficients of J_{v_6} as a function of r_C. Partial response coefficients are shown as light coloured solid lines, while the total response is shown as a dark dashed line.

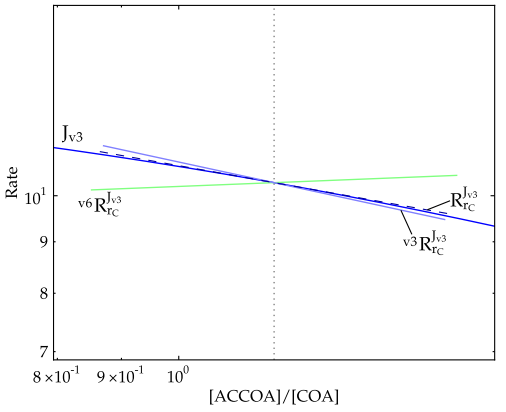

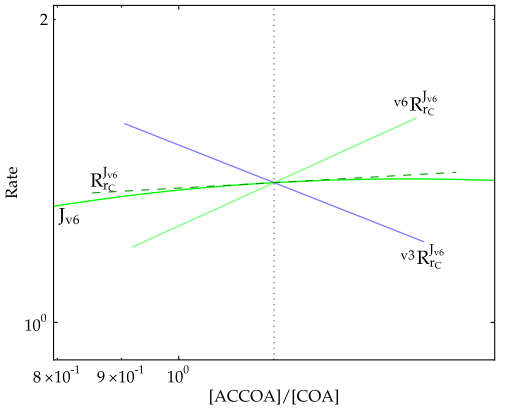

Figure 5.10: The rate characteristic plots for (A) J_{v_3} and (B) J_{v_6} with their partial responses towards r_C indicating the relative contribution of each route of interaction with the reaction blocks. Partial response coefficients are shown as light coloured solid lines, while the total response is shown as a dark dashed line. The steady-state is indicated by the grey dotted line.

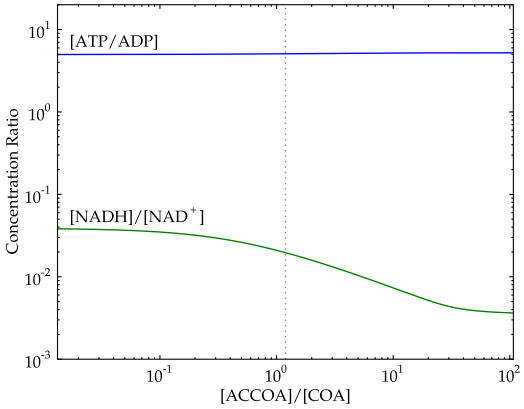

Figure 5.11: The values of the ratios r_A and r_N as a function of r_C.

towards the observed response as r_C is a product/substrate pair for this enzyme (Figure 5.10A). A small positive partial response ${}^{v_6}R^{J_{v_3}}_{r_C}$ was also observed. This positive effect was due to the positive response of J_{v_6} towards r_C. This positive response led to a negative response in r_N (${}^{v_6}R^{r_N}_{r_C} = -0.04$) (Figure 5.11), which acts as a product/substrate for PDH. The negative response of r_N towards J_{v_6} had an additional effect on the concentration of Pyr though the interaction with J_{v_1} and J_{v_2} (with ${}^{v_6}R^{Pyr}_{r_C} = 0.035$) which also affected the rate of PDH positively.

5.3.3.2 Routes of interaction of Acetyl-CoA/CoA with J_{v_6}

At the steady state, the response of J_{v_6} towards r_C was nearly zero (Figure 5.10B). This was due to two different routes of interaction of r_C with J_{v_6} having nearly equal, but opposite effects. The direct interaction of r_C with ACALDH had a positive effect on J_{v_6} with ${}^{v_6}R^{J_{v_6}}_{r_C} = 0.57$. The interaction of r_C with J_{v_6} via J_{v_3}, however, had a negative effect with ${}^{v_3}R^{J_{v_6}}_{r_C} = -0.50$. As with the response of J_{v_3} towards r_C via J_{v_6}, the negative response of the interaction of r_C with J_{v_6} via J_{v_3} was due to the mutual interaction these blocks with r_N. The negative response of J_{v_3} towards r_C led to a negative response in r_N (${}^{v_3}R^{r_N}_{r_C} = -0.34$) (Figure 5.11). In the r_C demand block J_{v_6}, r_N is a substrate/product ratio for both ACALDH and ADH. While the elasticity of J_{v_3} towards r_C was low, it had a considerable degree of control over J_{v_6} with $C^{J_{v_6}}_{v_3} = 0.73$.

At r_C values between 2 and 40, the rate of J_{v_6}, decreased (Figure 5.8). This effect was the result of the a decrease in magnitude of the positive partial response ${}^{v_6}R^{J_{v_6}}_{r_C}$ and an increase in magnitude of the negative partial response ${}^{v_3}R^{J_{v_6}}_{r_C}$ (Figure 5.9). The changes in these two partial responses led to a negative total response for this r_C range. The change in ${}^{v_6}R^{J_{v_6}}_{r_C}$ over this range can be predominantly attributed

to a decrease in $\varepsilon_{r_C}^{v_6}$, which decreased by a factor of nearly 4 while $C_{v_6}^{J_{v_6}}$ remained relatively constant. Similarly $\varepsilon_{r_C}^{v_3}$ decreased to nearly zero, while $C_{v_3}^{J_{v_6}}$ remained constant up to a r_C value of 20, from where it decreased to nearly zero, causing the observed increase in1 ${}^{v_3}R_{r_C}^{J_{v_6}}$ at ratios above 20 (data not shown).

5.3.4 NADH/NAD$^+$

The third and final moiety-conserved cycle in this pathway is NADH/NAD$^+$. The NAD$^+$ moiety interacts with more reaction blocks than either of the CoA and ADP moieties: r_N is produced by J_{v_1} and J_{v_3} and consumed by J_{v_2}, $J_{v_{11}}$, J_{v_6}, J_{v_7} and $J_{v_{13}}$ (Figure 5.17). As shown in Figure 5.12, over the tested r_N range, the rate of the supply block J_{v_1} increased as the ratio increased up to 0.001, whereafter the rate remained constant up to a r_N value of 0.03. The rate of the supply block J_{v_3}, on the other hand, decreased considerably more than J_{v_1} over the full r_N range. The demand block J_{v_2}, had the highest rate of the demand blocks interacting with r_N and showed an increase in rate for increasing r_N values up to 0.003, whereafter the shape of its curve was almost identical to that of J_{v_1}. The rates of J_{v_6} and J_{v_7} were equal as they form a linear chain of reactions in the pathway. Their rates were negative at r_N values below 0.001 and increased up to a ratio of 0.06 after which a further increase in r_N caused a decrease in the rate of J_{v_6} and J_{v_7}. Up to a r_N value of about 0.003, the rate of $J_{v_{11}}$ increased as the ratio increased, whereafter any increase in the ratio caused a decrease in the rate. At steady state, the rate of $J_{v_{11}}$ was negative. The rate of $J_{v_{13}}$ increased in response to an increase of r_N over the full range, showing saturation at ratios above 0.2.

The combined supply block $J_{v_{1+3}}$ and the combined demand block $J_{v_{2+6+7+11+13}}$ both had a responses of nearly zero (-0.04 and 0.05 respectively) towards r_N. This indicates that there was very little functional differentiation between r_N supply and demand at the steady state. There was also almost no homoeostasis of r_N. There was, however, functional differentiation between the combined supply block and the individual demand blocks with supply controlling flux, as each demand block had a non-zero response towards r_N. The demand block therefore determined some degree of r_N homoeostasis. The block J_{v_2} was the only exception as it did have a near zero response towards r_N.

5.3.4.1 Routes of interaction of NADH/NAD$^+$ with J_{v_2}

While the response of J_{v_2} towards r_N was very low at the steady state (Figures 5.12 and 5.13), three different routes of interaction made considerable contributions towards the observed response (Figure 5.13A). The direct interaction of r_N with

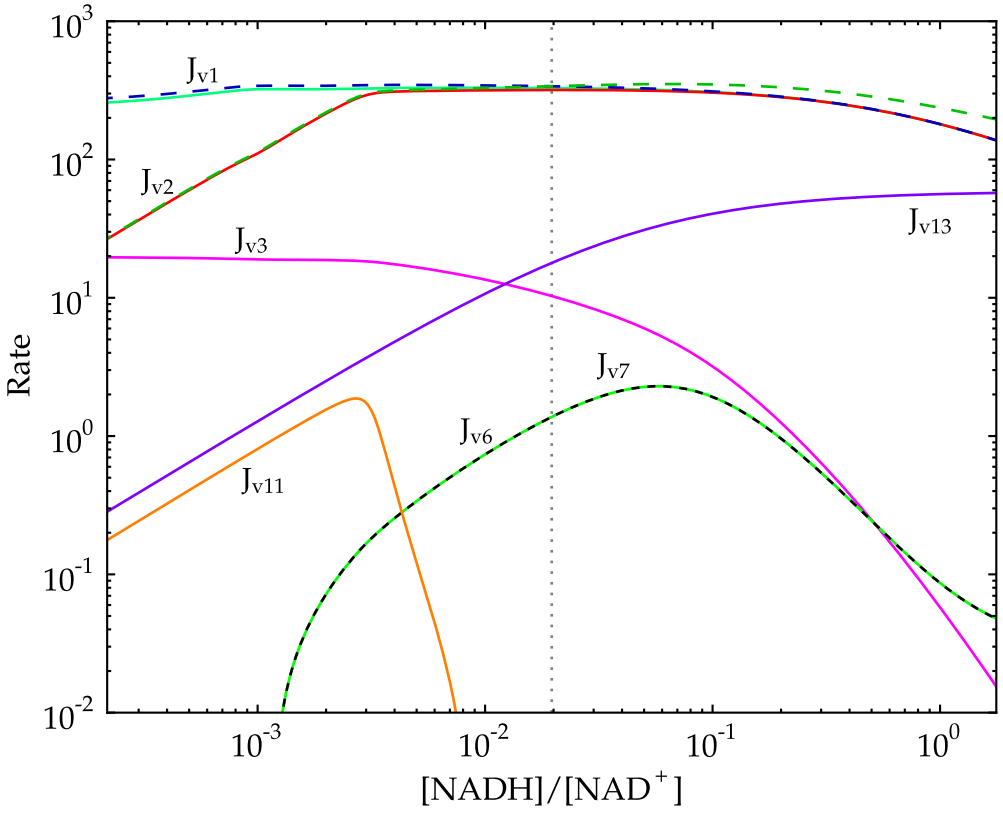

Figure 5.12: The rate characteristic plots for r_N. The green and black dashed line indicates the rates of J_{v_6} and J_{v_7}, as they were equal. Unlabelled dashed curves represent either total supply (blue) or total demand (green). The steady-state is indicated by the grey dotted line. $J_{v_{11}}$ is negative at the steady-state.

LDH in J_{v_2} as a substrate/product made the most significant positive contribution towards $R_{r_N}^{J_{v_2}}$. The partial response ${}^{v_3}R_{r_N}^{J_{v_2}}$ was also positive, while ${}^{v_1}R_{r_N}^{J_{v_2}}$ was negative. These two blocks are linked to J_{v_2} via Pyr.

The negative responses of J_{v_1} and J_{v_3} towards r_N caused negative and positive partial responses in [Pyr] respectively (${}^{v_1}R_{r_N}^{Pyr} = -0.024$ and ${}^{v_3}R_{r_N}^{Pyr} = 0.014$) which led to the observed partial responses in J_{v_2} (Figure 5.13A).

5.3.4.2 Routes of interaction of NADH/NAD$^+$ with J_{v_3}

There were four routes of interaction of r_N with J_{v_3} (Figure 5.13B). The direct interaction of r_N with PDH in J_{v_3} led to a negative partial response. An even more negative partial response was observed for the interaction of r_N with J_{v_3} via J_{v_2}. The interaction of r_N with J_{v_2} caused a negative partial response in [Pyr] (${}^{v_2}R_{r_N}^{Pyr} = -0.82$) which in turn affected the rate of J_{v_3}.

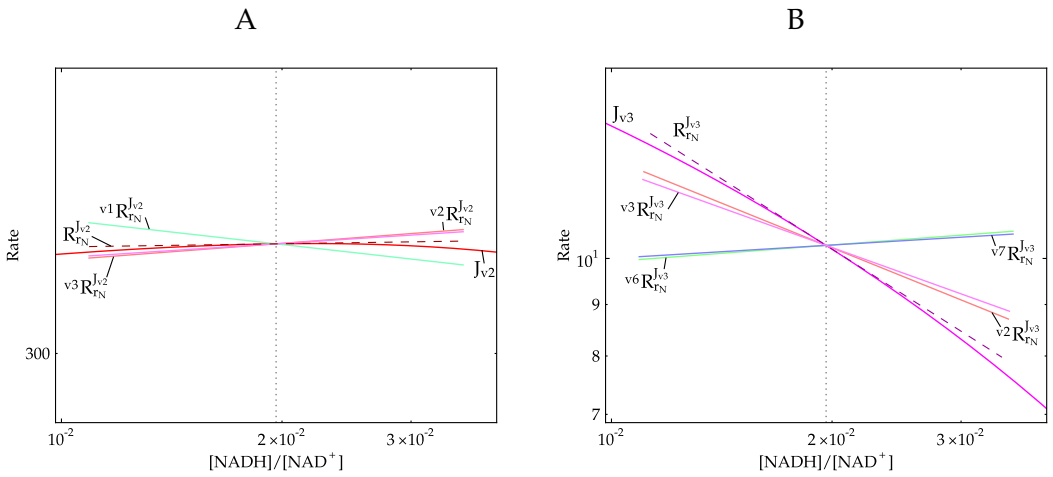

Figure 5.13: The rate characteristic plot for (A) J_{v_2} and (B) J_{v_3} with their partial responses towards r_N indicating the relative contribution of each route of interaction with the reaction blocks. Partial response coefficients are shown as light coloured solid lines, while the total response is shown as a dark dashed line. The steady-state is indicated by the grey dotted line.

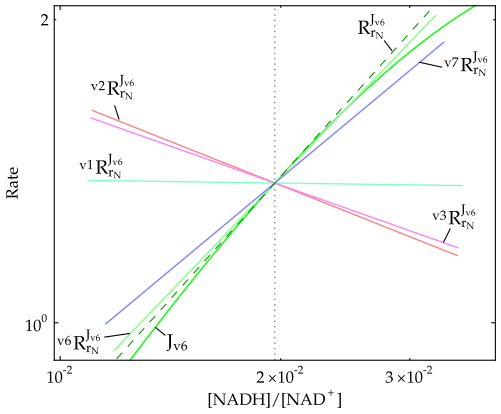

Figure 5.14: The rate characteristic plot for J_{v_6} with its partial responses towards r_N indicating the relative contribution of each route of interaction with the reaction block. Partial response coefficients are shown as light coloured solid lines, while the total response is shown as a dark dashed line. The steady-state is indicated by the grey dotted line.

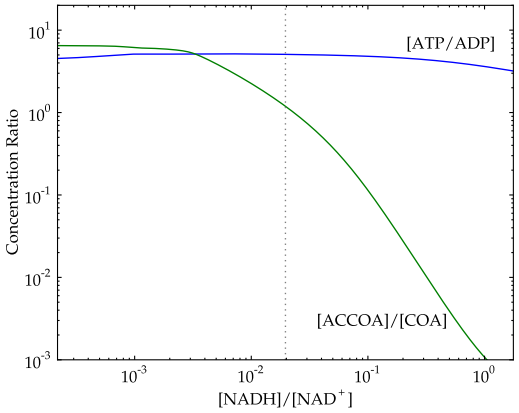

Figure 5.15: The values of the ratios r_A and r_C as a function of r_N.

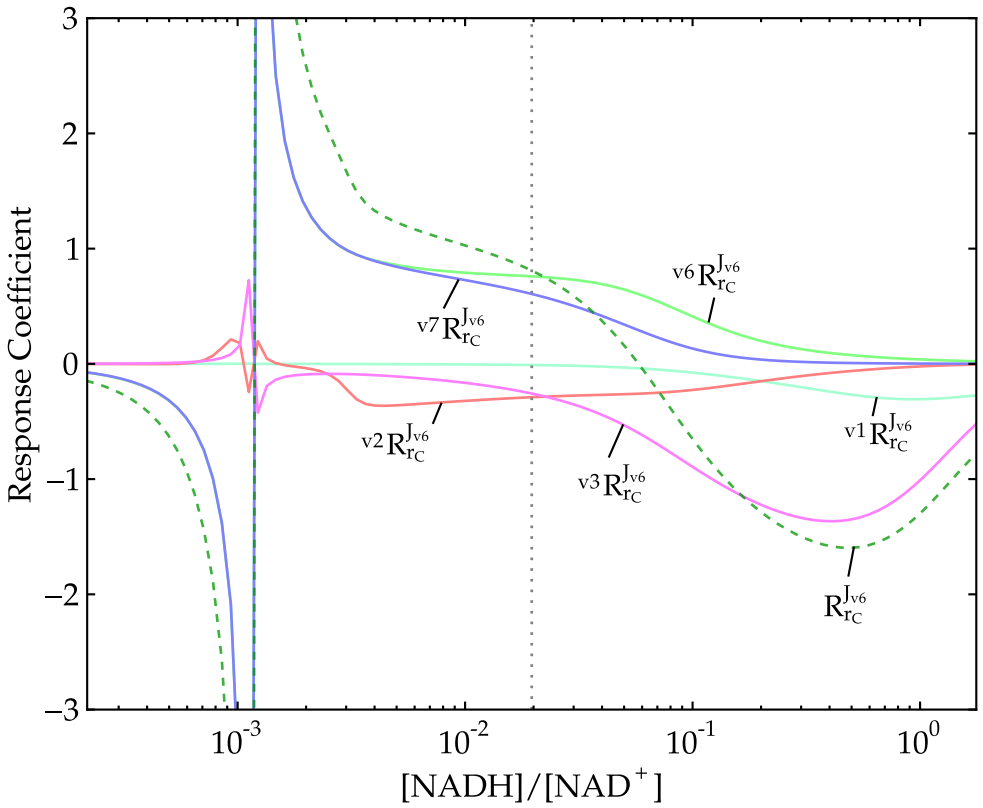

Figure 5.16: Partial response coefficients of J_{v_6} as a function of r_N. Partial response coefficients are shown as light coloured solid lines, while the total response is shown as a dark dashed line. There is a singularity at $r_N = 0.002$.

Two positive partial responses were observed for the interaction of r_N via J_{v_6} (ACALDH) and J_{v_7} (ADH) (Figure 5.13B). As the rates of these blocks were positively affected by r_N, their rate increased causing a negative responses in r_C (${}^{v_6}R^{r_C}_{r_N} = -0.083$ and ${}^{v_7}R^{r_C}_{r_N} = -0.067$) (Figure 5.15) which in turn caused the observed positive partial responses of J_{v_3}.

5.3.4.3 Routes of interaction of NADH/NAD$^+$ with J_{v_6} and J_{v_7}

While J_{v_6} and J_{v_7} are separate demand blocks for r_N, they are linked together via acetaldehyde (Acal) and form a single r_C demand block with their fluxes equal at steady-state. We will therefore consider the routes of interaction of r_N with these blocks at the same time and only refer to J_{v_6} wherever possible as the effects observed in both blocks were identical.

As shown in (Figure 5.14), at the steady state two routes of interaction of r_N with J_{v_6} made significant positive contributions towards the observed response. The direct interaction of r_N with ACALDH made the most significant contribution towards $R^{J_{v_6}}_{r_N}$. The interaction of r_N with ADH also resulted in a significant positive partial response of J_{v_6} (Figure 5.14).

Two negative responses were also observed for the interaction of r_N with J_{v_6} via J_{v_2} and J_{v_3} (Figure 5.14). As previously discussed, the direct interaction of r_N with J_{v_3} as well as the interaction with J_{v_3} via J_{v_2}, caused negative partial responses in J_{v_3}. Both these effects caused a negative response in r_C (${}^{v_3}R^{r_C}_{r_N} = -0.41$ and ${}^{v_2}R^{r_C}_{r_N} = -0.46$) (Figure 5.15). These effects on r_C in turn led to the observed negative values of the partial responses ${}^{v_2}R^{J_{v_6}}_{r_N}$ and ${}^{v_3}R^{J_{v_6}}_{r_N}$ (Figure 5.14).

At $r_N > 0.07$, the rate of J_{v_6} decreased (Figure 5.12). This was a result of the negative partial response ${}^{v_3}R^{J_{v_6}}_{r_N}$ increasing in magnitude and the positive partial responses ${}^{v_6}R^{J_{v_6}}_{r_N}$ and ${}^{v_7}R^{J_{v_6}}_{r_N}$ decreasing in magnitude, leading to a negative total response (Figure 5.16). At $r_N = 0.002$, there was a change in sign of the rate of J_{v_6} causing a mathematical singularity in the response coefficients (Figure 5.16). Additionally, there were irregular changes in the magnitude of the partial response coefficients ${}^{v_2}R^{J_{v_6}}_{r_N}$ and ${}^{v_2}R^{J_{v_6}}_{r_N}$ near this singularity. This non-monotonic behaviour was a result of the multiple interactions between supply and demand blocks.

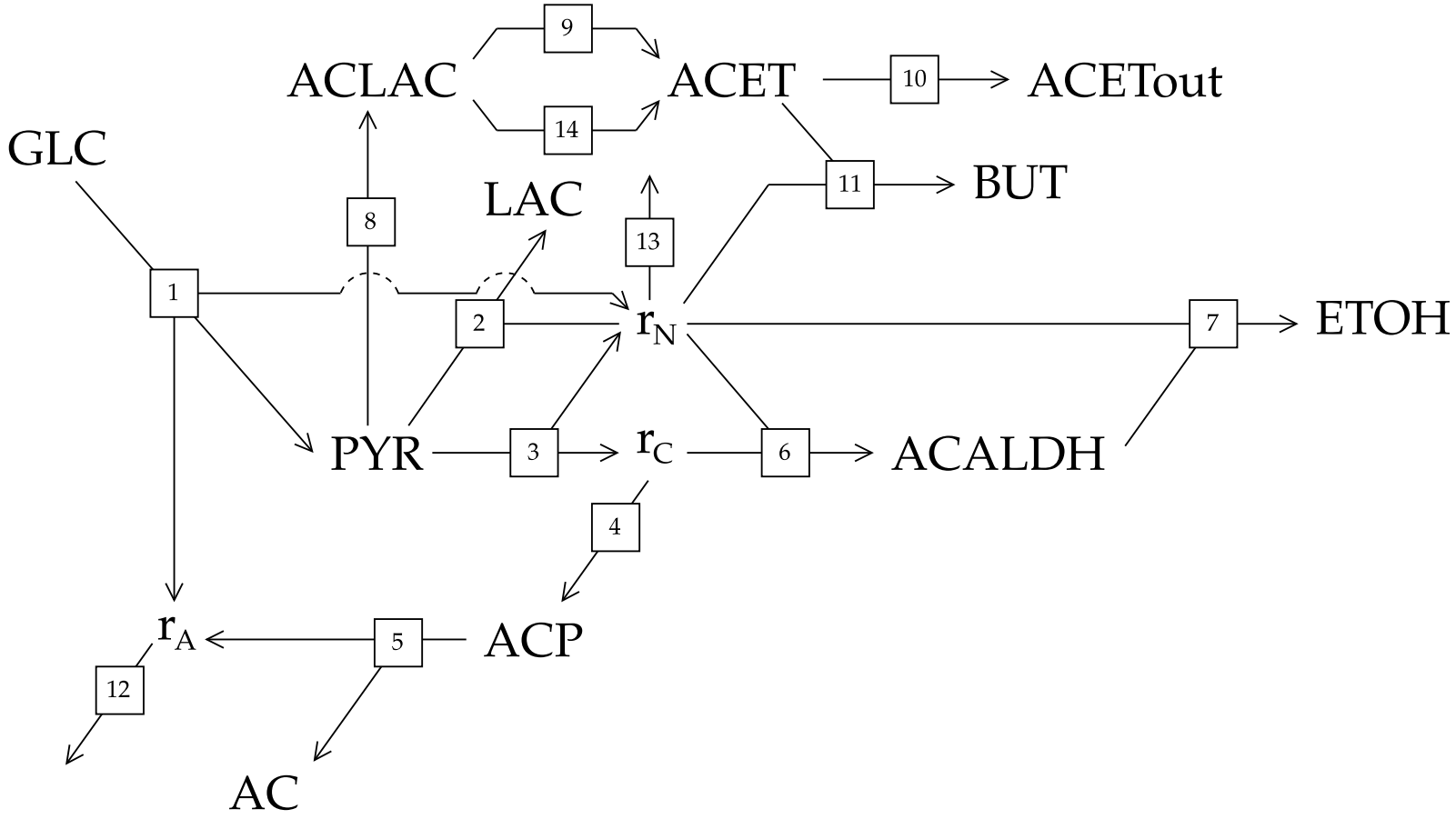

Figure 5.17: A version of the pyruvate branch pathway, as defined by Hoefnagel *et al.* [10], where each moiety only appears once. The moiety-conserved cycles are replaced with the ratios r_N, r_A and r_C. Reactions are numbered according to the key in Figure 5.1.

5.4 Discussion

Our findings demonstrate how the moiety-conserved cycles of ATP/ADP, NADH/ NAD^+ and Acetyl-CoA/CoA allow for different blocks of reactions to interact with each other, causing interesting and sometimes unexpected responses in flux.

When ignoring the interactions of ATP/ADP and NADH/NAD^+ with the metabolic pathway of the pyruvate branches, the structure of the pathway, while highly branched is fairly simple. Within the framework of generalised supply-demand analysis, demand and supply blocks for each variable metabolite can be defined where there are no routes of interaction between supply and demand, save for through the specific clamped metabolite. Even when ATP/ADP and NADH/NAD^+ are included in the pathway, simple inspection of a metabolic pathway does not necessarily give a full picture of how their supply and demand blocks are connected.

In the present study, conserved moieties were expressed as ratios of the metabolites between which they cycle, rather than as individual metabolites. This linearises the pathway allowing for parameter scans of the ratios of the members of the moiety-conserved cycles to be performed and for the pathway to be represented in a way where the connections between supply and demand blocks of the conserved moieties are clear (Figure 5.17). This representation paints a significantly more convoluted picture of supply and demand in the system, where supply and demand, supply and supply, and demand and demand blocks for certain metabolites may interact with each other via various routes, often involving the conserved moieties.

In the case of the two supply blocks of the r_A moiety, the one supply block (J_{v_1}) forms part of the other (J_{v_5}) when considering the chain of reactions v_1, v_3, v_4 and v_5. This allowed for the response in J_{v_1} towards r_A to be transmitted to J_{v_5} via this chain. Additionally J_{v_1} is a supply block of r_N. This allowed for additional routes of interaction with J_{v_5} by interacting with J_{v_3}, which forms part of the supply chain of J_{v_5}, and J_{v_6} and J_{v_7}, which forms part of the competing branch of J_{v_5} for Acetyl-CoA/CoA. We also showed that there was some functional differentiation between r_A supply and demand with supply having the most control over flux. This finding corresponds to a previous study where ATP supply had more control over flux than demand in glycolysis of growing *L. lactis* [5].

The numerous supply and demand blocks interacting with r_N, in addition to interacting with each other via alternative routes, lead to a great variety of effects of the moiety on its supply and demand blocks. An example of this was the effect of r_N

on J_{v_6}. The moiety ratio interacts directly with J_{v_6} as a substrate of ACALDH but also via J_{v_7} as a substrate for ADH which caused positive partial responses in J_{v_6}. r_N additionally interacted with PDH in J_{v_3} and LDH in J_{v_2} which caused negative partial responses. Previously it was shown that increased NADH oxidase (NOX) activity led to changes in the flux distribution towards the different end products of the pathway in lactic acid bacteria. Specifically increases in flux towards Acet (J_{v_8}) [10; 61], AcCoA (J_{v_3}) [10], AC (J_{v_5}) [61] and EtOH (J_{v_6}) [61] increased while flux towards Lactate decreased [10; 61].

Our results demonstrate that, in general, r_N homoeostasis was low and that, while there was very little functional differentiation between the total supply and total demand blocks, r_N supply had nearly complete control over flux when compared to the individual demand blocks. An increase in NOX ($J_{v_{13}}$) in our system would therefore not affect the total flux but rather just the flux towards $J_{v_{13}}$ and it would lead to a decrease in r_N. As shown in Figure 5.12, low r_N would indeed lead to a very different flux distribution, where the rates of J_{v_3}, $J_{v_{11}}$ (and by extension J_{v_8}) and J_{v_5} would increase, while the rate of J_{v_2} would decrease, specifically when considering r_N values below 0.001. In contrast to the previous results [61], our supply-demand analysis predicts a lower flux towards EtOH (J_{v_6}). This discrepancy may be the result of a difference in pH between the two systems as our model was built with pH = 6.5 and [10] the cell cultures used by Lopez de Felipe and Hugenholtz [61] had pH values ranging from 4.97 to 5.68.

Our data also showed that the importance of different interactions varied over a range of concentration ratios of the members of all three moiety-conserved cycles. In some cases the negative partial responses towards a substrate increased in magnitude as the substrate/product ratio increased, in turn causing negative complete responses and decreasing rates in response to increasing substrate. The opposite effect was also observed, where an increase in product caused an increase in rate of a supply block due to positive partial responses via a different route of interaction than the direct route, having a greater effect than the direct route itself.

Further work on this model could include a generalised supply-demand analysis of mutant strains of LAB, where either NOX concentration is increased or LDH concentration is decreased to show how the resulting change in flux distribution [10; 61] affects the interactions of the conserved moieties with their supply and demand blocks. Presumably, as flux in $J_{v_{11}}$ increases and flux in J_{v_2} decreases in both cases, there could possibly be significant changes in the responses of the supply and demand of r_N as the routes of interaction are greatly altered under these

conditions.

The current study demonstrates that the presence of the common moiety-conserved cycles, APT/ADP and NADH/NAD^+, result in pathways that have supply and demand blocks that are highly connected with each other. More generally we demonstrated that the individual members of a conserved moiety can be expressed as a ratio in order to perform GSDA. This framework enables us to trace the various routes of interaction of these, or any other two-membered moiety-conserved cycles, and quantify the relative contributions of each route of interaction. Previously, the analysis of the metabolic model in the present study led to a better understanding of the flux distribution and flux control of the pyruvate branch pathway [10]. In this study, however, we demonstrated that, while analysis of a model may already have produced noteworthy results, further analysis of a model using different tools or methods, such as GSDA in this case, may produce additional novel results. This demonstrates that, in general, kinetic models of metabolic pathways represent a powerful resource that may be tapped into using different analysis techniques, thereby leading to a better understanding of the regulation, control and behaviour of these pathways.

In the final chapter we will give a summary if the findings of this study and discuss their general significance within the context of GSDA and the field of Systems Biology.

Chapter 6

General discussion

This thesis had three main goals. The first was to develop methods to perform GSDA on two-membered and interlinked moiety-conserved cycles using PySCeS. Secondly, we wanted to build a software tool that can be used to interactively visualise rate characteristic data generated by the RateChar module for PySCeS. The final goal was to investigate the regulation, control and behaviour of two metabolic pathways by analysing kinetic models of these pathways using GSDA and the tools developed in this thesis. These goals were pursued order to reach a better understanding of the analysed pathways and to demonstrate the practical application of GSDA on real models of metabolism.

The next section is dedicated to providing a summary of the findings of this study. It will be followed by a discussion on the broader significance of our findings as well as a critique of the work. We will conclude this chapter with a brief discussion on future prospects relating to the work in this thesis.

6.1 Synopsis

6.1.1 RateChar and Conserved Moieties

In Section 3.3 we outlined methods for performing GSDA on two different types of moiety-conserved cycles. The first method relates to the commonly found two-membered conserved moiety such as ATP/ADP. Here we demonstrated that by expressing the members of the moiety-conserved cycle as a ratio of metabolites and by making slight modifications to the stoichiometry of a pathway model, parameter scans and MCA of these ratios can be performed. The second method relates to interlinked two-membered moiety-conserved cycles, where two cycles are interlinked by a shared metabolite. In this case the concentrations of the members of each of

the two conserved moieties are not free to change independently. As the ratio of the members of one moiety-conserved cycle changes, then so must the other. We demonstrated that expressing the concentrations of these members as a function of a fourth "linking metabolite", and by modifying the stoichiometry of the model to include the linking metabolite, we could also perform parameter scans and MCA of this metabolite in a GSDA.

In general, *in silico* supply-demand analysis can be performed utilising any metabolic analysis software application with the functionality to perform parameter scans of fixed metabolites and MCA of the supply and demand blocks for that metabolite [2]. While the requirements for GSDA are the same, performing the analysis for each individual metabolite in the pathway to generate results manually is a tedious and repetitive process and therefore more susceptible to human error. The RateChar module for PySCeS developed by Rohwer and Hofmeyr [7], utilises the features of PySCeS and its underlying platform, the Python programming language, to perform the analysis automatically. It also has the functionality to display and save results in the form of rate characteristic plots. These features are indispensable when performing GSDA on a metabolic model of any significant scope and complexity. While the original RateChar module relieves the user from the burden of manual analysis, the resulting rate characteristic plots that were generated with the software were at times difficult to interpret and often included erroneous results due to invalid steady-states being included on rate-characteristic plots. We therefore set out to improve this software package. The new features of RateChar as a result of the work done in this thesis include:

Error handling The previous implementation of RateChar did not differentiate between results that represent invalid steady states and those that do. The new feature discards invalid steady states without user intervention. Additionally provision was made for negative flux values, as they often caused unexpected behaviour of the plotting interface since the logarithm of these values is undefined.

Coloured rate characteristic plots Previously, only two colours were used to differentiate between the curves representing supply rates or those representing demand rates. In the new implementation, each reaction block interacting with a specific metabolite was assigned a different hue, with associated response or elasticity coefficients having a the same hue but a different shade.

Interactive rate characteristic plots The composition of a rate characteristic plots

may now be changed while they are displayed on screen. Specifically, the rate curves of reactions block and their associated elasticity, response and partial response coefficients may be enabled or disabled interactively as the user sees fit.

Integration with standard matplotlib This version of RateChar gives the user the ability to use standard matplotlib functions on the generated rate characteristic plots.

Additional options The dimensions of a rate characteristic plot and the output file format may now be specified.

6.1.2 Case studies with GSDA

This thesis also deals with the application of GSDA to metabolic models in an attempt to understand how the pathways they represent are regulated.

In Chapter 4 we used GSDA to analyse a metabolic model of aspartate-derived amino acid synthesis in *Aribidopsis thaliana*. The model used in this study is a very detailed and includes various features of the pathway such as isoenzymes, branch points and allosteric effectors. This pathway is also a determining factor in the nutritional qualities of plants [31; 47; 48; 51]. Therefore, increasing the yield of the amino-acids it produces presents an important biotechnological challenge. The first branch point in the pathway is at ASA and it leads to two branches. One of the branches leads to Thr and Ile, while the other leads to Lys. Thr and Lys also act as allosteric inhibitors for the first enzymes in their respective branches, as well as for the first enzymes in the pathway, where two of the four AK isoenzymes are inhibited by each. Previously it was shown that increasing the demand for either of Lys or Thr had the effect of increasing flux in its own branch, while flux in the other branch remained unaffected [31].

The major finding in this case study was an unexpected route of regulation from ASA towards its supply block. The production of ASA is catalysed by ASADH. This enzyme is both product sensitive and has a high elasticity towards ASA. However, the direct interaction of ASA with ASADH was only responsible for 7% of the observed response towards ASA. Instead, changes in ASA concentration were transmitted through the demand blocks and via the allosteric inhibitors, Lys and Thr, towards the AK enzymes in the supply block, thereby causing a response in the supply flux of ASA. In addition to demonstrating that responses are transmitted via demand, we were also able to quantify the contribution of each route of inter-

action towards the complete response. By determining the importance of different routes of regulation for different reaction blocks and combining this information, the percentage response of the ASA supply could be traced via each demand block and through the different AK isoenzymes in the supply block.

We also demonstrated that, while ASA is not well homoeostatically maintained by its supply and demand blocks, increases in demand for Lys did not affect the concentration of ASA. This was due to relieving of the inhibition of AK1 and AK2 by Lys as a result of lower Lys concentration during high Lys demand.

In Chapter 5, a model of the pyruvate branch pathway in lactic acid bacteria was investigated using GSDA. This pathway contains three different moiety-conserved cycles. Unlike many other models, these moiety-conserved cycles were explicitly included in the model as metabolic variables, and this introduced interactions between the different branches in the pathway. In this model we used the methods outlined in Section 3.3 to define the concentrations of the members of the moiety-conserved cycles as functions of their ratios and total moiety concentrations. This linearised the cycles and allowed GSDA to be performed around the ratios of the members of the moiety-conserved cycles.

Our findings demonstrate that the inclusion of these moiety-conserved cycles allowed for interactions between supply and demand blocks that would have gone unnoticed if they were excluded from the model. In the case of the two supply blocks of r_A, which represents the ratio of the ATP to ADP, the one block (J_{v_1}) forms part of the other (J_{v_5}). This interaction between the two blocks means that a change in r_A would, in addition to directly affecting each supply block via the enzymes that catalyse their respective r_A supply reactions, affect each block via interaction with the other.

In some cases multiple interactions were present. The ratio r_N, representing NADH/NAD$^+$, had four demand blocks and two supply blocks. These different blocks could interact with each other through different routes, and often multiple different routes, other than via NADH/NAD$^+$. The rate of these reaction blocks showed non-monotonic behaviour in response to NADH/NAD$^+$ as a result of these routes. Using GSDA, we could quantify the contribution of each of these routes towards the responses to the flux in each supply and demand block by examining at the partial responses for each route.

6.2 Significance and Critique

SDA and its generalised form are a result of a series of studies [7; 8; 11; 12; 62; 63]. This framework aims to provide a way to investigate and understand the behaviour, control and regulation of metabolic pathways within the metaphor of a supply-demand economy. By extending this framework and using it to analyse metabolic systems, we made various findings that fit into the broader context of cellular metabolism and systems biology.

In this thesis there was a significant focus on developing software tools that can be used for GSDA. The first of these tools was a method to perform parameter scans on two-membered moiety-conserved cycles in a GSDA. We demonstrated that, by expressing two-membered moiety-conserved cycles as ratios of the concentrations of the members, GSDA can be performed on model with conserved moieties. Neither the idea of expressing a moiety-conserved cycles as ratios of the individual members [14], nor performing MCA on moiety-conserved cycles [64] are new concepts. In fact, treating moiety-conserved cycles as a ratio of their members is a fairly common practice [65–67]. The method we outlined, however, presents a new opportunity in the study of metabolic models using GSDA. It proved invaluable in our own case study, which would have been impossible had it not been for this or a similar method. Previously, experimental SDA was used in the study of ATP supply and demand in *Lactococcus lactis* [5], *Escherichia coli* [5] and *Saccharomyces cerevisiae* [6] (as discussed in Section 2.6). In all three cases the [ATP]/[ADP] ratio was considered as opposed to just [ATP]. With the application of our method, *in silico* SDA or GSDA of the systems represented in these studies may now also be performed.

The second method we developed presents a way to deal with two interlinked two-membered moiety-conserved cycles. As of yet, this method has not been applied on real models of metabolism. Our search for a relevant model on the JWS online repository [32] was fruitless as only examples of models with interlinked moieties with multiple members were available [68].

We also developed an interactive plotting interface for the RateChar module for PySCeS. As GSDA is a method of analysis that relies heavily upon the visual interpretation of rate characteristic plots, this tool is very useful when performing GSDA. Most of the results in this study would have been difficult to generate without the use of RCFigure. In both case studies (Chapter 4 and 5) the models analysed were branched with multiple routes of interaction between supply and demand blocks.

Here RCFigure was invaluable in the generating easily interpretable results by allowing rate characteristic plots to be customised. This tool has the potential to enable GSDA on other metabolic models.

The fact that RateChar is built and integrated with PySCeS and Python is also very useful. PySCeS already provides a large number of methods that allow for MCA, structural analysis, steady-state analysis and time simulations of models of metabolic systems [39]. There are also a variety of scientific libraries available for Python such as SciPy and NumPy [69], which provide a variety of high level science and engineering modules, Biopython [70], which provides tools for biological computation, and SymPy [71], which is a library for symbolic mathematics. The significance of these tools all being built with Python libraries is that they are fully interoperable and open-source. This means that functionality provided by these tools may be integrated, providing a means to create new and unique implementations of technologies in order to solve specific problems and perform novel analyses. RateChar and PySCeS therefore form part of a much greater scientific computing ecosystem around the Python programming language.

Hofmeyr and Cornish-Bowden [2] argued that flux control by demand for a metabolic product is important and that supply is responsible for maintaining the homoeostasis of the metabolite when viewing metabolism as an economy. Our results in Chapter 4 confirm this notion. Demand for the end product Lys and Thr did indeed have the most control over flux. In our second case study, however, we found that flux control resided in the supply for most of the ratios of the members of the moiety-conserved cycles. Previous findings regarding flux control in this system have also been contrasting. Koebmann *et al.* [5] found that ATP flux control lies in either supply *or* demand in *L. lactis* depending on the level of ATP, where high demand conditions shifted flux control towards supply, while under low demand flux control lied in the demand. Under limiting glucose conditions, it was also shown that ATP flux was controlled by its supply in *S. cerevisiae*. GSH flux was controlled by supply under high GHS demand, and controlled by demand under low GSH demand. These results point to the levels of supply and demand activities being a factor determining flux control. This correlates well with the argument made by Hofmeyr and Cornish-Bowden [2], where they demonstrated that there are certain ranges of variation in demand where supply does not have any control over flux, but that these ranges are not infinite and when they are exceeded a shift in flux control can take place. In the aspartate-derived amino-acid pathway, Lys supply is within the range where supply still has the capacity to accommodate increases in demand. In the pyruvate branch model, however, flux from glycolysis remained constant,

regardless of product concentration, therefore shifting flux control to supply.

The case studies in this thesis involved GSDA of two previously published metabolic models. Both these models had already been analysed using methods such as flux-distribution analysis and MCA, and while these analyses provided various results, the potential wealth of knowledge these models provide was certainly not depleted. Further analysis using GSDA, revealed more novel findings. This clearly demonstrates the importance of both metabolic models and useful analysis tools in the study of metabolism. This conviction is shared by various other researchers. Snoep and Westerhoff [46] discussed the building of a "silicon cell" by integrating models of metabolism and the need for tools to analyse these models. Rohwer [36] also commented on the need for integration of different levels of cellular hierarchy in more complex models. Recently these ideas were realised in the form of a whole organism model of *Mycoplasma genitalium* [72]. In this thesis GSDA was shown to be an effective analysis tool in metabolic models of any size and, while its application to metabolic models does not lead to a full understanding of the pathway, it can provide an entry point into the further analysis of metabolic pathways.

6.3 Future Prospects

Analysing metabolic pathways with conserved moieties with multiple members, interlinked or not, with GSDA still provides a challenge. How this problem will be solved, remains to be seen, but will open up the possibility for previously impossible analyses, hopefully leading to greater understanding of metabolic regulation. The model used in Chapter 5 has a more detailed counterpart [68] that includes an interlinked moiety with multiple members. This model presents an ideal opportunity to gain a deeper knowledge of the effects of conserved moieties in metabolism as it contains a more complex conserved moieties than have been analysed with GSDA as yet and is an extension of the work that has already been done.

Software development is an iterative and incremental process. While RateChar already has significant functionality, there is always room for improvement. Future prospects in the development of this package include the refinement of current features, such as improving interactivity or parallelising parameter scans. New features could include the ability to save parameter scan data for later use with either the RCFigure class or for the use with other software plotting interfaces. The initial need for the development of RateChar and its subsequent improvement in the current study illustrates the need for software tools that are powerful, extensible and accessible for the use in metabolic analysis. GSDA and RateChar represent

the integration of MCA, parameter scans and rate characteristic plots to form a useful framework of metabolic analysis [7]. The visual and interactive features of RateChar also proved to be very powerful. Therefore the development of RateChar could pave the way for building more software tools that integrate different modes of analysis such as symbolic control analysis with GSDA, leading to a larger and more comprehensive frameworks of analysis.

List of References

[1] Boogerd, F., Bruggeman, F.J., Hofmeyr, J.-H.S. and Westerhoff, H.V. (eds.): *Systems Biology: Philosophical Foundations*. 1st edn. Elsevier Science, May 2007. ISBN 0444520856.

[2] Hofmeyr, J.S. and Cornish-Bowden, A.: Regulating the cellular economy of supply and demand. *FEBS Letters*, vol. 476, no. 1-2, pp. 47–51, June 2000. ISSN 0014-5793.

[3] Hofmeyr, J.-H.S. and Olivier, B.G.: The regulatory design of an allosteric feedback loop: the effect of saturation by pathway substrate. *Biochemical Society Transactions*, vol. 30, no. 2, p. 19, April 2001. ISSN 03005127.

[4] Hofmeyr, J.-H.S.: The harmony of the cell: the regulatory design of cellular processes. *Essays in Biochemistry*, vol. 45, pp. 57–66, 2008. ISSN 0071-1365. PMID: 18793123.

[5] Koebmann, B.J., Westerhoff, H.V., Snoep, J.L., Solem, C., Pedersen, M.B., Nilsson, D., Michelsen, O. and Jensen, P.R.: The extent to which atp demand controls the glycolytic flux depends strongly on the organism and conditions for growth. *Molecular Biology Reports*, vol. 29, no. 1, pp. 41–45, 2002. ISSN 0301-4851.

[6] Kroukamp, O., Rohwer, J., Hofmeyr, J.-H. and Snoep, J.: Experimental supply-demand analysis of anaerobic yeast energy metabolism. *Molecular Biology Reports*, vol. 29, no. 1, pp. 203–209, 2002. ISSN 0301-4851.

[7] Rohwer, J.M. and Hofmeyr, J.-H.S.: Identifying and characterising regulatory metabolites with generalised supply-demand analysis. *Journal of Theoretical Biology*, vol. 252, no. 3, pp. 546–554, June 2008. ISSN 1095-8541.

[8] Hofmeyr, J.-H.S. and Rohwer, J.M.: Supply-demand analysis: A framework for exploring the regulatory design of metabolism. In: *Methods in Enzymology*, vol. 500, pp. 533–554. Elsevier, 2011.

[9] Willey, J.M., Sherwood, L., Woolverton, C.J. and Prescott, L.M.: *Prescott, Harley, and Klein's microbiology*. 7th edn. McGraw-Hill Higher Education, New York, 2008. ISBN 9780072992915.

[10] Hoefnagel, M.H.N., Starrenburg, M.J.C., Martens, D.E., Hugenholtz, J., Kleerebezem, M., Swam, I.I.V., Bongers, R., Westerhoff, H.V. and Snoep, J.L.: Metabolic engineering of lactic acid bacteria, the combined approach: kinetic modelling, metabolic control

and experimental analysis. *Microbiology*, vol. 148, no. 4, pp. 1003–1013, January 2002. ISSN 1350-0872, 1465-2080.

[11] Hofmeyr, J.-H.S. and Cornish-Bowden, A.: Quantitative assessment of regulation in metabolic systems. *European Journal of Biochemistry*, vol. 200, no. 1, pp. 223–236, 1991. ISSN 1432-1033.

[12] Hofmeyr, J.S.: Metabolic regulation: A control analytic perspective. *Journal of Bioenergetics and Biomembranes*, vol. 27, no. 5, pp. 479–490, 1995. ISSN 0145-479X.

[13] Horton, H.R., Moran, L., Scrimgeour, K., Perry, M. and Rawn, D.: *Principles of Biochemistry*, chap. Introduction to metabolism, pp. 296–326. Pearson Education International, 2006.

[14] Reich, J. and Sel'kov, E.: *Energy Metabolism Of The Cell: A Theoretical Treatise*. Academic Press, 1981.

[15] Kacser, H., Burns, J.A. and Fell, D.A.: The control of flux: 21 years on. *Biochemical Society transactions*, vol. 23, no. 2, pp. 341–366, May 1995. ISSN 0300-5127. PMID: 7672373.

[16] Heinrich, R. and Rapoport, T.A.: A linear steady-state treatment of enzymatic chains: General properties, control and effector strength. *European Journal of Biochemistry*, vol. 42, no. 1, pp. 89–95, 1974. ISSN 1432-1033.

[17] Fell, D.A. and Sauro, H.M.: Metabolic control and its analysis. *European Journal of Biochemistry*, vol. 148, no. 3, p. 555–561, 1985. ISSN 1432-1033.

[18] Kahn, D. and Westerhoff, H.V.: Control theory of regulatory cascades. *Journal of Theoretical Biology*, vol. 153, no. 2, pp. 255–285, November 1991. ISSN 0022-5193.

[19] Koebmann, B.J., Westerhoff, H.V., Snoep, J.L., Nilsson, D. and Jensen, P.R.: The glycolytic flux in escherichia coli is controlled by the demand for ATP. *Journal of Bacteriology*, vol. 184, no. 14, pp. 3909–3916, July 2002. ISSN 0021-9193, 1098-5530.

[20] Schafer, J.R.A., Fell, D.A., Rothman, D. and Shulman, R.G.: Protein phosphorylation can regulate metabolite concentrations rather than control flux: The example of glycogen synthase. *Proceedings of the National Academy of Sciences of the United States of America*, vol. 101, no. 6, pp. 1485–1490, October 2004. ISSN 0027-8424, 1091-6490.

[21] Jørgensen, C.M., Hammer, K., Jensen, P.R. and Martinussen, J.: Expression of the pyrg gene determines the pool sizes of ctp and dctp in lactococcus lactis. *European Journal of Biochemistry*, vol. 271, no. 12, pp. 2438–2445, 2004. ISSN 1432-1033.

[22] Mendoza-Cozatl, D.G. and Moreno-Sanchez, R.: Control of glutathione and phytochelatin synthesis under cadmium stress. pathway modeling for plants. *Journal of Theoretical Biology*, vol. 238, no. 4, pp. 919–936, February 2006. ISSN 0022-5193.

[23] Aledo, J.C., Jiménez-Rivérez, S., Cuesta-Munoz, A. and Romero, J.M.: The role of metabolic memory in the ATP paradox and energy homeostasis. *FEBS Journal*, vol. 275, no. 21, pp. 5332–5342, 2008. ISSN 1742-4658.

[24] Hommes, F.A.: The integrated Michaelis-Menten equation. *Archives of Biochemistry and Biophysics*, vol. 96, pp. 28–31, January 1962. ISSN 0003-9861. PMID: 13908668.

[25] Schnell, S. and Maini, P.: A century of enzyme kinetics: Reliability of the K_M and v_{max} estimates. *Comments on Theoretical Biology*, vol. 8, no. 2-3, pp. 169–187, 2003.

[26] Walter, C.: Quasi-steady state in a general enzyme system. *Journal of Theoretical Biology*, vol. 11, no. 2, pp. 181–206, July 1966. ISSN 0022-5193.

[27] Walter, C.F. and Morales, M.F.: An analogue computer investigation of certain issues in enzyme kinetics. *The Journal of Biological Chemistry*, vol. 239, pp. 1277–1283, April 1964. ISSN 0021-9258. PMID: 14165939.

[28] Hoops, S., Sahle, S., Gauges, R., Lee, C., Pahle, J., Simus, N., Singhal, M., Xu, L., Mendes, P. and Kummer, U.: Copasi - a complex pathway simulator. *Bioinformatics*, vol. 22, no. 24, pp. 3067–3074, December 2006. ISSN 1367-4803, 1460-2059.

[29] Poolman, M.: Scrumpy: Metabolic modelling with Python. *IEE Proceedings: Systems Biology*, vol. 153, no. 5, pp. 375–378, 2006.
Available at: http://www.scopus.com/inward/record.url?eid=2-s2.0-33747193585&partnerID=40&md5=3b26d6e306377aaa3b697d70cb0562de

[30] Sauro, H.M.: Jarnac: a system for interactive metabolic analysis. In: Hofmeyr, J.-H.S., Rohwer, J.M. and Snoep, J.L. (eds.), *Animating the Cellular Map 9th International BioThermoKinetics Meeting*, no. 33 in Animating the Cellular Map 9th International BioThermoKinetics Meeting, pp. 221–228. Stellenbosch University Press, 2000.

[31] Curien, G., Bastien, O., Robert-Genthon, M., Cornish-Bowden, A., Cárdenas, M.L. and Dumas, R.: Understanding the regulation of aspartate metabolism using a model based on measured kinetic parameters. *Molecular Systems Biology*, vol. 5, p. 271, 2009. ISSN 1744-4292. PMID: 19455135.

[32] Olivier, B.G. and Snoep, J.L.: Web-based kinetic modelling using JWS online. *Bioinformatics*, vol. 20, no. 13, pp. 2143–2144, March 2004. ISSN 1460-2059.

[33] Le Novère, N., Bornstein, B., Broicher, A., Courtot, M., Donizelli, M., Dharuri, H., Li, L., Sauro, H., Schilstra, M., Shapiro, B., Snoep, J.L. and Hucka, M.: BioModels Database: a free, centralized database of curated, published, quantitative kinetic models of biochemical and cellular systems. *Nucleic Acids Research*, vol. 34, no. Database issue, pp. D689–D691, Jan 2006.

[34] Olivier, B.G., Rohwer, J.M. and Hofmeyr, J.H.S.: Modelling cellular processes with Python and Scipy. *Molecular Biology Reports*, vol. 29, no. 1-2, pp. 249–254, 2002. ISSN 0301-4851. PMID: 12241066.

[35] Olivier, B.G., Rohwer, J.M. and Hofmeyr, J.H.S.: Modelling cellular systems with PySCeS. *Bioinformatics*, vol. 21, no. 4, pp. 560–561, September 2004. ISSN 1460-2059.

[36] Rohwer, J.M.: Kinetic modelling of plant metabolic pathways. *Journal of Experimental Botany*, vol. 63, no. 6, pp. 2275–2292, January 2012. ISSN 0022-0957, 1460-2431.

[37] Pfau, T., Christian, N. and Ebenhöh, O.: Systems approaches to modelling pathways and networks. *Briefings in Functional Genomics*, vol. 10, no. 5, pp. 266–279, January 2011. ISSN 2041-2649, 2041-2657.

[38] Schallau, K. and Junker, B.H.: Simulating plant metabolic pathways with enzyme-kinetic models. *Plant Physiology*, vol. 152, no. 4, pp. 1763–1771, April 2010. ISSN 0032-0889, 1532-2548.

[39] Olivier, B., Rohwer, J. and Hofmeyr, J.: *PySCeS User Guide*, December 2008. Available at: http://pysces.sourceforge.net/docs/index.html

[40] Olivier, B.G.: *Simulation and Database Software for Computational Systems Biology: PySCeS and JWS Online*. Ph.D. thesis, University of Stellenbosch, 2005.

[41] du Preez, F., Conradie, R., Penkler, G., Holm, K., van Dooren, F. and Snoep, J.: A comparative analysis of kinetic models of erythrocyte glycolysis. *Journal of Theoretical Biology*, vol. 252, no. 3, pp. 488–496, 2008. Cited By (since 1996) 6. Available at: http://www.scopus.com/inward/record.url?eid=2-s2.0-43449086390&partnerID=40&md5=549ccb84e253776cd835e1b8f3bb435b

[42] Hunter, J.D.: Matplotlib: A 2d graphics environment. *Computing In Science & Engineering*, vol. 9, no. 3, pp. 90–95, 2007.

[43] Agoston, M.K.: *Computer graphics and geometric modeling: implementation and algorithms*. Springer, London, 2005. ISBN 1852338180.

[44] Fell, D.A.: Increasing the flux in metabolic pathways: A metabolic control analysis perspective. *Biotechnology and Bioengineering*, vol. 58, no. 2-3, p. 121–124, 1998. ISSN 1097-0290.

[45] Shimizu, K.: Toward systematic metabolic engineering based on the analysis of metabolic regulation by the integration of different levels of information. *Biochemical Engineering Journal*, vol. 46, no. 3, pp. 235–251, November 2009. ISSN 1369-703X.

[46] Snoep, J.L. and Westerhoff, H.V.: From isolation to integration, a systems biology approach for building the silicon cell. In: Alberghina, L. and Westerhoff, H.V. (eds.), *Systems Biology*, no. 13 in Topics in Current Genetics, pp. 13–30. Springer Berlin Heidelberg, January 2005. ISBN 978-3-540-22968-1, 978-3-540-31453-0.

[47] Galili, G. and Höfgen, R.: Metabolic engineering of amino acids and storage proteins in plants. *Metabolic Engineering*, vol. 4, no. 1, pp. 3–11, January 2002. ISSN 1096-7176. PMID: 11800569.

[48] Galili, G., Amir, R., Hoefgen, R. and Hesse, H.: Improving the levels of essential amino acids and sulfur metabolites in plants. *Biological Chemistry*, vol. 386, no. 9, pp. 817 – 831, 2005. ISSN 14316730.

[49] Stuttmann, J., Hubberten, H.-M., Rietz, S., Kaur, J., Muskett, P., Guerois, R., Bednarek, P., Hoefgen, R. and Parker, J.E.: Perturbation of arabidopsis amino acid metabolism causes incompatibility with the adapted biotrophic pathogen hyaloperonospora arabidopsidis. *The Plant Cell Online*, vol. 23, no. 7, pp. 2788–2803, July 2011. ISSN 1040-4651, 1532-298X.

[50] Rohwer, J.M. and Hofmeyr, J.-H.S.: Kinetic and thermodynamic aspects of enzyme control and regulation. *The journal of Physical Chemistry B*, vol. 114, no. 49, pp. 16280–16289, December 2010. ISSN 1520-5207. PMID: 21028763.

[51] Dewaele, E., Craciun, A., Vauterin, M., Frankard, V., Suharyanto, E., Tadesse, J. and Jacobs, M.: Metabolic engineering of a complex biochemical pathway: The lysine and threonine biosynthesis as an example. *Phytochemistry Reviews*, vol. 1, no. 1, pp. 125–133, January 2002. ISSN 1568-7767, 1572-980X.
Available at: http://link.springer.com.ez.sun.ac.za/article/10.1023/A%3A1015856925011

[52] Akhurst, T.J.: *Symbolic control analysis of cellular systems*. Ph.D. thesis, Stellenbosch University, 2011.

[53] Rohwer, J.M., Akhurst, T.J. and Hofmeyr, J.-H.S.: Symbolic control analysis of cellular systems. In: Hicks, M.G. and Kettner, C. (eds.), *Experimental Standard Conditions of Enzyme Characterizations. Proceedings of the 3rd International Beilstein Workshop*, pp. 137–148. Beilstein-Institut zur Förderung der Chemischen Wissenschaften, Frankfurt, 2008.

[54] Hofmeyr, J.-H.S.: Control-pattern analysis of metabolic pathways. *European Journal of Biochemistry*, vol. 186, no. 1-2, p. 343–354, 1989. ISSN 1432-1033.

[55] Butt, A.M.: ATP: a ubiquitous gliotransmitter integrating neuron–glial networks. *Seminars in Cell & Developmental Biology*, vol. 22, no. 2, pp. 205–213, April 2011. ISSN 1084-9521.
Available at: http://www.sciencedirect.com/science/article/pii/S108495211100036X

[56] Edwards, F.A. and Gibb, A.J.: ATP - a fast neurotransmitter. *FEBS Letters*, vol. 325, no. 1–2, pp. 86–89, June 1993. ISSN 0014-5793.

[57] Ansell, R., Granath, K., Hohmann, S., Thevelein, J. and Adler, L.: The two isoenzymes for yeast NAD^+-dependent glycerol 3-phosphate dehydrogenase encoded by GPD1 and GPD2 have distinct roles in osmoadaptation and redox regulation. *EMBO Journal*, vol. 16, no. 9, pp. 2179–2187, 1997. Cited By (since 1996) 228.

[58] Okun, J., Lümmen, P. and Brandt, U.: Three classes of inhibitors share a common binding domain in mitochondrial complex i (nadh:ubiquinone oxidoreductase). *Journal of Biological Chemistry*, vol. 274, no. 5, pp. 2625–2630, 1999. Cited By (since 1996) 213.

[59] Abbott, D.A., Van Den Brink, J., Minneboo, I.M., Pronk, J.T. and Van Maris, A.J.: Anaerobic homolactate fermentation with *Saccharomyces cerevisiae* results in depletion of ATP and impaired metabolic activity. *FEMS Yeast Research*, vol. 9, no. 3, p. 349–357, 2009. ISSN 1567-1364.

[60] Garrigues, C., Loubiere, P., Lindley, N.D. and Cocaign-Bousquet, M.: Control of the shift from homolactic acid to mixed-acid fermentation in lactococcus lactis: predominant role of the NADH/NAD+ ratio. *Journal of Bacteriology*, vol. 179, no. 17, pp. 5282–5287, January 1997. ISSN 0021-9193, 1098-5530.

[61] Lopez de Felipe, F. and Hugenholtz, J.: Pyruvate flux distribution in NADH-oxidase-overproducing lactococcus lactis strain as a function of culture conditions. *FEMS Microbiology Letters*, vol. 179, no. 2, p. 461–466, 1999. ISSN 1574-6968.

[62] Hofmeyr, J.H., Cornish-Bowden, A. and Rohwer, J.M.: Taking enzyme kinetics out of control; putting control into regulation. *European Journal of Biochemistry / FEBS*, vol. 212, no. 3, pp. 833–837, March 1993. ISSN 0014-2956. PMID: 8462553.

[63] Hofmeyr, J.-H.S. and Cornish-Bowden, A.: Co-response analysis: A new experimental strategy for metabolic control analysis. *Journal of Theoretical Biology*, vol. 182, no. 3, pp. 371–380, October 1996. ISSN 0022-5193.

[64] Hofmeyr, J.H.S., Kacser, H. and Merwe, K.J.: Metabolic control analysis of moiety-conserved cycles. *European Journal of Biochemistry*, vol. 155, no. 3, pp. 631–640, 1986.

[65] Golinska, M., Troy, H., Chung, Y.., McSheehy, P.M., Mayr, M., Yin, X., Ly, L., Williams, K.J., Airley, R.E., Harris, A.L., Latigo, J., Perumal, M., Aboagye, E.O., Perrett, D., Stubbs, M. and Griffiths, J.R.: Adaptation to HIF-1 deficiency by upregulation of the AMP/ATP ratio and phosphofructokinase activation in hepatomas. *BMC Cancer*, vol. 11, 2011.
Available at: www.scopus.com

[66] Brawand, F., Folly, G. and Walter, P.: Relation between extra- and intramitochondrial ATP/ADP ratios in rat liver mitochondria. *BBA - Bioenergetics*, vol. 590, no. 3, pp. 285–289, 1980. Cited By (since 1996): 5.
Available at: www.scopus.com

[67] Ainscow, E.K. and Brand, M.D.: Top-down control analysis of ATP turnover, glycolysis and oxidative phosphorylation in rat hepatocytes. *European Journal of Biochemistry*, vol. 263, no. 3, p. 671–685, 1999. ISSN 1432-1033.

[68] Hoefnagel, M.H.N., Burgt, A.v.d., Martens, D.E., Hugenholtz, J. and Snoep, J.L.: Time dependent responses of glycolytic intermediates in a detailed glycolytic model of lactococcus lactis during glucose run-out experiments. *Molecular Biology Reports*, vol. 29, no. 1-2, pp. 157–161, March 2002. ISSN 0301-4851, 1573-4978.

[69] Jones, E., Oliphant, T., Peterson, P. *et al.*: SciPy: Open source scientific tools for Python. 2001–.
Available at: http://www.scipy.org/

[70] Cock, P.J.A., Antao, T., Chang, J.T., Chapman, B.A., Cox, C.J., Dalke, A., Friedberg, I., Hamelryck, T., Kauff, F., Wilczynski, B. and Hoon, M.J.L.d.: Biopython: freely available Python tools for computational molecular biology and bioinformatics. *Bioinformatics*, vol. 25, no. 11, pp. 1422–1423, January 2009. ISSN 1367-4803, 1460-2059.

[71] SymPy Development Team: *SymPy: Python library for symbolic mathematics*, 2012.
Available at: http://www.sympy.org

[72] Karr, J.R., Sanghvi, J.C., Macklin, D.N., Gutschow, M.V., Jacobs, J.M., Bolival Jr., B., Assad-Garcia, N., Glass, J.I. and Covert, M.W.: A whole-cell computational model predicts phenotype from genotype. *Cell*, vol. 150, no. 2, pp. 389–401, July 2012. ISSN 0092-8674.
Available at: http://www.sciencedirect.com/science/article/pii/S0092867412007763

Appendices

Appendix A

RCFigure Class

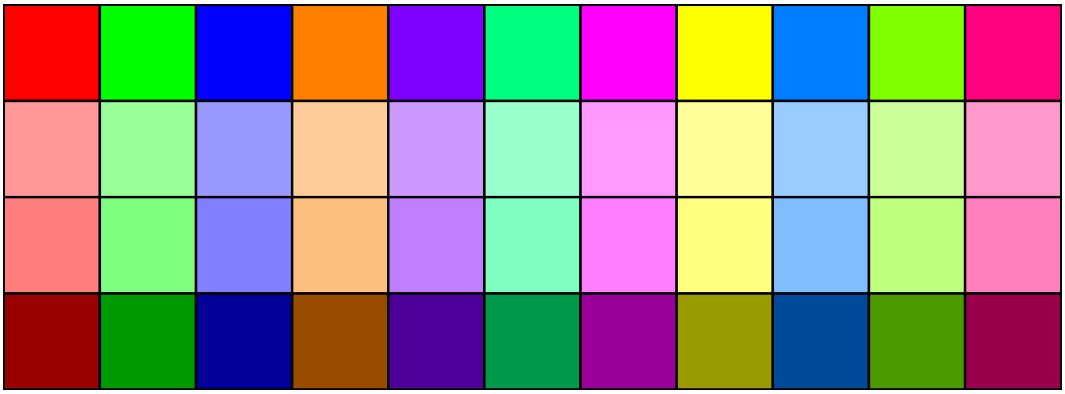

Figure A.1: A demonstration of the colours used by RCFigure. The rows from top to bottom represent the colours used for rate curves, elasticity coefficients, partial response coefficients and response coefficients. Colours are assigned to reaction blocks from left to right.

A description of the individual functions of the class follows below:

- set_visible() - This function is used to set the visibility of the lines associated with a certain reaction. It takes two arguments and has four keywords. The first arguments is name, which is the name of the reaction whose lines are to be manipulated. The possible keywords are p, f, e and r which affect the lines representing partial response coefficients, flux rate characteristics, elasticities and response coefficients associated with a certain reaction. They can take boolean values of True of False which make the lines visible or invisible respectively. The second argument is affzero which has a value of False by default and determines whether partial response coefficients with zero gradients are affected by the function.

- set_type_visible() - Like the previous function, this function sets the visibility of certain lines. Rather than changing the visibility of the lines associated with a certain reaction, it changes the visibility of a certain set of lines. It has three arguments, affzero which has the same function as in the previous method, visibility, which can take the values of True or False and either switches the visibility on or off, and finally, line_set_name which is the name of the set of lines to affect. line_set_name can take the following values:
  - supply_rc - For supply response coefficients
  - demand_rc - For demand response coefficients
  - supply_elas - For supply elasticity coefficients
  - demand_elas - For demand elasticity coefficients
  - mod_elas - For modifier elasticity coefficients
  - supply_flux - For supply fluxes
  - demand_flux - For demand fluxes
  - supply_partial_rc - For partial response coefficients associated with supply reactions
  - demand_partial_rc - For partial response coefficients associated with demand reactions
  - supply_total - For the total supply flux
  - demand_total - For the total demand flux
- update_legend() - This function updates the figure legend to reflect the lines that are set to visible.
- update_title() - The title of the figure can be set via the title variable. This function updates the figure title to reflect this change.
- show() - After the visibility of lines have been changed, this function is used to update the figure. It calls both update_legend and update_title.
- save() - Figures may be saved to the hard disk with this functionality. It takes file name as an argument which is a string that indicates file path and file name.
- clear() - This function resets the figure by removing all plots to give a blank set of axes.

In addition to these basic methods of RCFigure, there are some functions that combine the above methods to draw certain predefined types of rate characteristics. These functions all have one argument, file. When file is set to true the figure is saved to the default location on the disk, otherwise the figure is displayed on screen. When a function has to display multiple figures, they are shown one after the other as the and the user is prompted to switch to the next. These functions are:

- plotRateChar() - Plots supply and demand fluxes and excludes all other plots such as elasticity coefficients or response coefficients.
- plotElasRC() - This function plots all the rate characteristic data except partial response coefficients on the same figure.
- plotElasRCIndiv() - The same information is plotted as with the previous function, but instead of plotting every reaction on the same figure, a different figure is drawn for each reaction connected to the intermediate metabolite.
- plotPartialRCDemand() and plotPartialRCSupply() - plots the response coefficients, fluxes and partial response coefficients for the demand and supply reactions respectively.
- plotPartialRCIndiv() - Similar to plotElasRCIndiv, this function plots the same information as plotPartialRCDemand and plotPartialRCSupply, but on separate figures for each reaction.

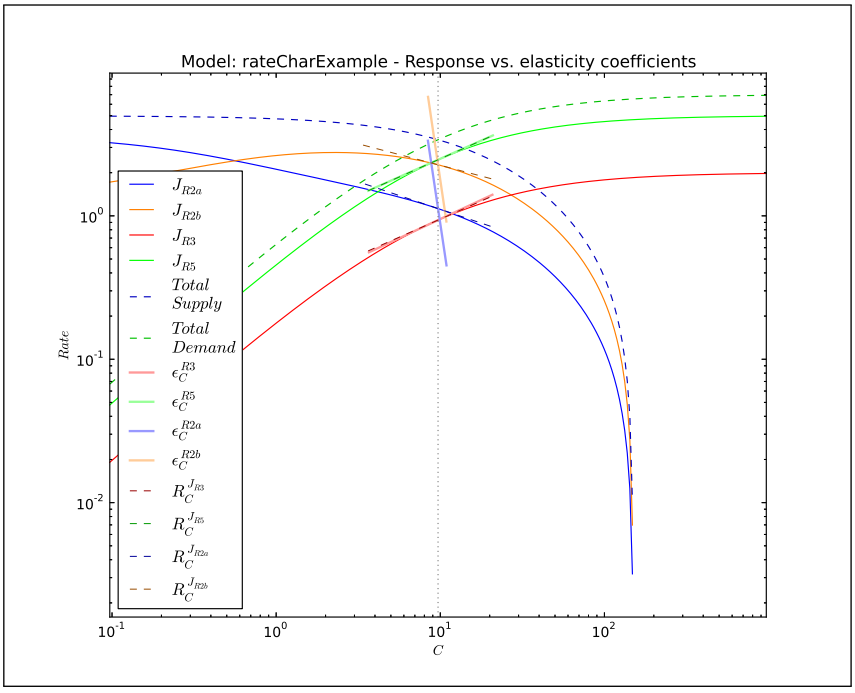

Figure A.2: A combined rate characteristic plot of the reaction blocks linked by metabolite *C* in Figure 3.6 as generated by the newly developed RCFigure class with the default settings.

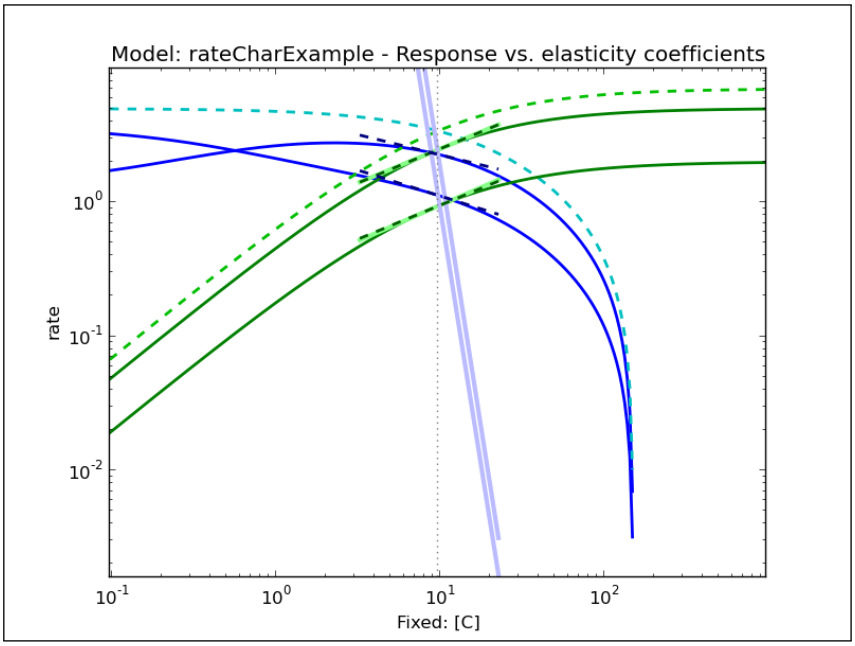

Figure A.3: A combined rate characteristic plot of the reaction blocks linked by metabolite *C* in Figure 3.6 as generated by the original version of RateChar with the default settings.

Appendix B

Response coefficients of the pyruvate branch model

x	${}^{x}R^{J_{v_3}}_{Pyr}$	ε^{x}_{Pyr}	$C^{J_{v_3}}_{x}$
v_2	0.18	0.81	0.22
v_3	0.36	0.73	0.49
v_8	6.17	2.40	2.57
v_1	0.00	0.00	-0.20
$R^{J_{v_3}}_{Pyr}$	0.53		

Table B.1: The individual control and elasticity coefficients that make up the partial response coefficients of $R^{J_{v_3}}_{Pyr}$.

x	${}^{x}R^{J_{v_5}}_{r_A}$	$\varepsilon^{x}_{r_A}$	$C^{J_{v_5}}_{x}$
v_{12}	0.00	1.61	0.00
v_1	-0.21	-0.93	0.23
v_5	-0.10	-0.98	0.10
$R^{J_{v_5}}_{r_A}$	-0.31		

Table B.2: The individual control and elasticity coefficients that make up the partial response coefficients of $R^{J_{v_5}}_{r_A}$

x	${}^{x}R^{J_{v_3}}_{r_C}$	$\varepsilon^{x}_{r_C}$	$C^{J_{v_3}}_{x}$
v_4	0.00	0.97	0.00
v_6	0.05	1.79	0.039
v_3	-0.27	-0.67	0.40
$R^{J_{v_3}}_{r_C}$	-0.22		

Table B.3: The individual control and elasticity coefficients that make up the partial response coefficients of $R^{J_{v_3}}_{r_C}$.

x	${}^{x}R^{J_{v_6}}_{r_C}$	$\varepsilon^{x}_{r_C}$	$C^{J_{v_6}}_{x}$
v_4	0.00	0.97	0.00
v_6	0.57	1.79	0.32
v_3	-0.49	-0.67	0.73
$R^{J_{v_6}}_{r_C}$	0.07		

Table B.4: The individual control and elasticity coefficients that make up the partial response coefficients of $R^{J_{v_6}}_{r_C}$

x	${}^{x}R_{r_N}^{J_{v_2}}$	$\varepsilon_{r_N}^{x}$	$C_{x}^{J_{v_2}}$
v_2	0.013	0.677	0.019
v_6	-0.001	2.303	-0.001
v_7	-0.001	1.001	-0.001
v_{11}	0.000	-8.838	0.000
v_{13}	0.000	-0.696	0.000
v_1	-0.019	-0.0297	0.651
v_3	0.011	-0.548	-0.020
$R_{r_N}^{J_{v_2}}$	0.002		

Table B.5: The individual control and elasticity coefficients that make up the partial response coefficients of $R_{r_N}^{J_{v_2}}$.

x	${}^{x}R_{r_N}^{J_{v_3}}$	$\varepsilon_{r_N}^{x}$	$C_{x}^{J_{v_3}}$
v_2	-0.29	0.68	-0.43
v_6	0.06	2.30	0.02
v_7	0.04	1.00	0.04
v_{11}	0.00	-8.84	0.00
v_{13}	0.00	-0.70	0.00
v_1	-0.01	-0.03	0.23
v_3	-0.26	-0.55	0.48
$R_{r_N}^{J_{v_3}}$	-0.46		

Table B.6: The individual control and elasticity coefficients that make up the partial response coefficients of $R_{r_N}^{J_{v_3}}$

x	${}^{x}R_{r_N}^{J_{v_6}}$	$\varepsilon_{r_N}^{x}$	$C_{x}^{J_{v_6}}$
v_2	-0.28	0.68	-0.43
v_6	0.76	2.30	0.33
v_7	0.60	1.00	0.61
v_{11}	0.00	-8.84	0.00
v_{13}	0.00	-0.70	0.00
v_1	-0.01	-0.03	0.33
v_3	-0.26	-0.55	0.47
$R_{r_N}^{J_{v_6}}$	0.81		

Table B.7: The individual control and elasticity coefficients that make up the partial response coefficients of $R_{r_N}^{J_{v_6}}$.

x	${}^{x}R_{r_N}^{J_{v_7}}$	$\varepsilon_{r_N}^{x}$	$C_{x}^{J_{v_7}}$
v_2	-0.28	0.68	-0.43
v_6	0.76	2.30	0.33
v_7	0.60	1.00	0.61
v_{11}	0.00	-8.84	0.00
v_{13}	0.00	-0.70	0.00
v_1	-0.01	-0.03	0.33
v_3	-0.26	-0.55	0.47
$R_{r_N}^{J_{v_7}}$	0.81		

Table B.8: The individual control and elasticity coefficients that make up the partial response coefficients of $R_{r_N}^{J_{v_7}}$

Appendix C

The aspartate-derived amino-acid pathway model

```
#Translated into .psc from madonna format

FIX: Aspartate S_Adenosyl_Methionine sink

# Keywords
Description: AspPathway
Modelname:
Output_In_Conc: True
Species_In_Conc: True

# GlobalUnitDefinitions
UnitSubstance: mole, 1.0, 0, 1
UnitArea: metre, 1.0, 0, 2
UnitVolume: litre, 1.0, 0, 1
UnitLength: metre, 1.0, 0, 1
UnitTime: second, 1.0, 0, 1


# Reactions
v_2:
        Aspartate = Aspartyl_Phosphate
        AKHSDHII*(AKII_kforward_app_exp - AKII_kreverse_app_exp*
    Aspartyl_Phosphate)/(1+(Threonine/ AKII_Thr_Ki_app_exp)**AKII_h_exp)
# VakII has modifier(s): AKHSDHII Threonine

v_10:
        Threonine > Isoleucine
        TD*TD_k_app_exp*Threonine/(1+(Isoleucine/( TD_Ile_Ki_no_Val_app_exp
    + TD_Val_Ka1_app_exp *Val/( TD_Val_Ka2_app_exp +Val)))**TD_h_app_exp)
# Vtd has modifier(s): TD Val Isoleucine

v_9:
        Phosphohomoserine > Threonine
        TS1*(TS1_kcatmin_exp + TS1_AdoMet_kcatmax_exp*
```

```
    S_Adenosyl_Methionine**TS1_h_exp / TS1_AdoMet_Ka1_exp)/
    (1+S_Adenosyl_Methionine**TS1_h_exp / TS1_AdoMet_Ka1_exp)*
    Phosphohomoserine/((1+Phosphate/TS1_Phosphate_Ki_exp)*
    ( TS1_AdoMEt_Km_no_AdoMet_exp*(1+S_Adenosyl_Methionine/
    TS1_AdoMet_Ka2_exp)/(1+S_Adenosyl_Methionine/ TS1_AdoMet_Ka3_exp))/
    (1+S_Adenosyl_Methionine**TS1_h_exp /TS1_AdoMet_Ka4_exp)+
    Phosphohomoserine)
# Vts1 has modifier(s): TS1 Phosphate S_Adenosyl_Methionine

v_8:
        Homoserine > Phosphohomoserine
        HSK*HSK_kcat_app_exp*Homoserine/(HSK_Hser_app_exp + Homoserine)
# Vhsk has modifier(s): HSK

v_1:
        Aspartate = Aspartyl_Phosphate
        AKHSDHI*(AKI_kforward_app_exp -
    AKI_kreverse_app_exp*Aspartyl_Phosphate)*1/
    (1+(Threonine/ AKI_Thr_Ki_app_exp)**AKI_h_exp)
# VakI has modifier(s): AKHSDHI Threonine

v_3:
        Aspartate = Aspartyl_Phosphate
        AK2*(AK2_kforward_app_exp -
    AK2_kreverse_app_exp*Aspartyl_Phosphate)/
    (1+(Lysine/ AK2_Lys_Ki_app_exp)**AK2_h_exp)
# Vak2 has modifier(s): AK2 Lysine

v_4:
        Aspartate = Aspartyl_Phosphate
        AK1*(AK1_kforward_app_exp -
    AK1_kreverse_app_exp*Aspartyl_Phosphate)/
    (1+(Lysine/(AK1_Lys_Ki_app_exp/
    (1+S_Adenosyl_Methionine/AK1_AdoMet_Ka_app_exp)))**AK1_h_exp)
# Vak1 has modifier(s): AK1 Lysine S_Adenosyl_Methionine

v_6:
        Aspartate_Semialdehyde > Homoserine
        AKHSDHI* HSDHI_kforward_app_exp *Aspartate_Semialdehyde*
    ( HSDHI_Thr_relative_residual_activity_app_exp+
    HSDHI_Thr_relative_inhibition_app_exp /
    (1+Threonine/ HSDHI_Thr_Ki_app_exp))
# Vhsdh1 has modifier(s): AKHSDHI Threonine

v_5:
        Aspartyl_Phosphate > Aspartate_Semialdehyde
        ASADH*(ASADH_kforward_app_exp*Aspartyl_Phosphate-
    ASADH_kreverse_app_exp*Aspartate_Semialdehyde)
# Vasadh has modifier(s): ASADH

v_7:
        Aspartate_Semialdehyde > Homoserine
        AKHSDHII* HSDHII_kforward_app_exp *Aspartate_Semialdehyde*
    ( HSDHII_Thr_relative_residual_activity_app_exp+
    HSDHII_Thr_relative_inhibition_app_exp /
```

```
    (1+Threonine/ HSDHII_Thr_Ki_app_exp))
# Vhsdh2 has modifier(s): AKHSDHII Threonine

v_13:
        Phosphohomoserine > S_Adenosyl_Methionine
        CGS*(CGS_kcat_exp /(1+ CGS_Cys_Km_exp /Cys))*
    Phosphohomoserine/(( CGS_Phser_Km_exp /(1+ CGS_Cys_Km_exp /Cys))*
    (1+Phosphate/ CGS_Phosphate_Ki_exp)+ Phosphohomoserine)
# Vcgs has modifier(s): CGS Cys Phosphate

v_14:
        Aspartate_Semialdehyde > Lysine
        DHDPS1* DHDPS1_k_app_exp*Aspartate_Semialdehyde*
    (1/(1+(Lysine/DHDPS1_Lys_Ki_app_exp)**DHDPS1_h_exp))
# Vdhdps1 has modifier(s): DHDPS1 Lysine

v_15:
        Aspartate_Semialdehyde > Lysine
        DHDPS2* DHDPS2_k_app_exp *Aspartate_Semialdehyde*
    (1/(1+(Lysine/ DHDPS2_Lys_Ki_app_exp)**DHDPS2_h_exp))
# Vdhdps2 has modifier(s): DHDPS2 Lysine

# additional reactions inferred from Madonna file
v_16:
        Lysine > sink
        Lys_tRNAS_Vmax *Lysine/(Lys_tRNAS_Lys_Km+Lysine)

v_11:
        Threonine > sink
        Thr_tRNAS_Vmax *Threonine/(Thr_tRNAS_Thr_Km+Threonine)

v_12:
        Isoleucine > sink
        Ile_tRNAS_Vmax *Isoleucine/(Ile_tRNAS_Ile_Km+Isoleucine)

Vtha:
        Threonine > sink
        THA*THA_kcat_exp*Threonine/(THA_Thr_Km_exp+Threonine)

Vlkr:
        Lysine > sink
        LKR*LKR_kcat_exp*Lysine/(LKR_Lys_Km_exp+Lysine)

##
#######
##
sink = 0.0
Lys_tRNAS_Vmax = 0.43
Ile_tRNAS_Vmax = 0.43
Thr_tRNAS_Vmax = 0.43
Lys_tRNAS_Lys_Km = 25.0
Ile_tRNAS_Ile_Km = 20.0
Thr_tRNAS_Thr_Km = 100.0
THA = 0.0
THA_kcat_exp = 1.7
```

```
THA_Thr_Km_exp = 7100.0
LKR = 0.0
LKR_kcat_exp = 3.1
LKR_Lys_Km_exp = 13000.0

# Variable species
Isoleucine = 0.0
Val = 100.0
ASADH = 11.6
Threonine = 0.0
Aspartyl_Phosphate = 0.0
Phosphate = 10000.0
DHDPS2 = 1.6
DHDPS1 = 1.6
Homoserine = 0.0
TD = 0.36
Cys = 15.0
Aspartate = 150.0
Lysine = 0.0
AK2 = 0.25
AK1 = 0.25
Phosphohomoserine = 0.0
AKHSDHII = 0.63
Aspartate_Semialdehyde = 0.0

AKHSDHI = 0.63
S_Adenosyl_Methionine = 20.0
HSK = 4.0
CGS = 0.7
TS1 = 7.4

# Parameters
AKII_kforward_app_exp = 1.35
AKII_kreverse_app_exp = 0.38
AKII_Thr_Ki_app_exp = 109.0
AKII_h_exp = 2.0
TD_k_app_exp = 0.0124
TD_Ile_Ki_no_Val_app_exp = 30.0
TD_Val_Ka1_app_exp = 73.0
TD_Val_Ka2_app_exp = 615.0
TD_h_app_exp = 3.0
TS1_kcatmin_exp = 0.42
TS1_AdoMet_kcatmax_exp = 3.5
TS1_AdoMet_Ka1_exp = 73.0
TS1_h_exp = 2.0
TS1_Phosphate_Ki_exp = 1000.0
TS1_AdoMEt_Km_no_AdoMet_exp = 250.0
TS1_AdoMet_Ka2_exp = 0.5
TS1_AdoMet_Ka3_exp = 1.09
TS1_AdoMet_Ka4_exp = 142.0
HSK_kcat_app_exp = 2.8
HSK_Hser_app_exp = 14.0
AKI_kforward_app_exp = 0.36
AKI_kreverse_app_exp = 0.10
AKI_Thr_Ki_app_exp = 124.0
```

```
AKI_h_exp = 2.0
AK2_kforward_app_exp = 3.15
AK2_kreverse_app_exp = 0.88
AK2_Lys_Ki_app_exp = 22.0
AK2_h_exp = 1.1
AK1_kforward_app_exp = 5.65
AK1_kreverse_app_exp = 1.57
AK1_Lys_Ki_app_exp = 550.0
AK1_AdoMet_Ka_app_exp = 3.5
AK1_h_exp = 2.0
HSDHI_kforward_app_exp = 0.84
HSDHI_Thr_relative_residual_activity_app_exp = 0.15
HSDHI_Thr_relative_inhibition_app_exp = 0.85
HSDHI_Thr_Ki_app_exp = 400.0
ASADH_kforward_app_exp = 0.9
ASADH_kreverse_app_exp = 0.23
HSDHII_kforward_app_exp = 0.64
HSDHII_Thr_relative_residual_activity_app_exp = 0.25
HSDHII_Thr_relative_inhibition_app_exp = 0.75
HSDHII_Thr_Ki_app_exp = 8500.0
CGS_kcat_exp = 30.0
CGS_Cys_Km_exp = 460.0
CGS_Phser_Km_exp = 2500.0
CGS_Phosphate_Ki_exp = 2000.0
DHDPS1_k_app_exp = 1.0
DHDPS1_Lys_Ki_app_exp = 10.0
DHDPS1_h_exp = 2.0
DHDPS2_k_app_exp = 1.0
DHDPS2_Lys_Ki_app_exp = 33.0
DHDPS2_h_exp = 2.0
```

Appendix D

The pyruvate branch pathway model

```
 FIX: Glucose  Lactate  Phosphate  O_2  ACETOUT  Butanediol  Acetate  Ethanol
dummy

v_1:
{0.5}Glucose = {1}Pyruvate + {1}R_N + {1}R_A
   (Vmax1*(Glucose/Km1GLC)*(NAD/Km1NAD)*(ADP/Km1ADP))/
   ((1+Glucose/Km1GLC+Pyruvate/Km1PYR)*
   (1+NAD/Km1NAD+NADH/Km1NADH)*(1+ADP/Km1ADP+ATP/Km1ATP))

 v_2:
{1}Pyruvate + {1}R_N = {1}Lactate
   (Vmax2*(Pyruvate/Km2PYR)*(NADH/Km2NADH)*
   (1-((Lactate*NAD)/(Pyruvate*NADH*Keq2))))/
   ((1+(Pyruvate/Km2PYR)+(Lactate/Km2LAC))*
   (1+(NADH/Km2NADH)+(NAD/Km2NAD)))

  v_3:
{1}Pyruvate = {1}R_N + {1}R_C
   Vmax3*((Pyruvate/Km3PYR)*(NAD/Km3NAD)*(CoA/Km3COA)/
   ((1+(Pyruvate/Km3PYR))*(1+(NAD/Km3NAD)+(NADH/Km3NADH))*
   (1+(CoA/Km3COA)+(Acetyl_CoA/Km3ACCOA))))*(1/(1+((Ki3*NADH)/NAD)))

 v_4:
{1}R_C + {1}Phosphate = {1}Acetyl_Phosphate
   ((Vmax4/(Ki4ACCOA*Km4P))*(Acetyl_CoA*Phosphate-
   ((Acetyl_Phosphate*CoA)/(Keq4))))/(1+(Acetyl_CoA/Ki4ACCOA)+
   (Phosphate/Ki4P)+(Acetyl_Phosphate/Ki4ACP)+(CoA/Ki4COA)+
   ((Acetyl_CoA*Phosphate)/(Ki4ACCOA*Km4P))+((Acetyl_Phosphate*CoA)/
   (Km4ACP*Ki4COA)))

 v_5:
{1}Acetyl_Phosphate = {1}Acetate + {1}R_A
   (Vmax5*(Acetyl_Phosphate/Km5ACP)*(ADP/Km5ADP)*
   (1-((Acetate*ATP)/(Acetyl_Phosphate*ADP*Keq5))))/
   ((1+(Acetyl_Phosphate/Km5ACP)+(Acetate/Km5AC))*
```

```
   (1+(ADP/Km5ADP)+(ATP/Km5ATP)))

 v_6:
{1}R_N + {1}R_C =  {1}Acetaldehyde
   (Vmax6*(NADH*Acetyl_CoA)/(Km6NADH*Km6ACCOA)-(Vmax6*NAD*CoA*
   Acetaldehyde)/(Km6NADH*Km6ACCOA*Keq6))/((1+NADH/Km6NADH+NAD/Km6NAD)*
   (1+Acetyl_CoA/Km6ACCOA+CoA/Km6COA)* (1+Acetaldehyde/Km6ACAL))

 v_7:
{1}Acetaldehyde + {1}R_N = {1}Ethanol
   (Vmax7*(Acetaldehyde/Km7ACAL)*(NADH/Km7NADH)*(1-((Ethanol*NAD)/
   (Acetaldehyde*NADH*Keq7))))/((1+(Acetaldehyde/Km7ACAL)+
   (Ethanol/Km7ETOH))*(1+(NADH/Km7NADH)+(NAD/Km7NAD)))

 v_8:
{1}Pyruvate = {0.5}Acetolactate
   Vmax8*(Pyruvate/Km8PYR)*(1-(Acetolactate/(Pyruvate*Keq8)))*
   (((Pyruvate/Km8PYR)+(Acetolactate/Km8ACLAC))**(h8-1))/
   (1+(((Pyruvate/Km8PYR)+(Acetolactate/Km8ACLAC))**h8))

 v_9:
{1}Acetolactate = {1}Acetoin
   (Vmax9*Acetolactate/Km9ACLAC)/
   (1 + Acetolactate/Km9ACLAC + Acetoin/Km9ACET)

 v_10:
{1}Acetoin = {1}ACETOUT
   Vmax10*Acetoin/(Km10ACET + Acetoin)

v_11:
{1}Acetoin + {1}R_N = {1}Butanediol
   (Vmax11*(Acetoin/Km11ACET)*(NADH/Km11NADH)*
   (1-((Butanediol*NAD)/(Acetoin*NADH*Keq11))))/
   ((1+(Acetoin/Km11ACET)+(Butanediol/Km11BUT))*
   (1+(NADH/Km11NADH)+(NAD/Km11NAD)))

 v_12:
{1}R_A = {1}Phosphate
   Vmax12*((ATP/ADP)**n12)/((KATP**n12 + ((ATP/ADP)**n12)))

 v_13:
{1}R_N + {1}O_2 = {1}dummy
   (Vmax13*NADH/Km13NADH*O_2/Km13O)/
   ((1+NADH/Km13NADH+NAD/Km13NAD)*(1+O_2/Km13O))

 v_14:
{1}Acetolactate = {1}Acetoin
   k14*Acetolactate

#initext
Glucose = 15
Lactate = 0.1
Phosphate = 10
O_2 = 0.2
ACETOUT = 0.001
```

```
Butanediol = 0.01
Acetate = 0.01
Ethanol = 0.1
dummy = 0


#initpar
Vmax1 = 4794 # 2397
Km1GLC = 0.1
Km1PYR = 2.5
Km1NAD = 0.1412
Km1NADH = 0.08999
Km1ADP = 0.04699
Km1ATP = 0.01867
Vmax2 = 5118
Km2PYR = 1.5
Km2NADH = 0.08
Km2LAC = 100
Km2NAD = 2.4
Keq2 = 21120.69
Vmax12 = 900
n12 = 2.58
KATP = 6.196
Vmax13 = 118
Km13NADH = 0.041
Km13NAD = 1
Km13O = 0.2
Vmax8 = 1200  # 600
Km8PYR = 50
Km8ACLAC = 100
h8 = 2.4
Keq8 = 9000000000000.0
Vmax9 = 106
Km9ACLAC = 10
Km9ACET = 100
Vmax10 = 200
Km10ACET = 5
k14 = 0.0003
Vmax11 =  105
Km11ACET = 0.06
Km11NADH = 0.02
Km11BUT = 2.6
Km11NAD = 0.16
Keq11 = 1400
Vmax4 = 42
Ki4ACCOA = 0.2
Km4P = 2.6
Keq4 = 0.0065
Ki4P = 2.6
Ki4ACP = 0.2
Ki4COA = 0.029
Km4ACP = 0.7
Vmax5 = 2700
Km5ACP = 0.16
Km5ADP = 0.5
```

```
Km5AC = 7
Km5ATP = 0.07
Keq5 = 174.217
Vmax3 = 259
Km3PYR = 1
Km3NAD = 0.4
Km3COA = 0.014
Km3NADH = 0.1
Km3ACCOA = 0.008
Ki3 = 46.4159
Vmax6 = 97
Km6NADH = 0.025
Km6ACCOA = 0.007
Km6NAD = 0.08
Km6COA = 0.008
Km6ACAL = 10
Keq6 = 1
Vmax7 = 162
Km7ACAL = 0.03
Km7NADH = 0.05
Km7ETOH = 1
Km7NAD = 0.08
Keq7 = 12354.9


#InitVar
#NAD       = 6.33
#ADP      = 4.9
Pyruvate      = 1
#NADH     = 3.67
#ATP      = 0.1
Acetolactate    = 0.000001
Acetoin     = 0.000001
#CoA      = 0.89
#Acetyl_CoA    = 0.11
Acetyl_Phosphate      = 0.03145
Acetaldehyde     = 0.11

#NADH/NAD
R_N = 0.57894
SN = 10.0

#ATP/ADP
R_A = 0.02040816326530612
SA = 5.0

#Acetyl_CoA/CoA
R_C = 0.12359550561797752
SC = 1.0

!F CoA = SC/(R_C+1)
!F Acetyl_CoA = (R_C*SC)/(R_C+1)

!F ADP = SA/(R_A+1)
!F ATP = (R_A*SA)/(R_A+1)
```

```
!F NAD = SN/(R_N+1)
!F NADH = (R_N*SN)/(R_N+1)
```